University of California
Santa Barbara

Probing Late-Stage Stellar Evolution Through Robotic Follow-Up of Nearby Supernovae

A dissertation submitted in partial satisfaction
of the requirements for the degree

Doctor of Philosophy
in
Physics

by

Griffin A. Hosseinzadeh

Committee in charge:

Professor D. Andrew Howell, Co-Chair
Professor Lars Bildsten, Co-Chair
Professor Crystal L. Martin
Professor Benjamin A. Mazin

June 2018

The dissertation of Griffin A. Hosseinzadeh is approved.

Professor Crystal L. Martin

Professor Benjamin A. Mazin

Professor Lars Bildsten, Committee Co-Chair

Professor D. Andrew Howell, Committee Co-Chair

June 2018

Probing Late-Stage Stellar Evolution Through Robotic Follow-Up of Nearby Supernovae

by

Griffin A. Hosseinzadeh

To my mother, UCSB alumna, class of 1972, with whom I first visited Santa Barbara and who sparked my interest in space with *Star Trek: The Next Generation*.

Acknowledgements

The work contained in this dissertation is the result of collaboration with many people, but in particular, I thank my advisor, Prof. Andy Howell, and the current and former postdocs in my research group, Prof. Stefano Valenti (now at UC Davis), Prof. Iair Arcavi (soon to be at Tel Aviv University), and Dr. Curtis McCully (now a research scientist at Las Cumbres Observatory) for teaching me everything I know about astronomy. I also thank the staff (and dogs) of Las Cumbres Observatory for (1) building and operating a world-class facility that is uniquely designed to carry out my research and (2) making me feel like I was part of the family from the very beginning.

Equally importantly, I thank my friends for supporting me through the stress of graduate school, especially my housemates Dr. Ryan Heller, Grace Butler, Dr. Charlotte Mason, Jon Bechtel, and Christina Knapp, and I thank my family for being proud of me throughout my educational career.

I thank the LSSTC Data Science Fellowship Program for teaching me the more advanced statistical and machine learning methods used in this work and for introducing me to an exceptional community of astronomers who worry about their data.

Lastly, I thank the National Science Foundation (grant number AST-1313484) for supporting me financially for the last four years.

Curriculum Vitæ

Griffin A. Hosseinzadeh

EDUCATION

University of California, Santa Barbara September 2012 – June 2018
Ph.D. Physics, Astrophysics Emphasis, June 2018
Certificate in College and University Teaching, June 2018
M.A. Physics, Astrophysics Emphasis, June 2016

University of California, Berkeley August 2008 – May 2012
B.A. Physics, Music Minor
High Distinction in General Scholarship

RESEARCH

Harvard-Smithsonian Center for Astrophysics starting September 2018
Postdoctoral Researcher
Berger Time-Domain Research Group

Las Cumbres Observatory January 2014 – June 2018
Graduate Student Researcher
Global Supernova Project

Planet November 2012 – June 2013
Spacecraft Engineer
Optical Systems/Instrumentation

Frascati National Laboratories August–October 2012
DOE–INFN Summer Exchange Student
MoonLIGHT–ILN Experiment

University of California, Berkeley May–July 2012
Emilio G. Segrè Intern
Physics 111 Advanced Laboratory

Lawrence Berkeley National Laboratory May 2010 – August 2011
Undergraduate Researcher
Daya Bay Reactor Neutrino Experiment

TEACHING

Santa Barbara City College August 2014 – May 2018
Adjunct Faculty
Department of Earth and Planetary Science
ERTH 102 – Observational Astronomy Lab

University of California, Santa Barbara September 2013 – June 2014
Teaching Assistant
Department of Physics
Astro 1 – Basic Astronomy
Astro 2 – History of the Universe

University of California, Berkeley June–August 2010 & 2011
Graduate Student Instructor
Department of Physics
Physics 8A & 8B – Introductory Physics

PROGRAMS

LSSTC Data Science Fellowship Program September 2017 – May 2019
Training program for dealing with big data in astronomy

Hubble Space Telescope Program Principal Investigator March–May 2018
GO-15236: UV observations of a Type Ibn supernova host galaxy

SERVICE

Peer Reviewer May 2018 – present
Monthly Notices of the Royal Astronomical Society

UCSB Astro Webmaster March 2017 – June 2018
Maintain https://web.physics.ucsb.edu/~astrogroup/

Santa Barbara Astro Lunch January 2017 – June 2018
Organizer of weekly lunch talks by locals and visitors

MENTORING

Worster Fellowship, UC Santa Barbara June–August 2016
Mentor for an undergraduate research project

Pioneers in Engineering, UC Berkeley Febuary–April 2011 & 2012
Robotics competition for Bay Area high school students

OUTREACH

AAS Astronomy Ambassadors January 2018
Workshop for effective communication with the public

Astronomy on Tap Santa Barbara March 2016 – June 2018
Free, public astronomy presentations at a bar

UCSB Physics Circus October 2013 – June 2018
Interactive physics demonstrations for local students

HOBBIES

UCSB Jazz Ensemble, bass trombone — January 2014 – June 2018

University of California Marching Band, trombone — August 2008 – May 2012
Student Director, Executuve Committee 2011
Musical Activities Committee 2010
Director's Assistant 2009

SOFTWARE

PyZOGY — doi:10.5281/zenodo.1043973

`lcogtsnpipe` — https://github.com/svalenti/lcogtsnpipe/

FLOYDS Pipeline — https://github.com/svalenti/FLOYDS_pipeline/

CONFERENCES

8. 231st AAS Meeting, Oxon Hill, MD, USA, January 2018
   "Probing Late-Stage Stellar Evolution through Robotic Follow-Up of Nearby Supernovae"
7. Southern Horizons in Time-Domain Astronomy (IAU Symposium 339), Stellenbosch, Western Cape, South Africa, November 2017
   "Early Blue Excess from the Type Ia Supernova 2017cbv"
   "Type Ibn Supernovae" (supernova workshop)
6. Generation-GW: Diving into Gravitational Waves, St. Thomas, VI, USA, June 2017
   "Las Cumbres Observatory: A Global Network of Robotic Telescopes for Time-Domain Follow-Up"
5. 229th AAS Meeting, Grapevine, TX, USA, January 2017
   "Short-Lived Circumstellar Interaction in a Low-Luminosity Type II Supernova"
4. Supernovae Through the Ages, Hanga Roa, Easter Island, Chile, August 2016
   "Type Ibn Supernovae Have Uniform Light Curves but Two Spectral Subclasses"
3. 227th AAS Meeting, Kissimmee, FL, USA, January 2016
   "Type Ibn Supernovae: Not a Single Class"
2. Hot-Wiring the Transient Universe IV, Santa Barbara, CA, USA, May 2015
   "FLOYDS: A Robotic Spectrograph for the Faulkes Telescopes"
1. 225th AAS Meeting, Seattle, WA, USA, January 2015
   "Diversity in Type Ibn Supernovae" (poster)

PUBLICATIONS

42. Anderson, J. P., Dessart, L., Gutiérrez, C. P., et al. 2018, NatAs, in press
    "The Lowest-Metallicity Type II Supernova from the Highest-Mass Red Supergiant Progenitor"

41. Astropy Collaboration 2018, AJ, in press
"The Astropy Project: Building an Inclusive, Open-Science Project and Status of the v2.0 Core Package"

40. Bose, S., Dong, S., Pastorello, A., et al. 2018, ApJ, 853, 57
"Gaia17biu/SN 2017egm in NGC 3191: The Closest Hydrogen-Poor Superluminous Supernova to Date Is in a Normal,' Massive, Metal-Rich Spiral Galaxy"

39. Gutiérrez, C. P., Anderson, J. P., Sullivan, M., et al. 2018, MNRAS, in press
"Type II Supernovae in Low Luminosity Host Galaxies"

38. Hosseinzadeh, G., Valenti, S., McCully, C., et al. 2018, ApJ, in press
"Short-Lived Circumstellar Interaction in the Low-Luminosity Type IIP SN 2016bkv"

37. Huang, F., Wang, X.-F., Hosseinzadeh, G., et al. 2018, MNRAS, 475, 3959
"SN 2016X: A Type II-P Supernova with a Signature of Shock Breakout from Explosion of a Massive Red Supergiant"

36. Inserra, C., Smartt, S. J., Gall, E. E. E., et al. 2018, MNRAS, 475, 1046
"On the Nature of Hydrogen-Rich Superluminous Supernovae"

35. Li, L., Wang, X., Zhang, J., et al. 2018, MNRAS, in press
"Optical Observations of the 2002cx-like Supernova 2014ek, and Characterizations of SNe Iax"

34. Maguire, K., Sim, S. A., Shingles, L., et al. 2018, MNRAS, 477, 3567
"Using Late-Time Optical and near-Infrared Spectra to Constrain Type Ia Supernova Explosion Properties"

33. Miller, A. A., Cao, Y., Piro, A. L., et al. 2018, ApJ, 852, 100
"Early Observations of the Type Ia Supernova iPTF 16abc: A Case of Interaction with Nearby, Unbound Material and/or Strong Ejecta Mixing"

32. Prentice, S. J., Ashall, C., Mazzali, P. A., et al. 2018, MNRAS, in press
"SN 2016coi/ASASSN-16fp: An Example of Residual Helium in a Type Ic Supernova?"

31. Sand, D. J., Graham, M. L., Botyánszki, J., et al. 2018, ApJ, in press
"Nebular Spectroscopy of the Blue Bump' Type Ia Supernova 2017cbv"

30. Tartaglia, L., Sand, D. J., Valenti, S., et al. 2018, ApJ, 853, 62
"The Early Detection and Follow-up of the Highly Obscured Type II Supernova 2016ija/DLT16am"

29. Arcavi, I., McCully, C., Hosseinzadeh, G., et al. 2017, ApJL, 848, L33
"Optical Follow-up of Gravitational-Wave Events with Las Cumbres Observatory"

28. Arcavi, I., Hosseinzadeh, G., Howell, D. A., et al. 2017, Natur, 551, 64
"Optical Emission from a Kilonova Following a Gravitational-Wave-Detected Neutron-Star Merger"

27. Arcavi, I., Howell, D. A., Kasen, D., et al. 2017, Natur, 551, 210
"Energetic Eruptions Leading to a Peculiar Hydrogen-Rich Explosion of a Massive Star"

26. Arcavi, I., Hosseinzadeh, G., Brown, P. J., et al. 2017, ApJL, 837, L2
"Constraints on the Progenitor of SN 2016gkg from Its Shock-Cooling Light Curve"

25. Barbarino, C., Botticella, M. T., Dall'Ora, M., et al. 2017, MNRAS, 471, 2463
"LSQ14efd: Observations of the Cooling of a Shock Break-out Event in a Type Ic Supernova"

24. Blagorodnova, N., Gezari, S., Hung, T., et al. 2017, ApJ, 844, 46
"iPTF16fnl: A Faint and Fast Tidal Disruption Event in an E+A Galaxy"

23. Cartier, R., Sullivan, M., Firth, R. E., et al. 2017, MNRAS, 464, 4476
"Early Observations of the Nearby Type Ia Supernova SN 2015F"

22. Graham, M. L., Bigley, A., Mauerhan, J. C., et al. 2017, MNRAS, 469, 1559
"Clues to the Nature of SN 2009ip – II. The Continuing Photometric and Spectroscopic Evolution to 1000 Days"

21. Graham, M. L., Kumar, S., Hosseinzadeh, G., et al. 2017, MNRAS, 472, 3437
"Nebular-Phase Spectra of Nearby Type Ia Supernovae"

20. Hosseinzadeh, G., Sand, D. J., Valenti, S., et al. 2017, ApJL, 845, L11
"Early Blue Excess from the Type Ia Supernova 2017cbv and Implications for Its Progenitor"

19. Hosseinzadeh, G., Arcavi, I., Valenti, S., et al. 2017, ApJ, 836, 158
"Type Ibn Supernovae Show Photometric Homogeneity and Spectral Diversity at Maximum Light"

18. IceCube Collaboration et al. 2017, A&A, 607, A115
"Multiwavelength Follow-up of a Rare IceCube Neutrino Triplet"

17. LIGO Scientific Collaboration & Virgo Collaboration et al. 2017, Natur, 551, 85
"A Gravitational-Wave Standard Siren Measurement of the Hubble Constant"

16. LIGO Scientific Collaboration & Virgo Collaboration et al. 2017, ApJL, 848, L12
"Multi-Messenger Observations of a Binary Neutron Star Merger"

15. McCully, C., Hiramatsu, D., Howell, D. A., et al. 2017, ApJL, 848, L32
"The Rapid Reddening and Featureless Optical Spectra of the Optical Counterpart of GW170817, AT 2017gfo, during the First Four Days"

14. Tartaglia, L., Fraser, M., Sand, D. J., et al. 2017, ApJL, 836, L12
"The Progenitor and Early Evolution of the Type IIb SN 2016gkg"

13. Yan, L., Lunnan, R., Perley, D. A., et al. 2017, ApJ, 848, 6
"Hydrogen-Poor Superluminous Supernovae with Late-Time Hα Emission: Three Events From the Intermediate Palomar Transient Factory"

12. Zheng, W., Filippenko, A. V., Mauerhan, J., et al. 2017, ApJ, 841, 64
"Discovery and Follow-up Observations of the Young Type Ia Supernova 2016coj"

11. Darnley, M. J., Henze, M., Bode, M. F., et al. 2016, ApJ, 833, 149
"M31N 2008-12a - The Remarkable Recurrent Nova in M31: Panchromatic Observations of the 2015 Eruption"

10. Ferretti, R., Amanullah, R., Goobar, A., et al. 2016, A&A, 592, A40
"Time-Varying Sodium Absorption in the Type Ia Supernova 2013gh"

9. Huang, F., Wang, X., Zampieri, L., et al. 2016, ApJ, 832, 139
"Optical and Ultraviolet Observations of the Very Young Type IIP SN 2014cx in NGC 337"

8. Leloudas, G., Fraser, M., Stone, N. C., et al. 2016, NatAs, 1, E2
"The Superluminous Transient ASASSN-15lh as a Tidal Disruption Event from a Kerr Black Hole"

7. Nicholl, M., Berger, E., Smartt, S. J., et al. 2016, ApJ, 826, 39
"SN 2015bn: A Detailed Multi-Wavelength View of a Nearby Superluminous Supernova"

6. Nicholl, M., Berger, E., Margutti, R., et al. 2016, ApJL, 828, L18
"Superluminous Supernova SN 2015bn in the Nebular Phase: Evidence for the Engine-Powered Explosion of a Stripped Massive Star"

5. Taddia, F., Sollerman, J., Fremling, C., et al. 2016, A&A, 588, A5
"Long-Rising Type II Supernovae from Palomar Transient Factory and Caltech Core-Collapse Project"

4. Terreran, G., Jerkstrand, A., Benetti, S., et al. 2016, MNRAS, 462, 137
"The Multifaceted Type II-L Supernova 2014G from Pre-Maximum to Nebular Phase"

3. Tomasella, L., Cappellaro, E., Benetti, S., et al. 2016, MNRAS, 459, 1018
"Optical and Near-Infrared Observations of SN 2014ck: An Outlier among the Type Iax Supernovae"

2. Valenti, S., Howell, D. A., Stritzinger, M. D., et al. 2016, MNRAS, 459, 3939
"The Diversity of Type II Supernova versus the Similarity in Their Progenitors"

1. Pastorello, A., Prieto, J. L., Elias-Rosa, N., et al. 2015, MNRAS, 453, 3650
"Massive Stars Exploding in a He-Rich Circumstellar Medium – VII. The Metamorphosis of ASASSN-15ed from a Narrow Line Type Ibn to a Normal Type Ib Supernova"

Plus 181 astronomical transient classification reports (128 as first author).

Abstract

Probing Late-Stage Stellar Evolution Through Robotic Follow-Up of Nearby Supernovae

by

Griffin A. Hosseinzadeh

Many of the remaining uncertainties in stellar evolution can be addressed through immediate and long-term photometry and spectroscopy of supernovae. The early light curves of thermonuclear supernovae can contain information about the nature of the binary companion to the exploding white dwarf. Spectra of core-collapse supernovae can reveal material lost by massive stars in their final months to years. Thanks to a revolution in technology—robotic telescopes, high-speed internet, machine learning—we can now routinely discover supernovae within days of explosion and obtain well-sampled follow-up data for months and years. Here I present three major results from the Global Supernova Project at Las Cumbres Observatory that take advantage of these technological advances. (1) SN 2017cbv is a Type Ia supernova discovered within a day of explosion. Early photometry shows a bump in the U-band relative to previously observed Type Ia light curves, possibly indicating the presence of a nondegenerate binary companion. (2) SN 2016bkv is a low-luminosity Type IIP supernova also caught very young. Narrow emission lines in the earliest spectra indicate interaction between the ejecta and a dense shell of circumstellar material, previously observed only in the brightest Type IIP supernovae. (3) Type Ibn supernovae are a rare class that interact with hydrogen-free circumstellar material. An analysis of the largest-yet sample of this class has found that their light curves are much more homogeneous and faster-evolving than their hydrogen-rich counterparts, Type IIn supernovae, but that their maximum-light spectra are more diverse.

Contents

Chapter 1

Introduction

1.1 Background

Baade & Zwicky (1934) first coined the term "super-novae" to refer to new sources of light (novae) that temporarily outshine the rest of their host galaxy. With the advent of astronomical spectroscopy, Minkowski (1941) "provisionally" divided supernovae into two classes based on the absence (Type I) or presence (Type II) of hydrogen in their spectra. We now know that (at least) two distinct physical mechanisms are responsible for these very bright transients, which do not correspond to the Type I vs. Type II classification: core-collapse supernovae are the explosions of massive ($> 8\,M_{\odot}$) stars after running out of fuel for fusion, while thermonuclear supernovae are the explosions of white dwarf stars in binary systems (Gal-Yam 2016). Unfortunately, despite the increasing diversity of observed supernovae, we still rely on an extended version of the 77-year-old classification scheme (Figure 1.1).

We study supernovae for many reasons. If you are interested in stellar evolution, supernovae are excellent probes of the last years to months of a star's life, when the fastest and most uncertain processes occur (e.g., this work). If you are interested in galaxy evolution, supernovae are major contributors to the energetic and chemical enrichment of galaxies (Heckman & Thompson 2017). If you are interested in cosmology, supernovae

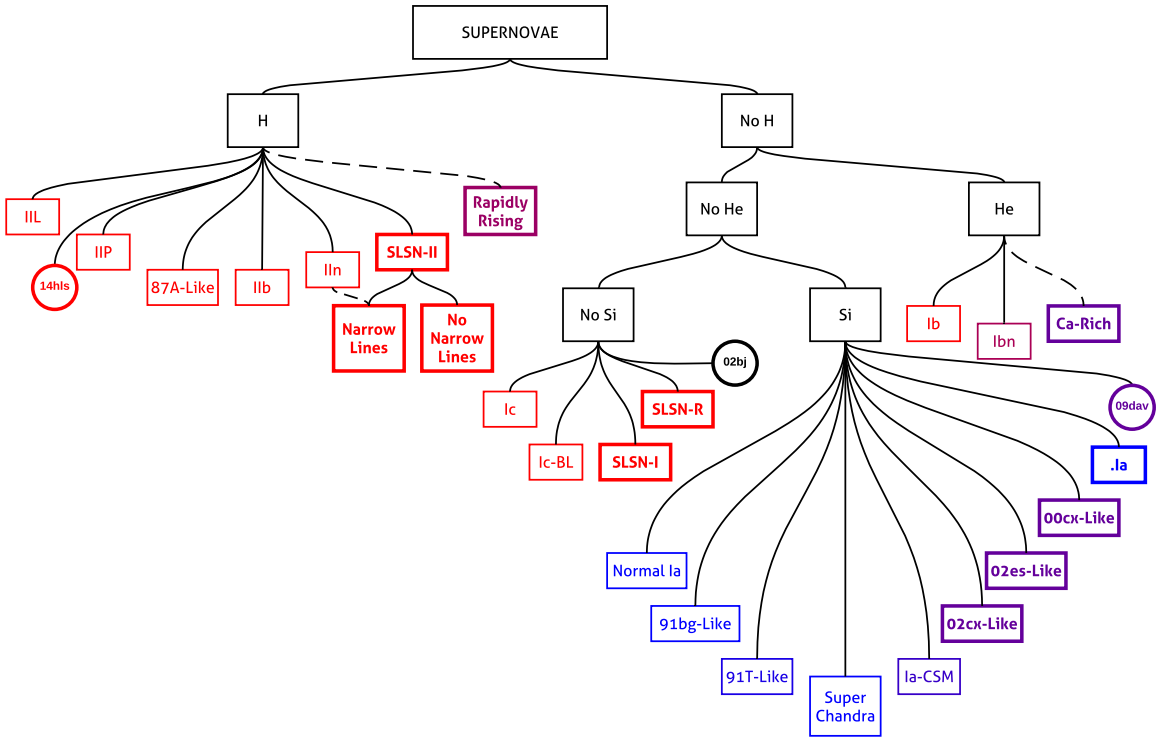

Figure 1.1: A modern supernova classification tree from Arcavi (in prep.). Colors represent the amount of certainty with which we know each class to come from massive stars (red) or white dwarfs (blue). Bold classes have been identified or proposed in the past decade.

are the most precise standard candles with which we can measure the expansion history of the universe (Riess et al. 1998; Perlmutter et al. 1999).

Most of our information about stars comes from our own galaxy, but because the supernova rate per galaxy is only one per century, almost all of our information about supernovae comes from other galaxies. As such, we still cannot directly connect the various types of supernovae to the types of stars that produce them, except in a few cases where the *Hubble Space Telescope* happened to have observed a star that later exploded (Van Dyk 2016). Instead, we rely on indirect evidence—mainly the photometric and spectroscopic evolution of the supernova itself—to infer the properties of the progenitor.

Historically, this evolution was only observed around maximum light, when the supernova was bright and easy to discover. The current frontier is to expand the range of observed phases in both directions, discovering supernovae early and obtaining well-sampled light curves and spectral series for months to years. These regimes allow us to probe physical processes that are otherwise inaccessible. For example, within a few days of explosion, the light curve of a core-collapse supernova is powered by shock cooling emission, the details of which depend strongly on the radius of the progenitor (Waxman & Katz 2017). Many months to years after explosion, when the material ejected in the supernova becomes mostly transparent, emission line strengths and ratios are sensitive to the progenitor mass (Jerkstrand 2017). The work presented in this dissertation takes advantage of these and other novel methods to constrain the nature of the progenitors of three types of supernovae, using data sets with unprecedented temporal coverage.

1.2 Las Cumbres Observatory

Most supernovae are now discovered by wide-field transient surveys that scan the night sky every few nights looking for changes. With sufficient depth and cadence, surveys can find supernovae very soon after they explode, within days or even hours. However, discovery is just the first step. To maximize the science return on a young discovery, we need to obtain a classification spectrum and start sampling its photometric evolution in multiple wavelength bands on similar timescales of hours to days.

While many surveys are currently in operation, very few facilities are dedicated to time-domain follow-up. One of those facilities—the tool that enabled much of the science in this dissertation—is Las Cumbres Observatory, a global network of robotic telescopes (Figure 1.2; Brown et al. 2013). Because the telescopes are distributed in longitude, at least one site will be in the dark and ready to observe a newly-discovered transient

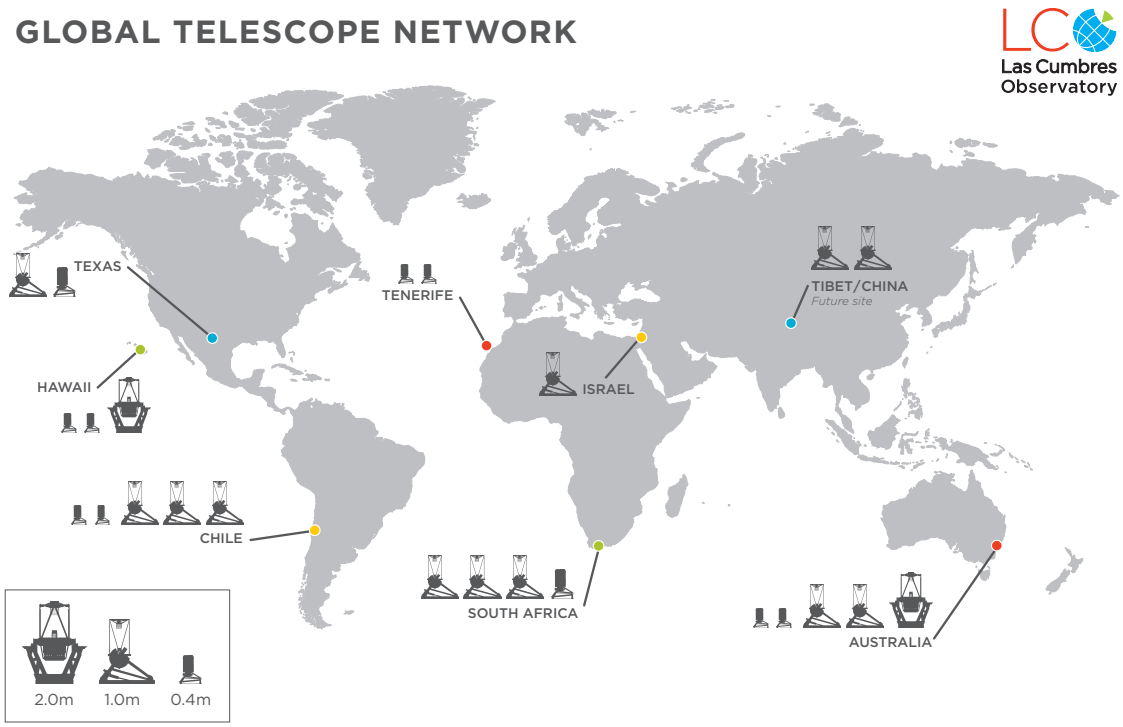

Figure 1.2: A map of Las Cumbres Observatory, a global telescope network, as of early 2018. Twenty-two robotic 2 m, 1 m, and 0.4 m telescopes distributed around the world give unprecedented time coverage of astronomical transients.

immediately. Furthermore, as the sun rises at that site, observations can continue at the next site to the west, allowing for nearly continuous coverage of the transient's early evolution. Weather can disrupt observations at any one site, but simultaneous bad weather at multiple sites is much less likely.

Particularly relevant for this work are FLOYDS: low-resolution ($\frac{\Delta\lambda}{\lambda} = 315-690$) long-slit spectrographs, mounted on Las Cumbres' two 2 m telescopes. FLOYDS are optimized for supernova classification and follow-up in that they are robotically controlled for rapid response and they cover the entire optical wavelength range ($300 - 1000$ nm) in a single exposure. Because supernovae have high velocities and therefore broad spectral features, higher-resolution spectra are not usually necessary. Since 2016, when the Transient Name

Server came online, our group has publicly classified 88 astronomical transients with FLOYDS (Arcavi et al. 2016a,b, 2017a,b; Hosseinzadeh et al. 2016a,b,c,d,e,f,g,h,i,j,k,l,m, n,o,p,q,r,s,t,u,w,v,x,y,z,aa,ab,ac,ad,ae,af,ag,ah, 2017a,b,c,d,e,f,g,h,i,j,k,l,m,n,o,p,q,r,s,t,u, v,w,x,y,aa,ab, 2018a,b,c,d,e; Valenti et al. 2017a,b,d; Burke et al. 2018; Hiramatsu et al. 2018a,b,c,d,e,f), many within a few days of discovery and some much sooner. In fact, two of the earliest classifications were of the supernovae presented in Chapters 2 and 3.

This work was carried out under the auspices of the LCOGT Supernova Key Project (May 2014 – March 2017) and the Global Supernova Project (April 2017 – May 2020), both consisting of over 100 collaborators led by P.I. Andy Howell. Each of these projects was allocated thousands of hours of time on the network to obtain well-sampled light curves and spectral series of hundreds of supernovae. Anyone in the collaboration can request observations, but our group schedules them and reduces the incoming data. To do this for dozens of supernovae simultaneously, we have built a large infrastructure of webpages, pipelines, and databases to automate the process. A significant portion of my graduate career was spent on this infrastructure work, which I will not discuss here.

The following chapters are three examples of how early discovery and rapid follow-up of transients can lead to advances in our understanding of stellar evolution. Chapter 2 focuses on the very early light curve of a Type Ia supernova that showed excess ultraviolet emission compared to a smooth power-law rise. We interpret this as a signature of the ejecta colliding with a nondegenerate binary companion star. Chapter 3 presents a low-luminosity Type IIP supernova whose early spectra show evidence of material around the progenitor star before it exploded. This is the lowest-luminosity supernova to show such evidence, suggesting that pre-supernova mass loss is common in red supergiant stars. Chapter 4 analyzes a sample of rare Type Ibn supernovae, in which the ejecta interact with hydrogen-poor circumstellar material. We find that their light curves relatively fast and homogeneous, but their spectra show some diversity at similar phases.

Chapter 2

Early Blue Excess from the Type Ia SN 2017cbv

This chapter is reproduced from Hosseinzadeh et al. (2017z) by permission of the American Astronomical Society. I would like to thank my coauthors, without whom this work would not have been possible: David J. Sand, Stefano Valenti, Peter Brown, D. Andrew Howell, Curtis McCully, Daniel Kasen, Iair Arcavi, K. Azalee Bostroem, Leonardo Tartaglia, Eric Y. Hsiao, Scott Davis, Melissa Shahbandeh, and Maximilian D. Stritzinger.

2.1 Introduction

Type Ia supernovae (SNe Ia) are the thermonuclear explosions of carbon-oxygen white dwarfs, and are standardizable candles vital for cosmological distance measurements. Despite intense study, the progenitor scenarios and explosion mechanisms for these events are still not understood, and may have multiple pathways (see Howell 2011; Maoz et al. 2014 for reviews). The two main progenitor pictures are the single-degenerate (SD) scenario, where the white dwarf accretes material from a nondegenerate secondary star (Whelan & Iben 1973), and the double-degenerate scenario (DD), where two white dwarfs are present in the pre-supernova system (Iben & Tutukov 1984; Webbink 1984). However,

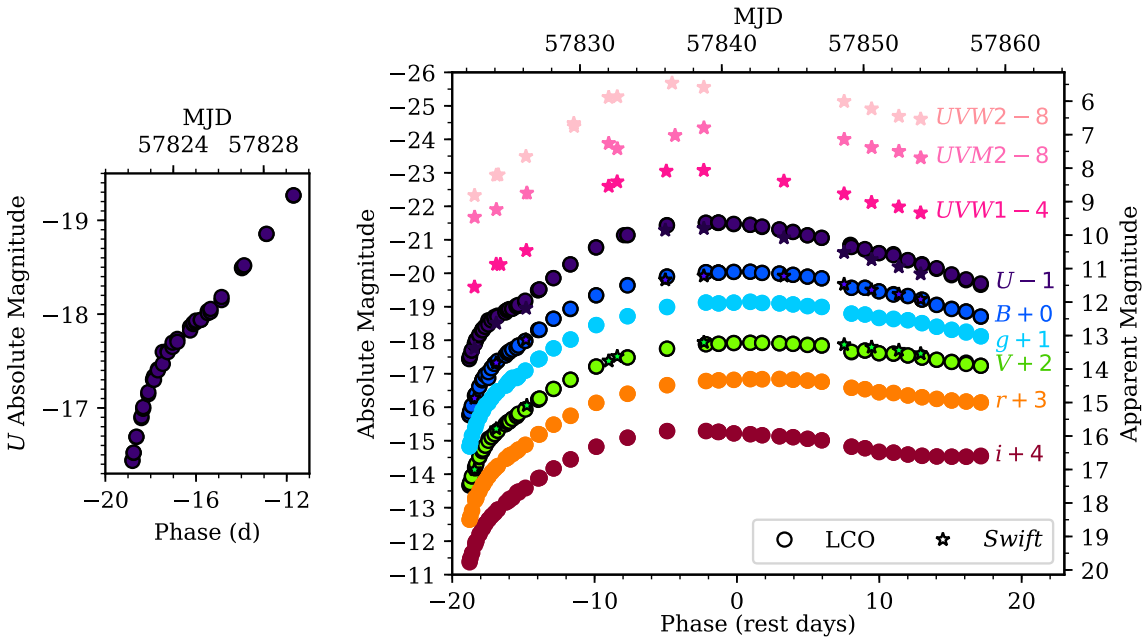

Figure 2.1: UV and optical photometry of SN 2017cbv, in absolute and extinction–corrected apparent magnitudes. The left panel shows a bump in the early U-band light curve. Data for this figure are available in the online journal.

the details of both scenarios are still under investigation (e.g., Pakmor et al. 2012; Kushnir et al. 2013; Shen & Bildsten 2014; Levanon & Soker 2017).

The early light curves of SNe Ia are promising ways to constrain the progenitor systems and the physics of the explosion. For instance, the collision of the SN ejecta with a nondegenerate companion star may manifest as an early blue or ultraviolet (UV) bump in the light curve, depending on the viewing angle (Kasen 2010). Early temperature or luminosity measurements can directly constrain the radius of the progenitor (Piro et al. 2010; Rabinak et al. 2012); observed limits have confirmed that the exploding star must be a white dwarf (e.g., Nugent et al. 2011; Bloom et al. 2012; Zheng et al. 2013). Recently, Piro & Morozova (2016) explored how early SN Ia light curve behavior depends on the amount and extent of circumstellar material (CSM), and the distribution of ^{56}Ni in the ejecta, which is expected to vary considerably with the location(s) of ignition in

the progenitor. Finally, different explosion mechanisms may also produce distinct early light curves (Noebauer et al. 2017).

Very early SN Ia light curve observations are becoming more common, and recent studies have shown that they display a range of early behaviors (Hayden et al. 2010; Bianco et al. 2011; Mo et al. 2010; Brown et al. 2012a; Zheng et al. 2013, 2014; Cao et al. 2015; Firth et al. 2015; Goobar et al. 2015; Im et al. 2015; Shappee et al. 2016; Marion et al. 2016; Zheng et al. 2017). iPTF14atg (Cao et al. 2015) and SN 2012cg (Marion et al. 2016) both showed early, UV/blue excesses in their light curves. iPTF14atg was a SN 2002es-like event, which are subluminous, do not follow the Phillips (1993) relation, have low velocities, and show Ti II absorption (Ganeshalingam et al. 2012). Cao et al. (2016) found that the UV excess in iPTF14atg was consistent with the SN ejecta interacting with a companion star, although Kromer et al. (2016) find the SD scenario incompatible with the observed spectral evolution. In SN 2012cg, a normal SN Ia, the early blue bump was again interpreted as a signature of ejecta-companion interaction, consistent with a $6\,M_{\odot}$ main-sequence companion $29\,R_{\odot}$ from the white dwarf, using the Kasen (2010) formulation.[1] However, Shappee et al. (2018) find that other probes of the progenitor system do not support the SD interpretation for SN 2012cg.

Here we present the early light curve and spectra of SN 2017cbv, which shows a clear blue excess during the first several days of observations. This excess may be a more subtle version of that seen in SN 2012cg and iPTF14atg, but seen more clearly here thanks to denser sampling.

[1]Note that the models of Kasen (2010) directly constrain the binary separation, not the companion mass. Masses can be inferred by assuming the companion is in Roche lobe overflow and applying a mass-radius relationship.

2.2 Observations and Data Reduction

SN 2017cbv (a.k.a. DLT17u) was discovered on MJD 57822.14 (2017 March 10 UT) at a magnitude of $R \approx 16$ by the Distance Less Than 40 Mpc survey (DLT40; Tartaglia et al. 2018), a one-day cadence SN search using a PROMPT 0.4 m telescope (Reichart et al. 2005), and was confirmed by a second DLT40 image during the same night (Valenti et al. 2017c). Our last nondetection was on MJD 57791. The SN is located on the outskirts of the nearby spiral galaxy NGC 5643. Within hours of discovery (MJD 57822.7), the transient was classified as a very young SN Ia with the robotic FLOYDS spectrograph mounted on the Las Cumbres Observatory (LCO; Brown et al. 2013) 2-meter telescope in Siding Spring, Australia (Hosseinzadeh et al. 2017aa).

UBVgri follow-up observations were obtained with Sinistro cameras on LCO's network of 1 m telescopes. Using `lcogtsnpipe` (Valenti et al. 2016), a PyRAF-based photometric reduction pipeline, we measured aperture photometry of the SN. Because the SN is bright and far from its host galaxy, image subtraction and PSF fitting are not required. Local sequence stars were calibrated to the L101 standard field observed on the same night at the same observatory site using *UBV* Vega magnitudes from Stetson (2000) and *gri* AB magnitudes from the SDSS Collaboration (2017).

The *Swift* satellite began observing SN 2017cbv on MJD 57822.52. Ultra-Violet Optical Telescope (UVOT; Roming et al. 2005) photometry is given in the UVOT Vega photometry system using the pipeline for the Swift Optical Ultraviolet Supernova Archive (SOUSA; Brown et al. 2014) and the zeropoints of Breeveld et al. (2010). Smaller hardware windows were used in the optical near maximum brightness in order to reduce coincidence loss and measure brighter magnitudes without saturation (Poole et al. 2007; Brown et al. 2012b). A few U- and B-band observations on the rising branch were saturated and are excluded.

Finally, we obtained absolute magnitudes by applying the distance modulus, $\mu = 31.14 \pm 0.40$ mag (16.9 ± 3.1 Mpc), of Tully (1988) and the Milky Way extinction corrections, $E(B-V) = 0.15$ mag, of Schlafly & Finkbeiner (2011). We assume no additional host galaxy extinction, given the SN's position in the outskirts of NGC 5643 and a lack of narrow Na I D absorption in high resolution spectra Ferretti et al. (2017).

Our photometry is shown in Figure 2.1. By fitting quadratic polynomials to the observed light curve, one around peak and one around +15 days, we find that SN 2017cbv reached a peak magnitude of $B = 11.72$ mag ($M_B = -20.04$ mag) on MJD 57841.07, with $\Delta m_{15}(B) = 1.06$ mag. The decline rate of SN 2017cbv is near the average for normal SNe Ia (see, e.g., Figure 14 of Parrent et al. 2014). The peak absolute magnitude appears to be on the bright end of SNe Ia (Parrent et al. 2014), but this is uncertain due to the poorly constrained distance to NGC 5643. All figures use MJD 57821 as the nominal explosion date (see §2.4).

2.3 Light Curve Morphology & Fitting

The very early light curve of SN 2017cbv shows a prominent blue bump in the U, B and g bands during the first 5 days of observation, also visible in its $U-B$ and $B-V$ colors (Figure 2.2). This indicates a high-temperature component of the early light curve in addition to the normal SN Ia behavior.

There are several possibilities for the origin of the early light curve bump (see §2.5 for a discussion), but here we fit the analytic models of Kasen (2010) for a nondegenerate binary companion shocking the SN ejecta, as might be expected from the SD scenario. While in reality such a collision would be highly asymmetric, we use Kasen's analytic expressions for the luminosity within an optimal viewing angle. By further assuming that the shock consists of a spherical blackbody, Kasen arrives at the following equations

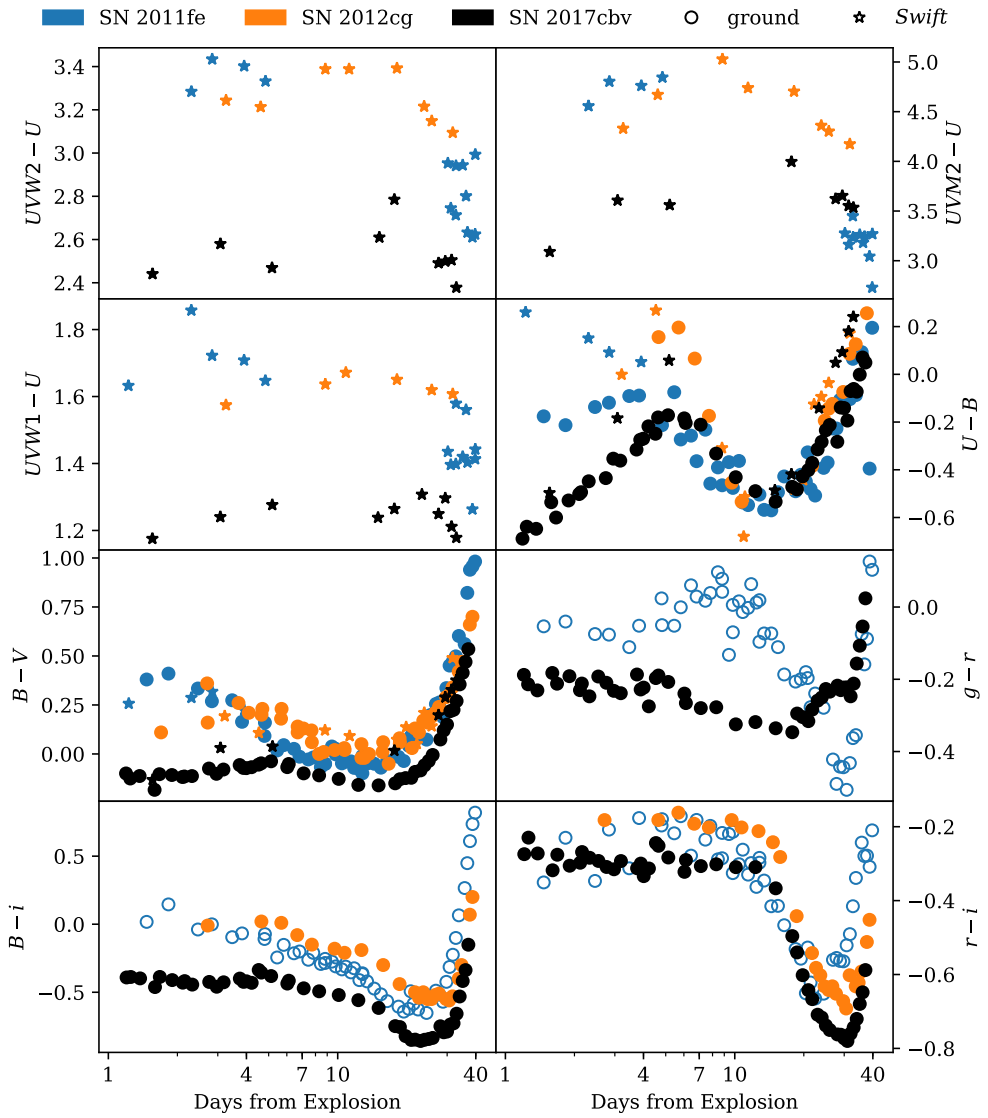

Figure 2.2: Milky Way extinction-corrected ultraviolet and optical colors of SN 2017cbv, compared to SN 2011fe (Zhang et al. 2016) and SN 2012cg (Marion et al. 2016). The colors of the subluminous SN Ia iPTF14atg are quite different than colors of the other events (Cao et al. 2015), so they are not shown. All *Swift* photometry is from SOUSA (Brown et al. 2014). Open circles indicate $V-R$, $B-I$, and $R-I$ colors that have been converted to $g-r$, $B-i$, and $r-i$, respectively, using the transformations of Jordi et al. (2006). Note the unusually blue $U-B$ and $B-V$ colors of SN 2017cbv during the bump (1–5 days after explosion).

for the photospheric radius and effective temperature[2]:

$$R_{\rm phot} = (2700\,R_\odot) x^{1/9} \kappa^{1/9} t^{7/9} \tag{2.1}$$

$$T_{\rm eff} = (25000\,{\rm K}) a^{1/4} x^{1/144} \kappa^{-35/144} t^{-37/72} \tag{2.2}$$

where a is the binary separation in units of 10^{11} m $(144, R_o dot)$, κ is the opacity in units of the electron scattering opacity (we fix $\kappa = 1$ in our fits), and t is the time since explosion in days. In addition, we define

$$x \equiv \frac{M}{{\rm M_{Ch}}} \left(\frac{v}{10000\,{\rm km\,s^{-1}}} \right)^7 , \tag{2.3}$$

where M is the ejected mass, ${\rm M_{Ch}} = 1.4\,M_\odot$ is the Chandrasekhar mass, and v is the transition velocity between power laws in the density profile.

Our light curve model is the sum of the SiFTO template (Conley et al. 2008), to account for the normal SN Ia emission, and Kasen's shock model, to account for the blue excess. We scale each band of the SiFTO template independently. In the U, B, V, and g bands, we fix the scaling factor to match the observed peak. In the r and i bands, we leave the scaling factor as a free parameter in order to account for any contribution from the shock in those bands around peak (predicted for some combinations of parameters). We also allow the time of B-band maximum light and the stretch (Perlmutter et al. 1997) of the SiFTO template to vary.

In total we have eight parameters:

- the explosion time,
- the binary separation, a,
- $x \propto M v^7$ (Eq. 2.3),
- factors on the r and i SiFTO templates,

[2]Eq. 2.2 corrects the exponent on κ in Kasen's Eq. 25.

- the time of peak,
- the stretch, and
- a factor on the shock component in U (see below).

We fit this combined model to our *UBVgri* light curve from LCO using a Markov-chain Monte Carlo routine based on the `emcee` package (Foreman-Mackey et al. 2013). We cannot include the *Swift* data in the fit due to a lack of early UV SN Ia templates. In addition to the photometric uncertainty, we add a 2% systematic (0.02 mag) uncertainty in quadrature as an estimate for our calibration uncertainties. For each of our observations, we find the expected $R_{\rm phot}$ and $T_{\rm eff}$ at that time, calculate the corresponding average L_ν in each filter, and compare that to our measured L_ν.

One caveat to our approach is that the SiFTO template may not describe the early light curve behavior of normal SNe Ia correctly in all filters. Given the small number of events observed 10–20 days before peak, reliable templates do not exist at these phases. However, we are encouraged by the fact that our SiFTO-based results qualitatively agree with other template fitters that we experimented with—SALT2 (Guy et al. 2007), MLCS2k2 (Jha et al. 2007), and the observed light curve of SN 2011fe (Zhang et al. 2016)—even at these early times.

We find that the SiFTO+Kasen model provides an excellent fit to our ground-based data (reduced $\chi^2 = 8.6$ after including our 2% calibration uncertainty), correctly predicting the blue bump at early times (Figure 2.3, top). Although at first glance our light curves do not look peculiar in the redder bands, emission from the shock model several weeks after explosion contributes to the observed luminosity around peak. Specifically, our best-fit model indicates that 5% and 15% of the r- and i-band peak luminosities, respectively, come from the shock component.

The best-fit binary separation is $56\,R_\odot$, implying a stellar radius of $\sim 20\,R_\odot$ (assuming Roche lobe overflow; Eggleton 1983). $56\,R_\odot$ is among the largest binary separations for

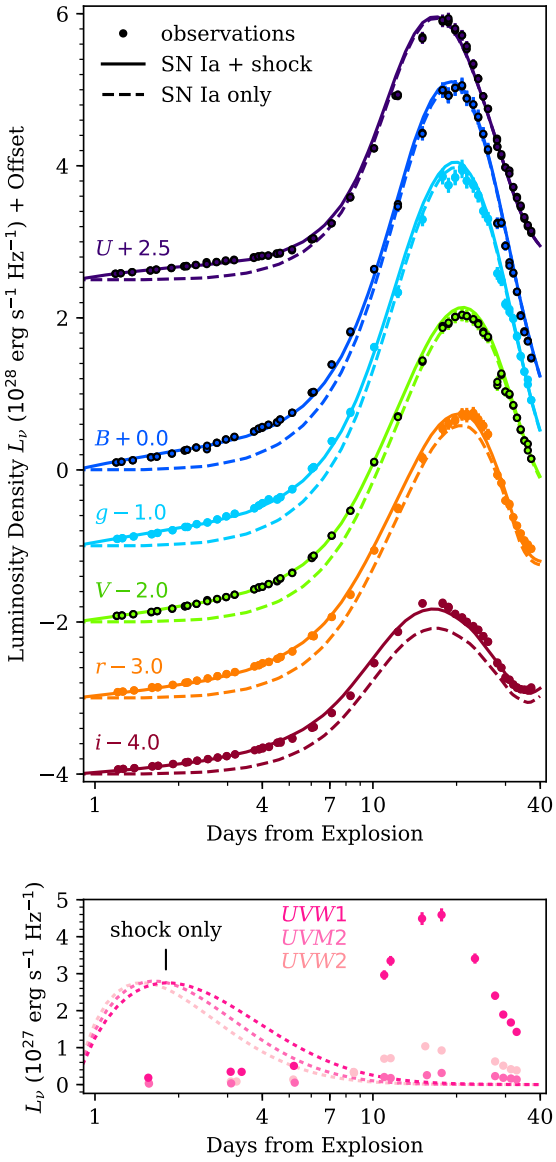

Figure 2.3: Best-fit model (solid lines), consisting of a SN Ia template (Conley et al. 2008) plus a companion shock component from Kasen (2010), to the ground-based light curve of SN 2017cbv. The dashed lines show the best-fit model with the companion shock subtracted. The model provides a good fit to the early light curve bump but the shock model alone (dotted lines) overpredicts the early *UVW1* to *UVW2* luminosity.

SD SN Ia progenitors from binary population synthesis calculations (Liu et al. 2015). However, this value is quite sensitive to the early color evolution of our SN Ia template. Since these templates may not be valid 15–20 days before peak, this result should be treated with caution. Furthermore, our simplified spherical model ignores the degeneracy between binary separation (a) and viewing angle; a bright (large a) off-angle shock looks similar to a faint (small a) shock along the line of sight.

Given the strong dependence of x on the transition velocity ($\propto v^7$), which is not observable, we cannot robustly estimate the ejecta mass. However, taking our best-fit value of $x = 3.84 \pm 0.19$ and assuming a Chandrasekhar mass of ejecta, we find a reasonable transition velocity of $v \approx 12000$ km s^{-1} (subject to uncertainty in the distance modulus). The best-fit explosion time is MJD 57821.9, about 7 hours before discovery, and the best-fit time of B-band peak for the SiFTO component is MJD 57840.2. The best-fit stretch from the SiFTO template is 1.04.

Despite the success of the binary companion shock model in the optical, we required a scaling factor of 0.61 on the U-band shock component in order to fit the data. The *UVW1*, *UVM2* and *UVW2* emission are even further overpredicted by the shock model (Figure 2.3, bottom). We discuss the potential causes of this discrepancy in §2.5.

2.4 Early Spectra

We obtained several additional optical and near-infrared (NIR) spectra of SN 2017cbv with FLOYDS and the SpeX NIR spectrograph (Rayner et al. 2003) at the NASA Infrared Telescope Facility, a selection of which are presented in Figure 2.4. As the event is ongoing at the time of publication, the full data set and analysis will be presented elsewhere (D. J. Sand et al., in prep.). In summary, the spectrum of SN 2017cbv greatly resembles the spectrum of SN 2013dy (Zheng et al. 2013) during the two weeks before

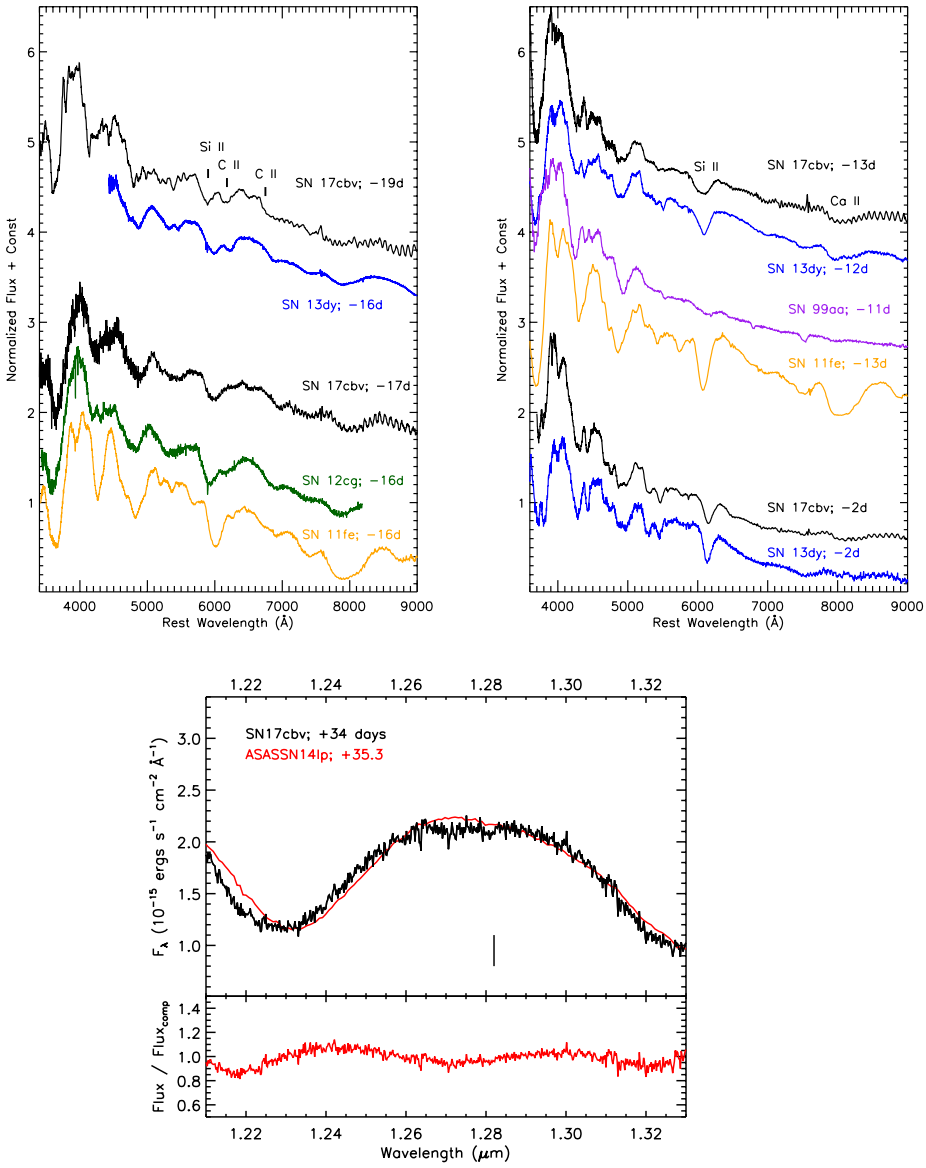

Figure 2.4: *Top Left:* The smoothed −19 day spectrum of SN 2017cbv shows conspicuous carbon similar to SN 2013dy, which persists at least until day −17. The −17 day spectrum is quite similar to the −16 day spectrum of SN 2012cg, which also showed an early blue bump in its light curve, but not the −16 day spectrum of SN 2011fe. *Top Right:* Spectra of SN 2017cbv at −13 and −2 days are very similar to SN 2013dy at similar epochs. Si II and Ca II are present and too strong to be SN 1999aa-like, but not as strong as in SN 2011fe. *Bottom:* NIR spectrum of SN 2017cbv in the region of Paβ (marked by the vertical line) compared to a spectrum of ASASSN-14lp. The bottom panel shows the ratio of the two spectra, yielding no evidence of narrow hydrogen emission from interaction with a companion star.

maximum light, with Si II and Ca II absorption features weaker than the prototypical Type Ia SN 2011fe but stronger than the somewhat overluminous SN 1999aa (Garavini et al. 2004). Despite the spectroscopic similarity to SN 2013dy, the light curve of SN 2017cbv declines slightly faster: $\Delta m_{15}(B) = 1.06$ mag for SN 2017cbv versus 0.92 mag for SN 2013dy (Pan et al. 2015).

We measure a Si II λ6355 velocity of 22800 km s^{-1} in the initial spectrum of SN 2017cbv, 19 days before maximum light. The absorption feature just redward of Si II could either be a lower-velocity component (9400 km s^{-1}) of the same line or C II λ6580 at 19800 km s^{-1}. We prefer the latter interpretation, since (1) it correctly predicts the tentative position of C II λ7234 in the same spectrum and (2) 9400 km s^{-1} would be uniquely low among very early SN Ia spectra (Silverman et al. 2012). The detection of unburned carbon can directly discriminate between the proposed SN Ia explosion mechanisms but is rarely seen in optical spectra even at these early times (Parrent et al. 2011; Silverman & Filippenko 2012), except for in super-Chandrasekhar SNe Ia (Howell et al. 2006). In SN 2017cbv, this feature disappears by day -13, reinforcing the need for early spectroscopy to fully account for unburned carbon.

The Si II absorption feature at -13 days clearly shows signs of two velocity components at 16500 and 10500 km s^{-1}. It is likely that the earlier spectra of SN 2017cbv are dominated by the high-velocity component of Si II, but we cannot fully trace the transition to low velocity Si II due to our lack of FLOYDS spectra between -13 and -2 days. We note that -13 days was also the approximate epoch at which SN 2012fr, another SN Ia with a prominent high-velocity Si II component, began showing low-velocity Si II (Childress et al. 2013). A similar multi-component velocity structure is evident for the Ca II H&K feature in our pre-maximum spectra.

We fit the early velocity evolution of Ca II H&K and the Si II high-velocity component (the only one we can clearly identify at early times) to a $t^{-0.22}$ power law, as suggested by

Piro & Nakar (2013) for finding the explosion time for SNe Ia. To do this, we mimicked the methodology of Piro & Nakar (2014) and allowed the power-law dependence to vary between $t^{-0.20}$ and $t^{-0.24}$ to estimate our uncertainties. This fit implies an explosion on MJD 57821.0 ± 0.3, 1.1 days prior to discovery and 0.9 days before the implied explosion time from our binary shock + standard SN Ia model presented in §2.3.

If SN 2017cbv had a SD progenitor, we might expect to see hydrogen in its late-time spectra (Mattila et al. 2005; Leonard 2007; Maeda et al. 2014). However, we do not detect Paβ emission in a NIR spectrum taken 34 days after maximum light (Figure 2.4, bottom). Following the method of Sand et al. (2016), we calculate a rough limit of $\lesssim 0.1\,M_{\odot}$ of hydrogen by comparing to a spectrum of ASASSN-14lp at a similar phase, although this limit depends on the viewing angle.

2.5 Discussion

The companion-shocking models provide a good fit to our optical data, but not to our UV data. This discrepancy is not likely to be a reddening effect (unless the reddening varies very quickly with time) because the UV luminosities around peak are not unusual for SNe Ia. However, it could stem from several simplifying assumptions in our model:

- **Blackbody:** The analytic models assume a blackbody spectrum for the shock component. However, the observed spectral energy distribution (SED) during the bump deviates significantly from a blackbody spectrum in the UV (Figure 2.5). A *Swift* grism spectrum taken during the bump is similar to UV spectra of other SNe Ia, showing significant absorption relative to a blackbody continuum (D.J. Sand et al., in prep.). This UV suppression is likely due to line blanketing (e.g., from iron lines). Any alternative model, companion shocking or otherwise, will need to account for this deviation from a blackbody spectrum.

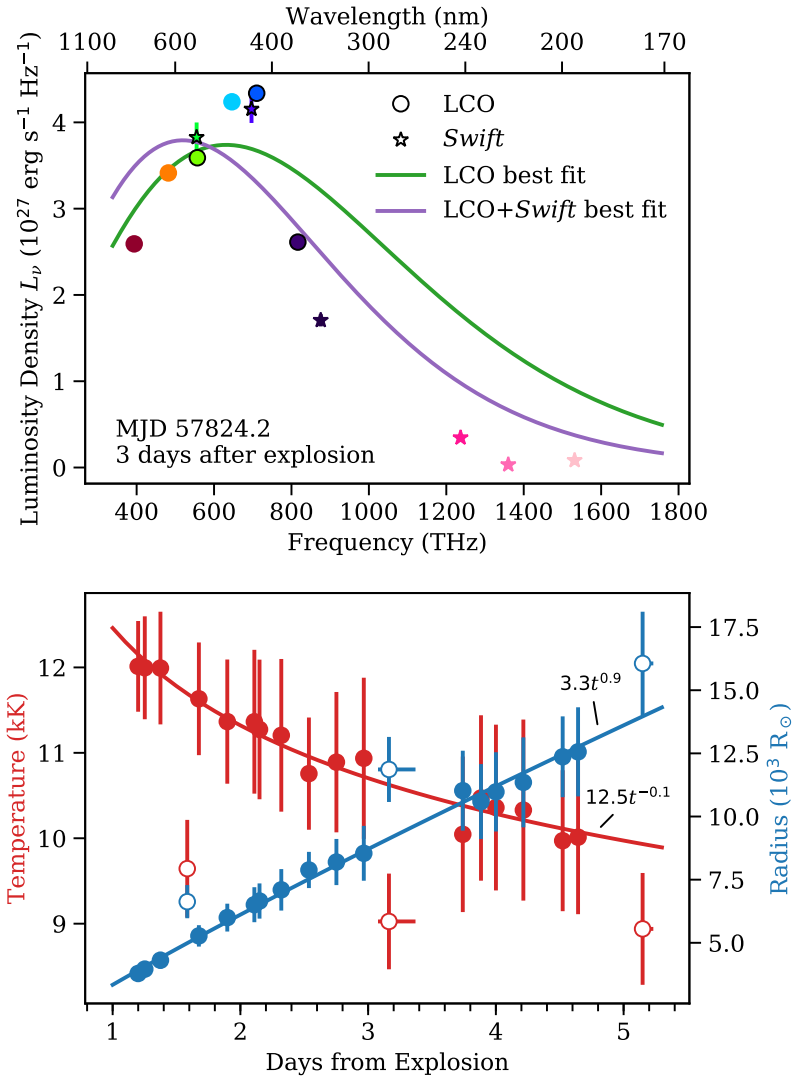

Figure 2.5: *Top:* Example SED of SN 2017cbv (3 days after explosion) and two blackbody fits, with and without the *Swift* observations. Including these filters pulls down the temperature, but neither blackbody spectrum is a good match to the data. *Bottom:* Blackbody temperature and radius evolution of SN 2017cbv during the first five days after explosion, presumably when the shock component dominates the light curve. The filled points use only *UBVgri* data, while the open points include *Swift* photometry. Lines are best-fit power laws, excluding the open points. The temperature evolution may not be reliable, since the SED is not well-described by a blackbody, but the radius evolution is well-constrained and close to what is expected for the Kasen (2010) models ($t^{7/9}$).

- **Constant Opacity:** We fixed the opacity to be that of electron scattering throughout the first 40 days of evolution, whereas in reality the opacity should change over time as the ejecta cool. Opacity and/or line blanketing that vary with time could potentially explain the discrepancy between the models and our UV data.
- **Density Profile:** The shock models we quote here assume a broken power law density profile for the ejecta: $\rho_{\rm inner} \propto r^{-1}$ and $\rho_{\rm outer} \propto r^{-10}$. The earliest emission, which should peak in the UV bands, depends strongly on the density of the outermost ejecta layers. In particular, a steeper density profile could suppress the early luminosity.
- **Spherical Symmetry:** In order to make the problem analytically tractable, we have ignored the asymmetry that must be present in a binary system. The analytic predictions are roughly equivalent to numerical predictions for a favorable viewing angle (see Figure 2 of Kasen 2010). If in reality we are viewing the collision off-axis, we might invoke a larger binary separation, ejecta mass, or ejecta velocity to match our observations. However, 3D numerical modeling of the ejecta–companion interaction would be needed to disentangle the early SN color diversity from the angular dependence of the shock component's color.

If the companion-shocking scenario is correct, but the model is inaccurate in the UV, then the companion sizes found by Marion et al. (2016) and Cao et al. (2015) and the constraints of Brown et al. (2012a) would have to be reevaluated. However, if the UV overprediction is only due to line blanketing, which depends on temperature, the models may be more susceptible to failure in relatively low-temperature events. Alternatively, there could be another cause of early bumps in the UV or optical.

The observed bump could also be interpreted as a collision with CSM, rather than a collision with a companion star, as has recently been modeled by Piro & Morozova (2016). Kasen (2010) estimates that 0.01–0.1 $M_\odot$ of CSM would be needed for a significant effect,

and that the material would have to be located at distances comparable to the binary separation. Stellar winds would be unlikely to produce such a configuration, but a DD system could potentially eject enough mass to large enough distances during the pre-supernova accretion phase (Kasen 2010) or during the merger itself (Levanon & Soker 2017). A large mass of CSM would likely have decelerated the ejecta below the velocities we measure in §2.4, although an unshocked high-velocity component could still persist.

A third possibility is that the bump arises from a bubble of radioactive nickel that escaped most of the ejecta, allowing it to radiate light away faster than the typical diffusion timescale. Piro & Morozova (2016) explored various nickel distributions and their effect on early SN light curves. Shallow nickel distributions result in steeper, bluer early light curves. The early light curves in Piro & Morozova (2016) that included both CSM interaction and significant nickel mixing bear a qualitative resemblance to the light curve of SN 2017cbv. Likewise, Noebauer et al. (2017) find an early blue bump in their sub-Chandrasekhar double-detonation model, in which the initial helium detonation on the surface produces a small amount of radioactive material. We cannot rule out these possibilities, but more detailed modeling of this event in particular would be necessary to distinguish them from the companion-shocking case.

2.6 Summary

We have presented early photometry and spectroscopy of the Type Ia SN 2017cbv, which was discovered within ∼1 day of explosion. Its light curve shows a conspicuous blue excess during the first five days of observations. We find a good fit between our *UBVgri* data and models of binary companion shocking from Kasen (2010), but the fit overpredicts the observed UV luminosity at early times. This discrepancy might be due to several simplifying assumptions in the models. Alternatively, the excess emission could

be due to interaction with CSM or the presence of radioactive nickel in the outer ejecta.

We observe no indication of ejecta interaction with hydrogen-rich material stripped from a companion star in the spectra of SN 2017cbv. However, more deep optical and near-infrared spectra out to the nebular phase are needed to confirm this finding.[3] Intriguingly, we do detect unburned carbon in the earliest spectra at a level rarely seen in normal SNe Ia. A connection between an early light curve bump and the presence of unburned carbon could provide an important clue about SN Ia progenitors, but the scarcity of events with either of these observations prevents us from drawing any conclusions now.

Our analysis demonstrates the importance of (1) discovering and announcing SNe as early as possible and (2) obtaining extremely well-sampled follow-up light curves and spectral series. The DLT40 survey and LCO follow-up network are uniquely suited to find very young SNe and follow them with sub-day cadence for long periods. Such observations, which will become increasingly common in the coming years, greatly enhance our ability to confront theoretical models.

[3]Since this work was originally published, Sand et al. (2018) have used nebular spectroscopy to place very strong constraints on the mass of material that could have been stripped from a nondegenerate companion star.

Chapter 3

Circumstellar Interaction in the Low-Luminosity Type IIP SN 2016bkv

This chapter is reproduced from Hosseinzadeh et al. (2018f) by permission of the American Astronomical Society. I would like to thank my coauthors, without whom this work would not have been possible: Stefano Valenti, Curtis McCully, D. Andrew Howell, Iair Arcavi, Anders Jerkstrand, David Guevel, Leonardo Tartaglia, Liming Rui, Jun Mo, Xiaofeng Wang, Fang Huang, Hao Song, Tianmeng Zhang, and Koichi Itagaki.

3.1 Introduction

The majority of massive ($M_{\rm ZAMS} \gtrsim 8\ M_{\odot}$) stars end their lives as Type II supernovae (SNe), i.e., those with hydrogen-rich spectra (Smartt 2009; Arcavi 2016). Broadly speaking, SNe II can be divided into two subclasses. SNe IIP/L have light curves that plateau (P) or decline linearly (L) for roughly 100 days before falling to a radioactive-decay-powered tail (Barbon et al. 1979). SNe IIn have spectra dominated by narrow (n) hydrogen emission lines, indicating strong interaction with circumstellar material (CSM; Schlegel 1990; Chugai 1991). Hereinafter, we will use "SNe II" to refer to SNe IIP and

IIL as a single class, excluding SNe IIb and IIn.

SNe II peak in the range of $-14 \gtrsim M_B \gtrsim -18$ mag (Patat et al. 1994) and show a correlation between plateau luminosity and photospheric expansion velocities (Hamuy & Pinto 2002; Pejcha & Prieto 2015). Pumo et al. (2017) claim that the ratio of the explosion energy to the ejected mass controls the plateau luminosity of SNe II, where smaller ratios are less luminous (see their Figure 5). At the faint/slow end of this distribution is a group of events referred to as low-luminosity (LL) SNe II (Pastorello et al. 2004; Spiro et al. 2014), exemplified by the nearby, well-studied SN 2005cs, whose red supergiant (RSG) progenitor star was detected by Maund et al. (2005) and Li et al. (2006) in pre-explosion images taken by the *Hubble Space Telescope* (*HST*). Several models have been proposed to explain LL SNe II, including high-mass RSGs exploding as fallback SNe (Turatto et al. 1998; Zampieri et al. 1998) and low-mass RSGs exploding as electron-capture SNe (Chugai & Utrobin 2000).

Interaction with CSM traditionally has not been considered significant in SNe II, since broad P Cygni lines dominate their spectra. However, recent efforts to obtain spectra of SNe within days of explosion have resulted in the discovery of narrow emission features in a significant fraction of early spectra of SNe II (18% of those observed within 5 days of explosion; Khazov et al. 2016). Early examples of these features include SNe 1983K (Niemela et al. 1985), 1993J (Benetti et al. 1994; Garnavich & Ann 1994; Matheson et al. 2000), 1998S (Leonard et al. 2000; Shivvers et al. 2015), and 2006bp (Quimby et al. 2007). Gal-Yam et al. (2014) first coined the term "flash spectroscopy" to describe this emission, produced as the CSM recombines after being ionized by the initial shock breakout flash. More recently, Yaron et al. (2017) observed flash spectra of the Type II SN 2013fs changing on hour time scales.

Intriguingly, Khazov et al. (2016) suggest that the presence of flash ionization features may be correlated with luminosity; in fact, all of their flash ionization spectra are

from events with peak absolute magnitudes $M_R < -17.5$ mag. This implies that more luminous events maintain higher temperatures at early times, enabling high-ionization lines to persist in their spectra long enough to be detected.

The object presented here, SN 2016bkv, is a SN II that was discovered soon after explosion. With a peak absolute magnitude of $M_V = -16$ mag and Hα expansion velocities under 1350 km s^{-1}, it greatly resembles SN 2005cs and other LL events in the literature. However, unlike any previous LL SN II, its pre-maximum spectra are dominated by narrow emission lines from high-ionization species, making it the least luminous SN for which flash ionization of the CSM has been detected. In this chapter, we report observations of SN 2016bkv and discuss their implications for the role of CSM interaction in SNe II. We also investigate the progenitor of SN 2016bkv, in particular, whether it exploded due to iron core collapse or electron capture.

3.2 Discovery

Itagaki (2016) discovered SN 2016bkv on 2016 March 21.70 UT at 17.5 mag using an unfiltered Celestron 14 inch (35 cm) telescope. Ross et al. (2016) do not detect the supernova on March 19.29, but only to an unfiltered limiting magnitude of 17 mag. Since this limit is not as deep as the first detection, in order to determine the explosion time, we fit $F(t) = F_1(t - t_0)^2$ to the first three unfiltered photometry points, after which the light curve appears to rise more slowly. This yields March 20.5 ($\mathrm{MJD}_0 = 57467.5 \pm 1.2$) as the explosion epoch, where we have adopted the time between estimated explosion and first detection as the uncertainty. Coincidentally, this uncertainty range includes the entire period from nondetection to first detection. Hosseinzadeh et al. (2016x) obtained the first spectrum on March 23.5, classifying the transient as a young SN II.

At right ascension $10^{\mathrm{h}}\,18^{\mathrm{m}}\,19\overset{\mathrm{s}}{.}31$ and declination $+41^{\circ}\,25'\,39\overset{''}{.}3$ (J2000), SN 2016bkv

lies 30.″3 (2.11 kpc projected) from the center of the spiral galaxy NGC 3184, which has a redshift of $z = 0.001975 \pm 0.000003$ (Strauss et al. 1992) and a Cepheid-based distance modulus of $\mu = 30.79 \pm 0.05$ mag (Ferrarese et al. 1999),[1] corresponding to a luminosity distance of $d_L = 14.4 \pm 0.3$ Mpc. In the past century, NGC 3184 has hosted at least four other SNe—1921B, 1921C, 1937F (Shapley 1939),[2] and 1999gi (Type II; Schlegel 2001; Smartt et al. 2001)—and one SN impostor—2010dn, which Smith et al. (2011) identify as the outburst of a luminous blue variable star.

As noted by Milisavljevic et al. (2016), images of NGC 3184 from *HST* show a star cluster at the position of SN 2016bkv. When the SN fades, it may be possible to determine the luminosity and colors of the progenitor star based on the change in flux from the cluster.

3.3 Observations and Data Reduction

In addition to unfiltered photometry from the 35 and 60 cm telescopes at the Itagaki Astronomical Observatory (Yamagata, Japan), we obtained *UBVgri* photometry of SN 2016bkv using Las Cumbres Observatory's (Brown et al. 2013) robotic 1 m telescope located at the McDonald Observatory (TX, USA) and *UBVRI* photometry using the 0.8 m Tsinghua University–National Astronomical Observatory of China Telescope (TNT; Huang et al. 2012) located at the Xinglong Observatory (Hebei Province, China). Unfortunately, the *Swift* satellite could not observe the SN in ultraviolet due to a nearby bright star.

Photometry measurements were complicated by the fact that the SN occurred in a bright but unresolved H II region (number 62 in the list of Hodge & Kennicutt 1983)

[1]Note, however, that other methods give distance moduli ranging from 29.3 mag (Pierce 1994) to 31.2 mag (Jones et al. 2009).

[2]Spectra of these SNe from E. Hubble's and F. Zwicky's programs were never obtained, but they have been photometrically classified as Types II, I, and IIP, respectively (Barbon et al. 2008).

and about 7.″7 away from an even brighter star (SDSS J101819.82+412544.3; Adelman-McCarthy et al. 2007). We obtained *BVgri* reference images with Las Cumbres approximately 600 days after explosion, when the SN was much fainter than the H II region, and subtracted them from the images of the supernova using PyZOGY (Guevel & Hosseinzadeh 2017), a new open-source Python image subtraction pipeline based on the optimal algorithm of Zackay et al. (2016). We then measured aperture photometry on the difference images using `lcogtsnpipe` (Valenti et al. 2016). The *U*-band light curve is PSF photometry on unsubtracted images, because host contamination in our reference images is much weaker in *U*. *UBV* photometry is calibrated in the Vega system to Landolt (1992) standard fields observed on the same night as the SN. *gri* photometry is calibrated in the AB system to stars in the Sloan Digital Sky Survey Data Release 8 (SDSS DR8; Aihara et al. 2011).

We obtained a *U*-band reference image with TNT approximately 300 days after explosion and *BVRI* references approximately 600 days after explosion. We subtracted these from the TNT images of the supernova using HOTPANTS (Becker 2015) and measured PSF photometry using a custom pipeline based on PyRAF tasks (Science Software Branch at STScI 2012). TNT *UBVRI* photometry is calibrated in the Vega system to SDSS DR13 stars (Albareti et al. 2017).

We measured PSF photometry from the remaining unsubtracted images using standard PyRAF tasks. Unfiltered photometry is calibrated to 20 nearby stars in SDSS DR6 (Adelman-McCarthy et al. 2007) by fitting blackbody spectra to their *ugriz* photometry and, for stars with reasonable fits, convolving the spectra with the spectral response curve of K. Itagaki's KAF-1001E CCD (both telescopes use the same CCD) to produce AB magnitudes. The resulting unfiltered magnitudes are not relevant to the bolometric light curve we produce in Section 3.4.2, but we do consider them when fitting the early light curve in Section 3.4.3. The photometry is plotted in Figure 3.1.

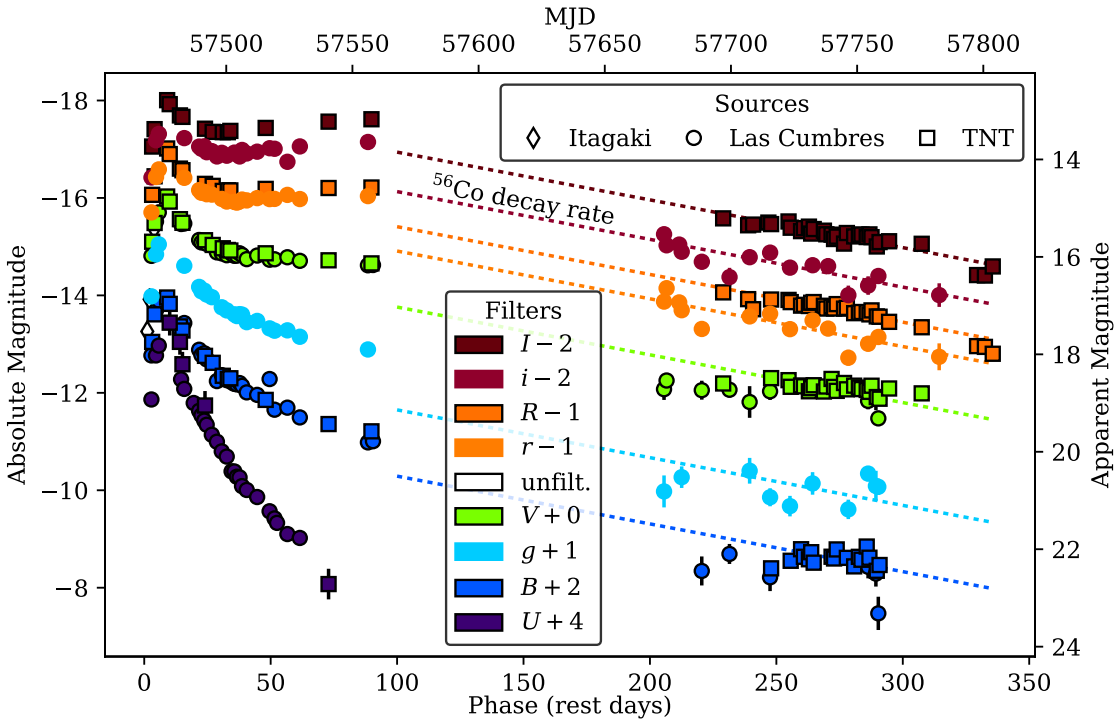

Figure 3.1: One year of photometry of SN 2016bkv. Late nondetections are hidden for clarity. Note the strong early bump and the small fall from plateau, which happened while the supernova was behind the sun. (The data used to create this figure are available.)

We obtained 17 optical spectra of SN 2016bkv during the flash ionization (Figure 3.2) and photospheric (Figure 3.3) phases using the robotic FLOYDS instrument, mounted on Las Cumbres Observatory's 2 m telescope on Haleakalā (HI, USA), and the Beijing Faint Object Spectrograph and Camera (BFOSC) and the Optomechanics Research Inc. (OMR) low-resolution spectrograph, both mounted on the 2.16 m telescope at Xinglong (Fan et al. 2016). Note that these low-resolution spectrographs cannot resolve lines with velocities below $\sim$800 km s^{-1}, meaning that we cannot constrain the photospheric velocity of SN 2016bkv during most of its evolution. Four additional spectra were obtained during the nebular phase using the Kast Double Spectrograph (Miller & Stone 1994)

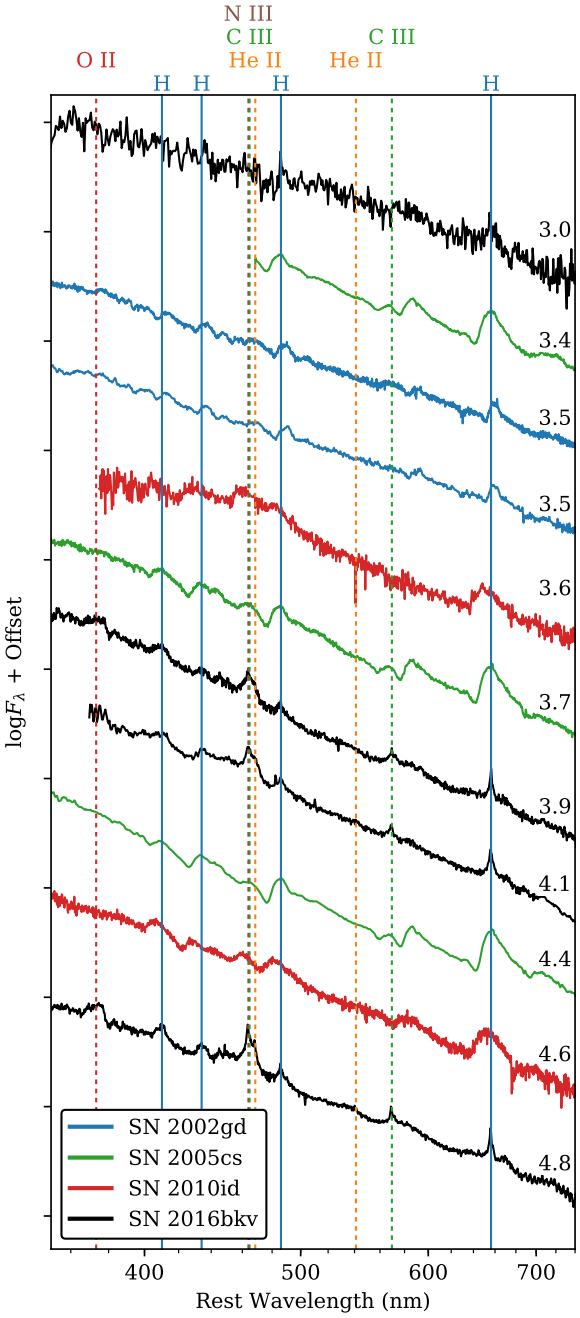

Figure 3.2: Flash-ionized spectra of SN 2016bkv compared with all spectra of LL SNe II observed within five days of estimated explosion: SNe 2002gd (Faran et al. 2014; Spiro et al. 2014), 2005cs (Pastorello et al. 2006; Faran et al. 2014), and 2010id (Gal-Yam et al. 2011). Phases in days from estimated explosion are marked to the right of each spectrum. SN 2016bkv is the only one that shows narrow emission of high-ionization species (dotted vertical lines).

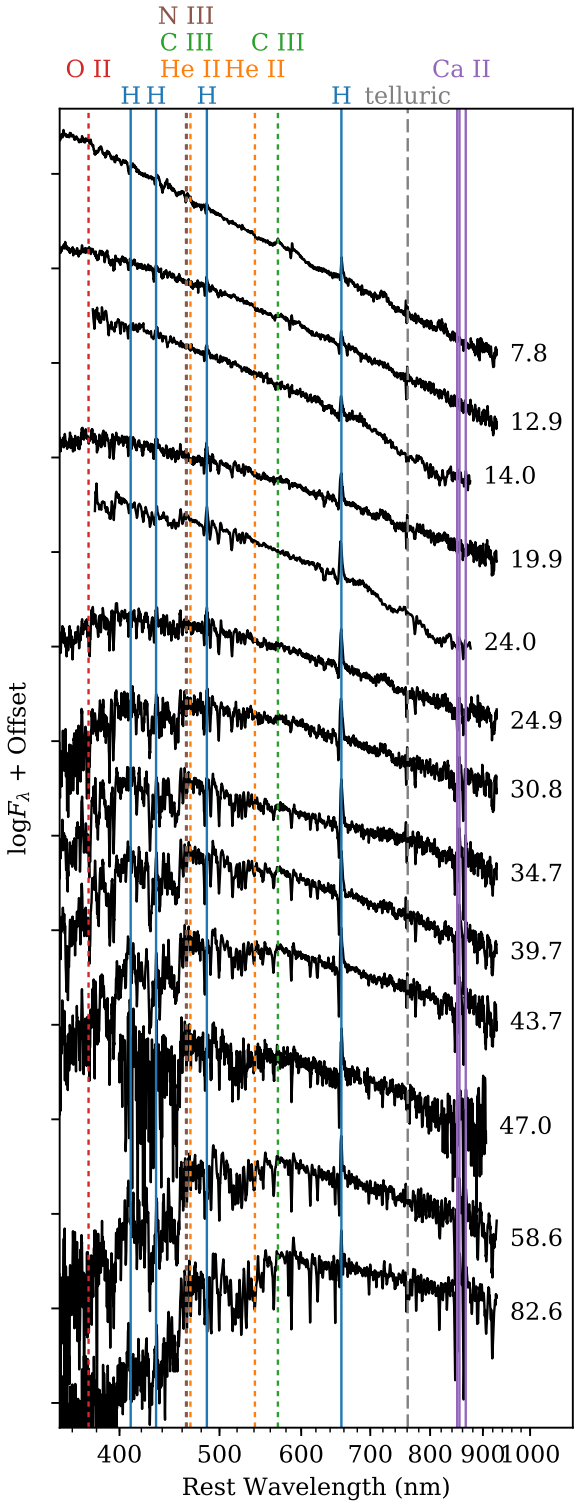

Figure 3.3: Photospheric spectra of SN 2016bkv; see Figure 3.7 for a more detailed line identification during the photospheric phase. Phases in days from estimated explosion are marked to the right of each spectrum. The early high-ionization lines in Figure 3.2 disappear after 5 days, giving way to typical SN II spectra with very low photospheric velocities (Hα velocity $< 1350\,\mathrm{km\,s^{-1}}$).

on the C. Donald Shane Telescope at the Lick Observatory (CA, USA) and the Low-Resolution Imaging Spectrometer (LRIS; Oke et al. 1995; Rockosi et al. 2010) on the Keck I telescope at the W. M. Keck Observatory (HI, USA). All spectra are available for download from the Weizmann Interactive Supernova Data Repository (Yaron & Gal-Yam 2012).

3.4 Analysis

3.4.1 Flash Spectroscopy

Initially, the spectrum of SN 2016bkv shows narrow emission lines of hydrogen (410.1, 434.0, 486.1, and 656.3 nm), He II (468.6 and 541.1 nm), C III (464.8 and 569.6 nm), N III (464.0 nm), and possibly O II (371.3–374.9 nm). With the exception of O II, these lines are a subset of those identified by Gal-Yam et al. (2014) in the Type IIb SN 2013cu (modeled by Groh 2014) and by Yaron et al. (2017) in the Type II SN 2013fs. The line widths are likely unresolved by our low-resolution spectrographs.

Previously, only three LL SNe II were observed spectrally this soon after explosion: SNe 2002gd (Faran et al. 2014; Spiro et al. 2014), 2005cs (Pastorello et al. 2006; Faran et al. 2014), and 2010id (Gal-Yam et al. 2011). Although their spectra are similarly blue, none of them show narrow emission features, instead being dominated by the same P Cygni profiles as during the photospheric phase (see Figure 3.2). Notably, Gal-Yam et al. (2014) identify a feature around 468 nm as He II, an indicator of very high temperatures, in their second spectrum of SN 2010id. However, Pastorello et al. (2004) identify a similar feature as high-velocity Hβ in their spectra of SN 2005cs (see their Figure 5).

Because of the very low photospheric velocity of SN 2016bkv, lower than these other three events, we suggest that its CSM may have lasted longer before being swept up

by supernova ejecta. This would have made flash spectroscopy easier by allowing us more time after explosion to observe the narrow emission lines. A larger sample size of well-observed flash-ionized SNe II would allow us to search for a correlation between photospheric velocity and duration of flash spectra.

3.4.2 Blackbody Fitting and Bolometric Light Curve

We construct a bolometric light curve of SN 2016bkv by fitting each epoch of photometry with a blackbody spectrum. In order to compare to pseudobolometric light curves from the literature, typically constructed using only optical photometry, we then integrate the blackbody spectrum from U to I. The result is shown in Figure 3.4, where it is compared to pseudobolometric light curves of other SNe II from Valenti et al. (2016).

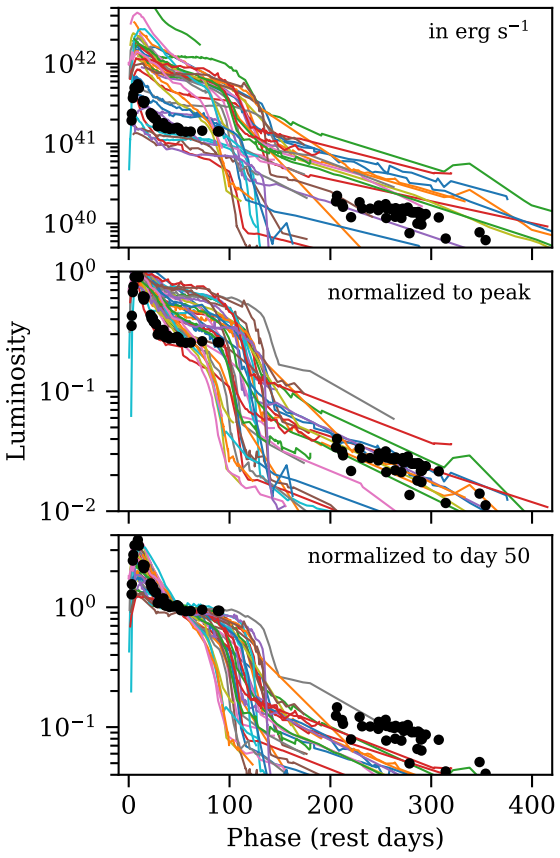

Figure 3.4: Pseudobolometric light curve of SN 2016bkv (black dots) compared to the Valenti et al. (2016) sample of SNe II (colored lines). SN 2016bkv has among the most extreme initial decline slopes and the smallest plateau-to-tail luminosity ratios.

The pseudobolometric light curve of SN 2016bkv is extreme in two ways. First, it has a very strong peak around 7 days after explosion with respect to the day-50 plateau luminosity (L_{50}). Integrating the light curve over the first 40 days, we find an excess $\Delta E = \int_0^{40}(L - L_{50})dt = 4.3 \times 10^{47}\,\mathrm{erg}$ above the plateau. If all of this energy were the result of converting ejecta kinetic energy into light with 100% efficiency, the mass of ejecta stopped would have to be

$$M = \frac{2\Delta E}{v_{\mathrm{ej}}^2} = 0.04\,M_\odot \left(\frac{1000\,\mathrm{km\,s^{-1}}}{v_{\mathrm{ej}}}\right)^2,$$

and the CSM mass would have to be comparable (Smith 2016). For comparison, Yaron et al. (2017) estimate that an order of magnitude less, a few $10^{-3}\,M_\odot$, CSM was necessary to produce the flash ionization lines in the spectra of SN 2013fs. However, the light-curve peak of SN 2016bkv may be powered by a combination of shock cooling and circumstellar interaction, in which case less CSM would be required.

Second, the luminosity ratio between the plateau (day 50) and the radioactive nickel tail (day 200) is relatively small. This implies that the amount of nickel produced in the explosion is unusually large for a LL SN II. Comparing the luminosity on the tail to SN 1987A, as in Hamuy (2003), we find that SN 2016bkv produced $M_{\mathrm{Ni}} = 0.0216 \pm 0.0014\,M_\odot$ of nickel. The uncertainty in this measurement is almost entirely due to the 2% uncertainty on the distance to the supernova, the 5% assumed uncertainty on the host-galaxy extinction ($A_V = 0.00 \pm 0.05$ mag), and the 1.2% uncertainty from the explosion epoch.

This measurement is surprisingly higher than those for previous LL SNe IIP and merits a careful consideration of the uncertainties. If supernova light was still present in the reference images we used to create our subtracted light curve, the luminosity we derived would be lower than the true luminosity, making the nickel mass even higher. Likewise, if extinction from dust in the ejecta were important, the true underlying luminosity would

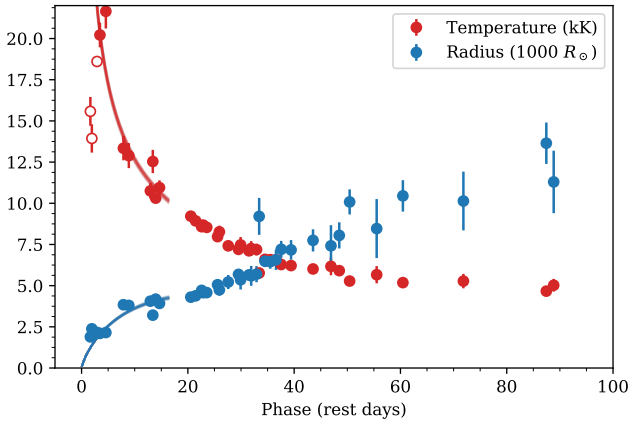

Figure 3.5: Best-fit blackbody temperature (red points) and radius (blue points) of SN 2016bkv during the photospheric phase, compared to the temperature (red lines) and radius (blue lines) from the best-fit Sapir & Waxman (2017) models in Section 3.4.3. The open red points are likely underestimates of the temperature from when the SED peaks blueward of our observations.

be higher than we observe, again making the nickel mass higher. In order to obtain a nickel mass similar to those of other LL SNe IIP, the true luminosity would have to be about three times lower than what we observe.

Figure 3.5 shows the evolution of the blackbody temperature and radius from the fit. The temperature evolution shows an unexpected rise during the first six days. Because we lack photometry blueward of U, the blackbody fits are not strongly constrained at these early times, when the spectral energy distribution peaks in the ultraviolet. If this rising behavior is real, it might be related to the flash ionization of the CSM, which manifests itself in the spectra during the same time period. However, given the uncertainties in the fits, we cannot claim to have observed a significant rise in temperature.

3.4.3 Shock Cooling Model Fitting

Sapir & Waxman (2017) present a method for modeling early supernova light curves powered by shock cooling emission—the radiation of energy deposited in the stellar envelope by the core-collapse shock wave. Here we test whether their models alone can reproduce the unusually sharp peak of SN 2016bkv or whether another power source is needed.

We fit our multiband light curve up to MJD 57485.0 (16.3 days after estimated explosion) to the Sapir & Waxman model, with $n = 1.5$ for a RSG, using a Markov chain Monte Carlo (MCMC) routine and flat priors for all parameters. This results in posterior probability distributions for the temperature 1 day after explosion (T_1), the total luminosity ≈1 day after explosion (L_1), the time at which the envelope becomes transparent ($t_{\rm tr}$), and the time of explosion (t_0). For each set of these parameters, the model gives the blackbody temperature and total luminosity as a function of time, which we then convert to observed fluxes for each photometry point, simultaneously fitting all bands. Figure 3.6 shows the light-curve fits, posterior probability distributions, and 1σ credible intervals centered on the medians.

Sapir & Waxman's models are valid starting when the supernova shock traverses the progenitor radius ($t > \frac{R}{5v}$) and ending when the ejecta cool below 8000 K. For our best-fit parameters, the latter occurs 27 days after explosion, well after the range of points we fit, but the former occurs 1–2 days after explosion. The most notable feature of our fits is that the explosion time is pushed as late as possible (5 minutes before discovery). If we believe this value, we should exclude the first two unfiltered points from our fit. However, this is in conflict with our earlier estimate of the explosion date, and as we discuss below, we do not consider these models to be a good fit.

Although the fit appears to converge on an optimal set of parameters (see also Figure 3.5), the models are not able to reproduce the sharpness of the peak around 8 days after explosion. This may be evidence that ejecta-CSM interaction contributes significant luminosity during the week around maximum light, which we might expect given our observation of the presence of CSM through flash spectroscopy. Indeed, Morozova et al. (2017, 2018) have shown that numerical light-curve models that include CSM reproduce these bumps much more faithfully than those with no CSM. In fact, there may be a correlation between the strength of the flash spectroscopy features and the luminosity in

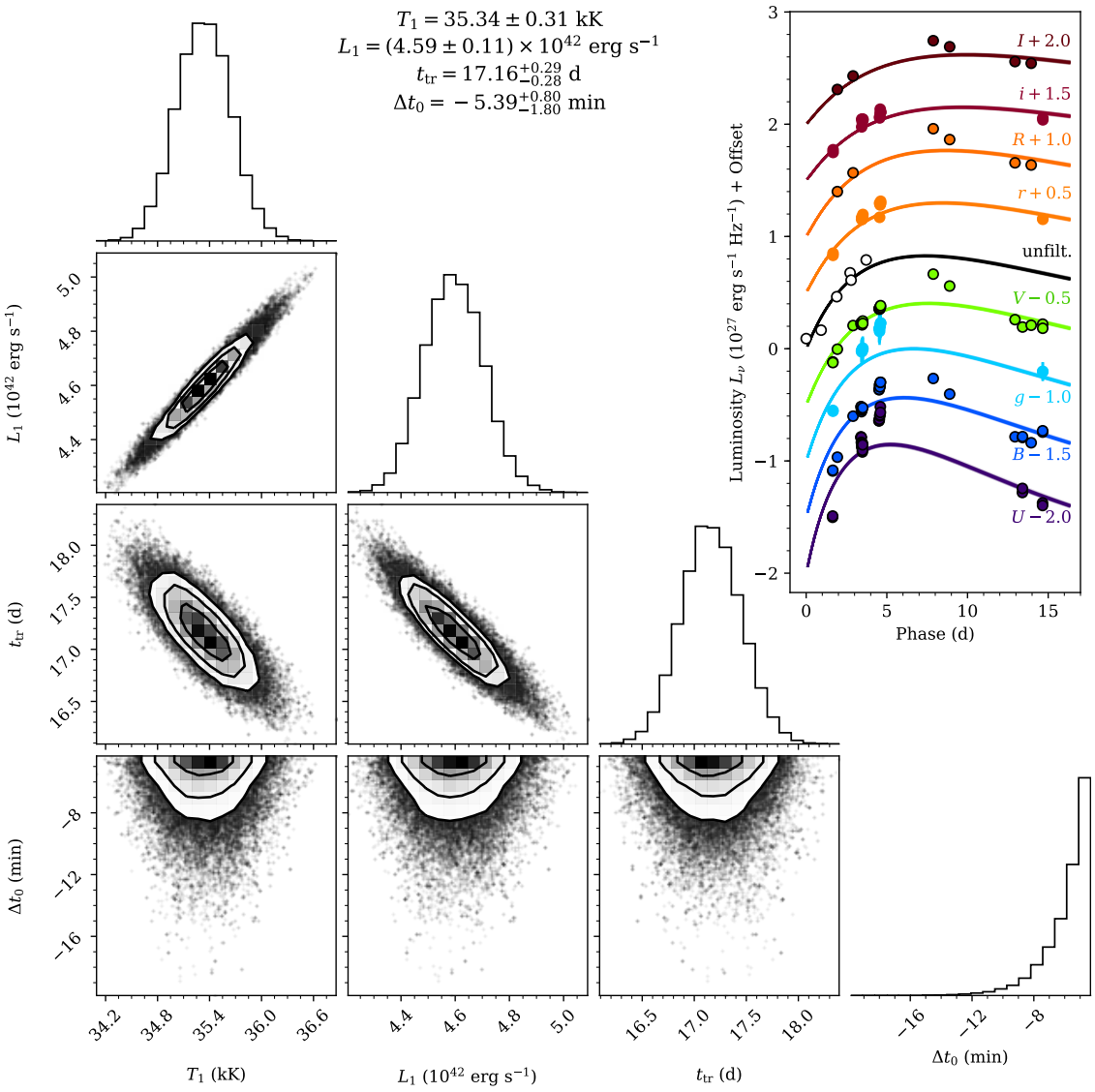

Figure 3.6: Posterior probability distributions of and correlations between the temperature 1 day after explosion (T_1), the total luminosity ≈1 day after explosion (L_1), the time at which the envelope becomes transparent ($t_{\rm tr}$), and the time between explosion and discovery (Δt_0). The 1σ credible intervals centered around the median are given at the top. The top-right panel shows 100 fits randomly drawn from our MCMC routine compared to the data. (The fits appear to be single lines because the spread in the parameters is small.) We do not consider the shock cooling models to be a good fit to the light-curve peak, leaving circumstellar interaction as a possible additional power source.

the initial light-curve peak, but more events with both types of measurements are needed to investigate such a correlation further.

3.4.4 Spectral Modeling

Because of their low photospheric velocities, LL SNe IIP provide a good opportunity to identify which elements contribute to their photospheric spectra. To aid in this identification, we use SYN++ (Thomas et al. 2011) to produce a synthetic spectrum that resembles our observed spectrum from 34.7 days after explosion. We chose this spectrum because it has a high signal-to-noise ratio, and many strong P Cygni lines are visible. Figure 3.7 compares the synthetic and observed spectra. The synthesis parameters are listed in the SYN++ input file, which is available in the online journal.

At this phase, the blue half of the optical spectrum is dominated by iron and titanium lines. These two elements plus calcium, sodium, and hydrogen can account for nearly all of the observed features. The most notable feature of our result is that the range of input velocities necessary to reproduce the observed spectrum is only 100–2000 km s^{-1}. Likewise, the photospheric velocity is 1000 km s^{-1}. Since this is near the resolution of our spectrograph, the true ejecta velocity may be lower. The photospheric temperature of our model is 7500 K, close to the blackbody temperature we calculate for this phase in Section 3.4.2, and the ion temperatures of 10^4 K are reasonable for the interior of the ejecta (although the synthetic spectrum is not very sensitive to these parameters).

Although the line positions match the observed spectrum quite well, a quadratic warping function is necessary to suppress the blue end of the model to match the observations. This function has no physical basis, but deviations from a perfect blackbody continuum with no electron scattering are conceivable. Another possibility is that our spectrograph has lost some of the blue light from the supernova in a way we have not

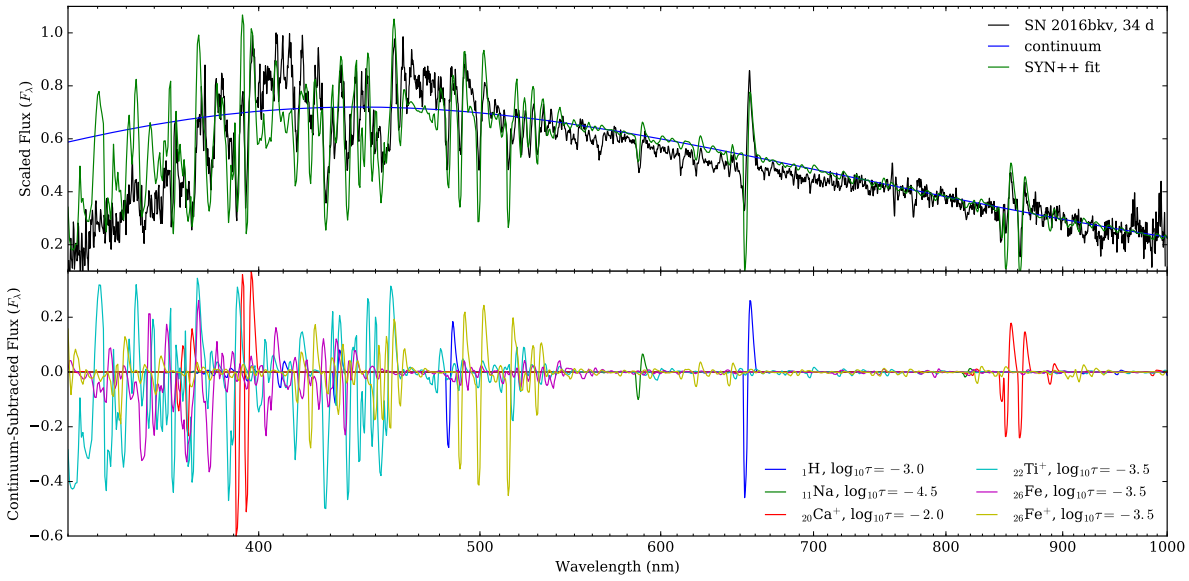

Figure 3.7: SYN++ model for the spectrum of SN 2016bkv 34.7 days after maximum light. The top panel shows the observed spectrum, the assumed continuum (a 7500 K blackbody warped by a quadratic polynomial; see Section 3.4.4), and the total synthetic spectrum (also warped). The bottom panel shows the contributions to the synthetic spectrum of each of the six ions we consider. (The SYN++ input file used to create this figure is available.)

sufficiently accounted for.

3.4.5 Nebular Spectra

Nebular spectra, taken after the ejecta are mostly transparent to optical light, provide several clues about the progenitor structure. We obtained four late-time spectra of SN 2016bkv, from 257 to 607 days after explosion. Because the SN was faint at these phases, the spectra are significantly contaminated by light from the host H II region. No spectrum of this H II region exists, so for each SN spectrum, we simply modeled the continuum using a Gaussian process with a kernel width of 100 nm and subtracted it from the observed spectrum. (Note, however, that this will not remove the contamina-

tion of the hydrogen lines.) We then scaled the result by a constant factor to match an extrapolation of the host-subtracted r- and i-band photometry.

In Figure 3.8, we compare these to the nebular spectral models of Jerkstrand et al. (2018) for a 9 $M_{\odot}$ RSG progenitor. These models were calculated using solar metallicity, which is not necessarily applicable for this H II region, but the literature contains very few other models that are appropriate for LL SNe II (e.g., Lisakov et al. 2017, 2018). The model spectra have been scaled to match the nickel luminosity of SN 2016bkv at the observed phase. Although Jerkstrand et al. do not model an electron-capture supernova, they expect nebular spectra from such an explosion to resemble their "pure hydrogen-zone" model, in which the progenitor is composed entirely of material from the hydrogen envelope (see their Figure 2). Specifically, Mg I], Fe I, [O I], He I, [C I], and O I 777.4 nm would be weaker to nonexistent and O I 844.6 nm would be stronger in the hydrogen-zone model. We plot this zone of the model in blue in Figure 3.8.

There are several discrepancies between the observed spectra and the full model, particularly the absence of observed iron lines, but the agreement between the observed spectra and the hydrogen-zone model is significantly better. As such, we consider the possibility that SN 2016bkv is an electron-capture supernova, although this conclusion is far from certain. An important caveat is that electron-capture supernovae are expected to yield very little radioactive nickel. On one hand, our spectra do not show any unambiguous lines from iron, the decay product of ^{56}Ni, but on the other hand, we inferred an unusually large mass of ^{56}Ni to power the late-phase light curve in Section 3.4.2. Furthermore, Moriya et al. (2014) expect electron-capture supernovae to come from super-asymptotic giant branch stars, in which case they would explode inside denser and more massive wind than we infer here. More observations and further modeling of LL SNe IIP in the nebular phase will be critical to understanding which, if any, supernovae are caused by electron capture.

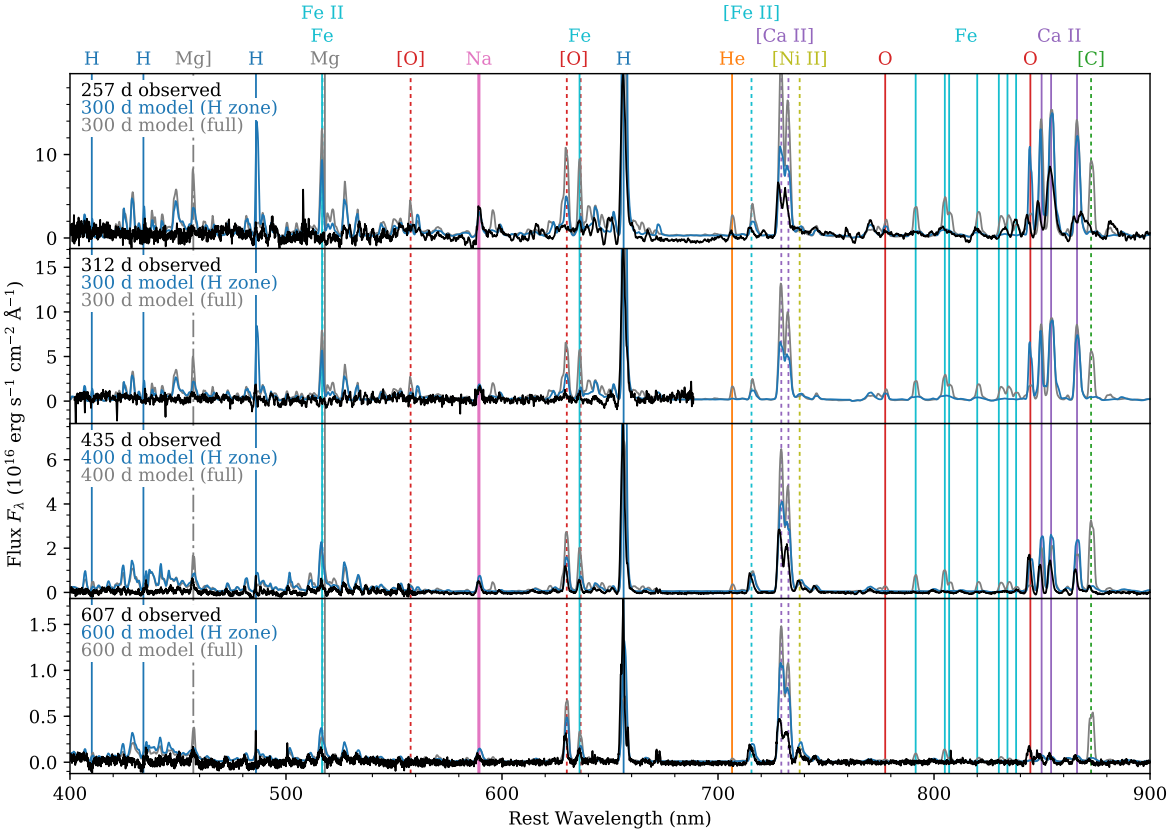

Figure 3.8: Late-time spectra of SN 2016bkv (black) compared to the 9 $M_\odot$ model of Jerkstrand et al. (2018): the full model in gray and hydrogen-zone model in blue. The observed spectra are calibrated to extrapolated r- and i-band photometry, and the model spectra are scaled to match the nickel mass and phase of the observed spectra. The agreement is not perfect, but there is a notable similarity between the observed spectra and the hydrogen-zone model, especially around 400 days. This raises the possibility that SN 2016bkv may be an electron-capture supernova from a low-mass RSG progenitor, although more specific models are required before we can make a firm conclusion.

3.5 Conclusions

Two lines of evidence point to strong but short-lived circumstellar interaction in SN 2016bkv. First, flash spectroscopy during the first five days reveals the presence of material around the progenitor star. A few days later, the light curve shows a strong peak that cannot be fit with the Sapir & Waxman (2017) shock cooling models alone, where the excess could represent luminosity from ejecta-CSM interaction. Even with this strong early peak at $M_V = -16$, SN 2016bkv is the lowest-luminosity supernova to show flash ionization lines, suggesting that late-stage mass loss is common even among LL SN II progenitors.

SN 2016bkv is also exceptional in its short fall from plateau, indicating a large nickel production ($0.022\,M_\odot$) compared to other LL SNe II. Certain emission lines in the nebular spectra of SN 2016bkv hint at the possibility of its being an electron-capture supernova, although we cannot yet definitively distinguish between this case and the traditional iron core-collapse model.

This and other work suggests that analyses of SNe II should be careful to distinguish between the properties of the progenitor star itself and the properties of its circumstellar environment. Peak luminosity, for example, can be strongly affected by circumstellar interaction, whereas luminosity after settling on the plateau may be related to the intrinsic properties of the star. Future data sets like the one presented here, with early and long-term coverage of young supernovae, will allow us to constrain progenitor properties and mass-loss history separately, by comparing to numerical light-curve and spectral models.

Chapter 4

Hydrogen-Poor Interacting (Type Ibn) Supernovae

This chapter is reproduced from Hosseinzadeh et al. (2017z) by permission of the American Astronomical Society. I would like to thank my coauthors, without whom this work would not have been possible: Iair Arcavi, Stefano Valenti, Curtis McCully, D. Andrew Howell, Joel Johansson, Jesper Sollerman, Andrea Pastorello, Stefano Benetti, Yi Cao, S. Bradley Cenko, Kelsey I. Clubb, Alessandra Corsi, Gina Duggan, Nancy Elias-Rosa, Alexei V. Filippenko, Ori D. Fox, Christoffer Fremling, Assaf Horesh, Emir Karamehmetoglu, Mansi Kasliwal, G. H. Marion, Eran Ofek, David Sand, Francesco Taddia, WeiKang Zheng, Morgan Fraser, Avishay Gal-Yam, Cosimo Inserra, Russ Laher, Frank Masci, Umaa Rebbapragada, Stephen Smartt, Ken W. Smith, Mark Sullivan, Jason Surace, and Przemek Woźniak.

4.1 Introduction

Supernovae (SNe) strongly interacting with circumstellar material (CSM) provide a unique window into the final evolutionary stages of certain types of massive ($\gtrsim 8M_{\odot}$) stars. For example, observations of CSM interaction probe a star's composition and mass-loss rate immediately prior to its terminal explosion. This can provide insight into the

state of the progenitor star in ways that are not available for non-interacting supernovae.

Interaction usually manifests itself as narrow emission lines in spectra of the supernova—broader than lines from H II regions in the host galaxy but not as broad as lines produced in the ejecta—indicative of the pre-explosion CSM velocity or of the velocity of CSM accelerated by the interaction. Three major spectral classes have been identified (see Figure 4.1). SNe IIn (Schlegel 1990; Filippenko 1997), the most commonly observed interacting supernovae, are core-collapse explosions of hydrogen-rich massive stars (SNe II) surrounded by hydrogen-rich CSM (Chugai 1991). Type Ia-CSM supernovae, though similar in appearance to SNe IIn, are thought to be the explosions of white dwarfs (SNe Ia) that interact with material stripped from a hydrogen-rich companion (see Silverman et al. 2013 and references therein). Finally, the Type Ibn classification was first proposed by Pastorello et al. (2007) to describe several hydrogen-poor (Type Ib/c) supernovae whose spectra were dominated by relatively narrow ($\sim$ 2000 km s^{-1}) helium features. A few objects with roughly equal-strength narrow hydrogen and helium features have been classified as transitional SNe Ibn/IIn (Pastorello et al. 2008b). In all these cases, interaction also adds extra luminosity to the light curves of these events by converting kinetic energy of the ejected material into radiation, placing interacting supernovae near the boundary of normal supernovae and the so-called superluminous supernovae (Gal-Yam 2012).

Of these classes, only Type IIn supernovae have had direct progenitor detections. The first such case was for SN 2005gl, which Gal-Yam & Leonard (2009) reported to be an explosion of a luminous blue variable (LBV) star, a class of objects known to undergo episodic mass loss. LBV progenitors were later suggested for Type IIn SNe 2009ip and 2010jl as well (Smith et al. 2010b,a; Foley et al. 2011; Fox et al. 2017), although there is still no consensus that the former was a genuine supernova. Detections of pre-explosion variability at the locations of other Type IIn supernovae, indicative of eruptions or outbursts (e.g., Mauerhan et al. 2013; Ofek et al. 2013, 2014), further support this scenario.

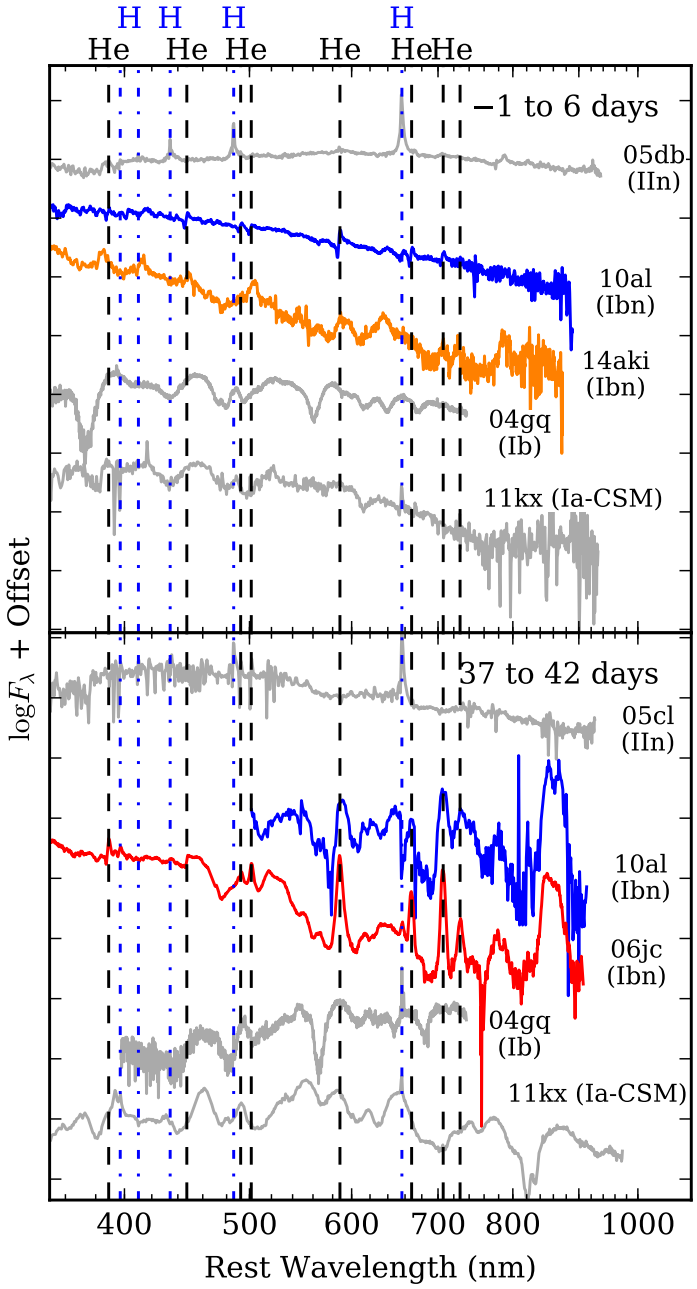

Figure 4.1: Representative spectra of SNe Ibn compared to those of Type IIn, Type Ib, and Type Ia-CSM supernovae. The upper panel shows spectra near maximum light, while the lower panel shows spectra more than one month later. Spectra of SNe 2005cl and 2005db are from Kiewe et al. (2012). Spectra of SN 2010al are from Pastorello et al. (2015a). The spectrum of SN 2006jc is from Pastorello et al. (2007). Spectra of SN 2004gq are from Modjaz et al. (2014). Spectra of PTF11kx are from Dilday et al. (2012).

SNe Ibn, on the other hand, have only indirect progenitor evidence. One popular narrative, first put forward by Pastorello et al. (2007), is that these supernovae are the core-collapse explosions of very massive Wolf–Rayet (WR) stars embedded in helium-rich CSM. WR atmospheres are nearly hydrogen-free, and their strong winds could eject material at velocities consistent with the widths of the relatively narrow lines observed in SNe Ibn (1000–2000 km s^{-1}; see review by Crowther 2007). Alternatively, Type Ibn progenitors could be members of massive binaries, in which CSM is produced by stripping material from the envelopes of one or both stars (Foley et al. 2007). We discuss possible progenitor channels for SNe Ibn in more detail in Section 4.5.

The best-studied SN Ibn is SN 2006jc (Foley et al. 2007; Pastorello et al. 2007, 2008a; Immler et al. 2008; Smith et al. 2008), discovered by Nakano et al. (2006) in the relatively nearby ($z = 0.006$) galaxy UGC 4904. Nakano et al. (2006) noted the detection of an optical transient at the coordinates of the supernova two years before the final explosion, as seen in some Type IIn supernovae. This was seen as evidence for unstable mass loss from a WR progenitor, although no such outbursts have ever been seen from a known WR star (Pastorello et al. 2007). Unfortunately, the light curve of SN 2006jc was already declining at the time of discovery, so we do not have data from immediately after explosion.

However, not all evidence points to a massive progenitor. PS1-12sk, for example, was a SN Ibn with spectra nearly identical to those of SN 2006jc that exploded in an apparently non-star-forming host (Sanders et al. 2013). Given the extremely low fraction of core-collapse supernovae that occurs in elliptical galaxies ($\lesssim 0.2\%$; Hakobyan et al. 2012), observing one out of fewer than two dozen SNe Ibn with an elliptical host is unlikely by chance, calling into question whether these are truly explosions of massive stars. Sanders et al. (2013), for example, suggest several degenerate progenitor scenarios for SNe Ibn.

One way to distinguish between the various progenitor scenarios is to obtain a large sample of well-observed events, both photometrically and spectroscopically. Unfortunately, many events, especially those discovered prior to 2010, do not have well-observed light curves and spectral series. In the most comprehensive study to date, Pastorello et al. (2016) point out that the Type Ibn class, defined by their spectra, include some light curve outliers. OGLE-2012-SN-006 (hereinafter OGLE12-006), for example, has a very slow decline, whereas LSQ13ccw has a very fast decline and an unusually faint peak magnitude. SNe 2005la and 2011hw, both transitional Type Ibn/IIn events, as well as iPTF13beo, have double-peaked light curves. SN 2010al, still the earliest observed SN Ibn relative to maximum light, had an unprecedented premaximum spectrum and an unusually slow rise. However, we show below that Type Ibn light curves, when taken as a whole, are much more homogeneous and faster evolving than their Type IIn counterparts.

Here we present photometry and spectroscopy for six new SNe Ibn: PTF11rfh, PTF12ldy, iPTF14aki, iPTF15ul, SN 2015G, and iPTF15akq. With the addition of these objects, the sample size of SNe Ibn with published data increases to 22. We also present new data for SN 2015U, previously discussed by Tsvetkov et al. (2015), Pastorello et al. (2015b), and Shivvers et al. (2016). We then examine light curves and spectra of objects in this sample to infer the properties of the class as a whole. Finally, we discuss the implications of these findings for possible progenitors.

Throughout this paper, times are given as dates in coordinated universal time (UTC) or as modified Julian dates (MJD). "Phase" denotes days since maximum light, in the r- or R-band where available, in the rest frame of the supernova.

PTF11rfh and PTF12ldy were discovered by the Palomar Transient Factory (PTF; Law et al. 2009; Rau et al. 2009) on 2011 December 8 and 2012 November 12, respectively. iPTF14aki, iPTF15ul, and iPTF15akq were discovered by the Intermediate Palomar Transient Factory (iPTF; Kulkarni 2013) on 2014 April 10, 2015 March 10, and

2015 April 17, respectively. iPTF14aki was independently discovered by the Catalina Real-Time Transient Survey (Drake et al. 2009) on 2014 April 21, given the name CSS140421:142042+031602, and classified by the Public ESO Spectroscopic Survey of Transient Objects (PESSTO; Polshaw et al. 2014; Smartt et al. 2015). SN 2015U was discovered by the Lick Observatory Supernova Search (Filippenko et al. 2001; Kumar et al. 2015) on 2015 February 13 and classified by Polshaw et al. (2014). SN 2015G was discovered by Kunihiro Shima on 2015 March 23 (Yusa et al. 2015) and classified by Foley et al. (2015).

Multiband optical photometry was obtained using the Catalina Sky Survey (CSS; Drake et al. 2009) telescope at Steward Observatory (AZ, USA), the 0.76 m Katzman Automatic Imaging Telescope (KAIT; Filippenko et al. 2001) at Lick Observatory (CA, USA), the 1 m and 2 m telescopes of the Las Cumbres Observatory Global Telescope Network (LCOGT; Brown et al. 2013), the Nordic Optical Telescope (NOT) at the Observatorio del Roque de los Muchachos (ORM; Canary Islands, Spain), the New Technology Telescope (NTT) at La Silla Observatory (Coquimbo Region, Chile), the 48 inch (1.2 m) Samuel Oschin Telescope (P48) and the 60 inch (1.5 m) telescope (P60; Cenko et al. 2006) at Palomar Observatory (California, USA). Ultraviolet photometry was obtained with the Ultra-Violet/Optical Telescope (UVOT; Roming et al. 2005) on board the *Swift* satellite.

Each photometry point is plotted in Figure 4.2. All upper limits reported in the tables and figures are 3σ nondetections. *Swift* magnitudes are in the UVOT system (Poole et al. 2007). All other magnitudes are in the Vega system for $UBVRI$ points and in the AB system for $ugriz$ points. (Note that P48 uses a Mould R filter.) See Appendix A.1 of Hosseinzadeh et al. (2017z) for details on the reduction process for photometry.

After calibration, apparent magnitudes were corrected for Milky Way extinction according to the dust maps of Schlafly & Finkbeiner (2011), obtained via the NASA/IPAC

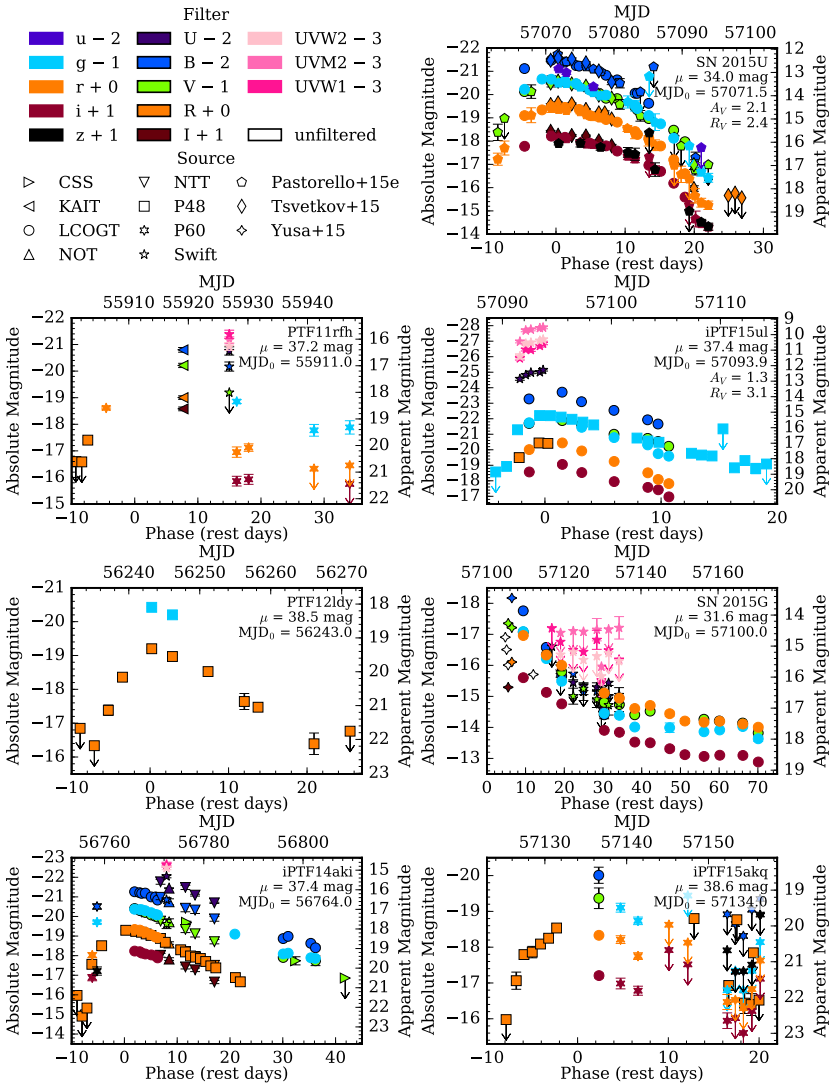

Figure 4.2: Light curves of PTF11rfh, PTF12ldy, iPTF14aki, SN 2015U, iPTF15ul, SN 2015G, and iPTF15akq. Marker shape denotes the source of the photometry (acronyms are defined in the text), and marker color denotes the filter band. Downward-pointing arrows mark 3σ nondetection upper limits. The right axis for each frame gives the *extinction-corrected* (including host extinction, if A_V and R_V are given) apparent magnitudes in the UVOT system for *Swift* points, in the Vega system for other $UBVRI$ points, and in the AB system for $ugriz$ points. The left axis gives the absolute magnitude assuming the distance modulus (μ) given at the top right of each panel. The bottom axis shows rest-frame days from the estimated peak date (MJD_0). For SN 2015U, the photometry published by Tsvetkov et al. (2015) and Pastorello et al. (2015b) is plotted for comparison. For SN 2015G, photometry from the discovery CBET (Yusa et al. 2015) is plotted for comparison.

Extragalactic Database (NED). SN 2015U and iPTF15ul were also corrected for their high host-galaxy extinction using the extinction law of Cardelli et al. (1989) with the best-fit parameters derived in Section 4.2. Absolute magnitudes were obtained using the distance moduli calculated from host-galaxy redshifts, if available, or redshifts obtained from the supernova spectra, and the cosmological parameters presented by the Planck Collaboration (2016). None of the mean redshift-independent distance moduli listed on NED for these objects are more than 3σ away from the values used here.

For iPTF14aki, two epochs of near-infrared photometry were obtained with the Near Infrared Camera Spectrometer (NICS) on the Telescopio Nazionale Galileo (TNG) at ORM. Magnitudes were measured using aperture photometry and calibrated to nearby stars in the 2MASS catalog (Skrutskie et al. 2006). We only detect the supernova at $> 3\sigma$ significance in the J-band: MJD 56779.9, $J = 18.4 \pm 0.2$ mag, $H > 18.9$ mag, $K_s > 18.9$ mag; MJD 56794.1, $J = 19.4 \pm 0.2$ mag, $H > 18.7$ mag, $K_s > 18.0$ mag.

We also observed PTF11rfh, along with the necessary calibrators, with the Karl G. Jansky Very Large Array (VLA; Perley et al. 2009) under our Target of Opportunity program (VLA/11A-227; PI: A. Corsi) on 2011 December 31.8 with the VLA in its D configuration. VLA data were reduced and imaged using the Common Astronomy Software Applications (CASA) package (McMullin et al. 2007). Our observation yielded a nondetection, with a 3σ upper limit of $\lesssim 81\,\mu$Jy at 6.4 GHz.

Optical spectra were obtained using the Andalucia Faint Object Spectrograph and Camera (ALFOSC) on NOT; the Double Spectrograph (DBSP; Oke & Gunn 1982) on the 200 inch (5.1 m) Hale Telescope (P200) at Palomar Observatory; the Double Imaging Spectrograph (DIS) on the Apache Research Consortium (ARC) 3.5 m telescope at Apache Point Observatory (NM, USA); the Device Optimized for the Low Resolution (DOLORES) on TNG; the ESO Faint Object Spectrograph and Camera (EFOSC2) on NTT; the FLOYDS robotic spectrographs on the LCOGT 2 m telescopes at Haleakalā

Observatory (HI, USA) and Siding Spring Observatory (New South Wales, Australia); the Kast Double Spectrograph on the 3 m C. Donald Shane Telescope at Lick Observatory; and the Low-Resolution Imaging Spectrometer (LRIS; Oke et al. 1995) on the Keck I telescope, the Deep Imaging Multi-Object Spectrograph (DEIMOS; Faber et al. 2003) on the Keck II telescope, and the Gemini Multi-Object Spectrograph (GMOS; Hook et al. 2004) on the Frederick C. Gillett Gemini North telescope, all on Mauna Kea (HI, USA). The near-infrared spectrum of SN 2015U was obtained with the SpeX instrument (Rayner et al. 2003) at the NASA Infrared Telescope Facility (IRTF), also on Mauna Kea.

Each spectrum is plotted in Figures 4.3–4.6. They are not corrected for reddening. See Appendix A.2 of Hosseinzadeh et al. (2017z) for details on the reduction process for spectroscopy. All spectra presented here have been submitted to the Weizmann Interactive Supernova Data Repository (WISeREP; Yaron & Gal-Yam 2012).

4.2 Extinction Estimation

As first noted by Ochner et al. (2015), SN 2015U suffers from significant host-galaxy extinction. The extinction parameters, parametrized using the extinction law of Cardelli et al. (1989 hereafter CCM89) have been estimated previously by at least two groups: Pastorello et al. (2015b) estimate $E(B-V) = 0.99 \pm 0.48$ mag assuming a fixed $R_V = 3.1$, and Shivvers et al. (2016) estimate $E(B-V) = 0.94^{+0.1}_{-0.4}$ mag for $R_V = 2.1$ by fitting reddened blackbody models to photometry of SN 2015U.

We compare our optical through near-infrared spectrum of SN 2015U at +5 days to broadband photometry and spectra of SN 2010al around the same phase. This yields a best-fit extinction law with $E(B-V) = 0.86 \pm 0.10$ mag and $R_V = 2.4 \pm 0.2$ (as parametrized by CCM89). Figure 4.5 shows a reddened optical–near-infrared spectrum

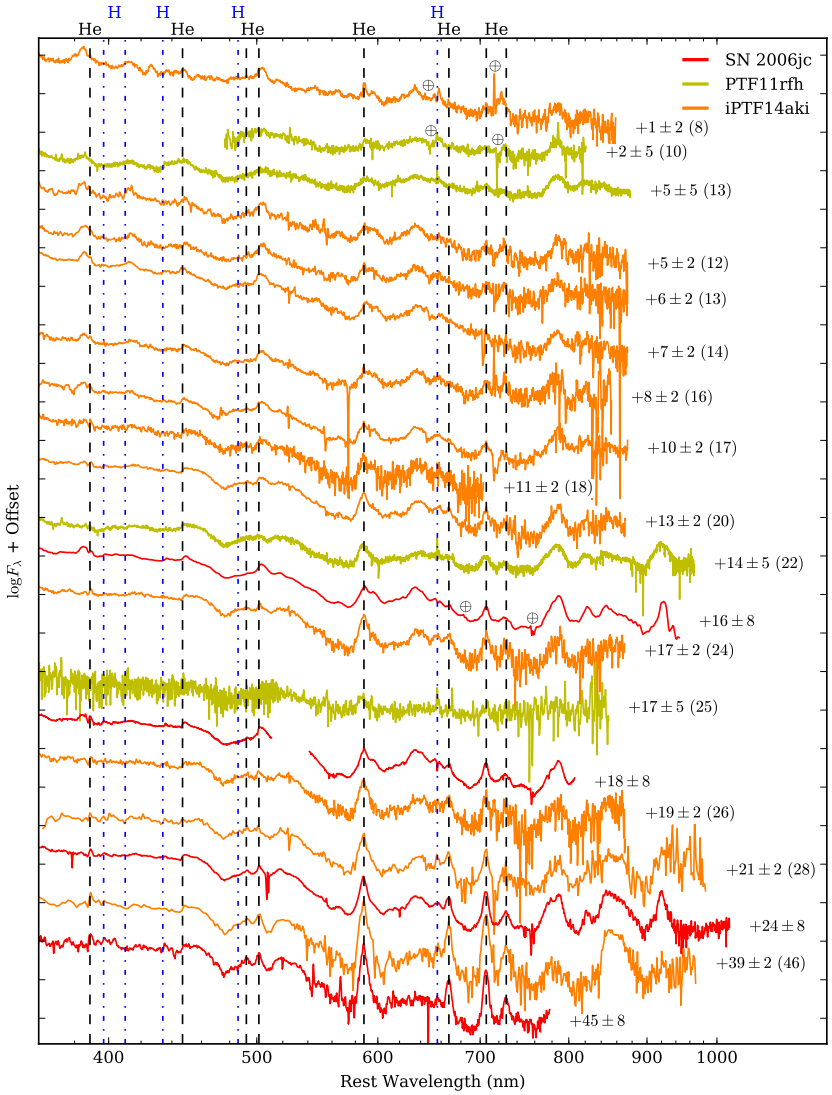

Figure 4.3: Combined spectral series of PTF11rfh and iPTF14aki with representative spectra of SN 2006jc for comparison. Phase is indicated to the right of each spectrum, with rest-frame days from explosion in parentheses, where available. Vertical lines mark emission wavelengths of various elements, listed along the top axis. The Earth symbol (⊕) marks wavelengths affected by telluric absorption once for each supernova. Tick marks on the vertical axes are 0.5 dex apart. Note the similarity between these three objects and the contrast with the early spectra in Figure 4.4.

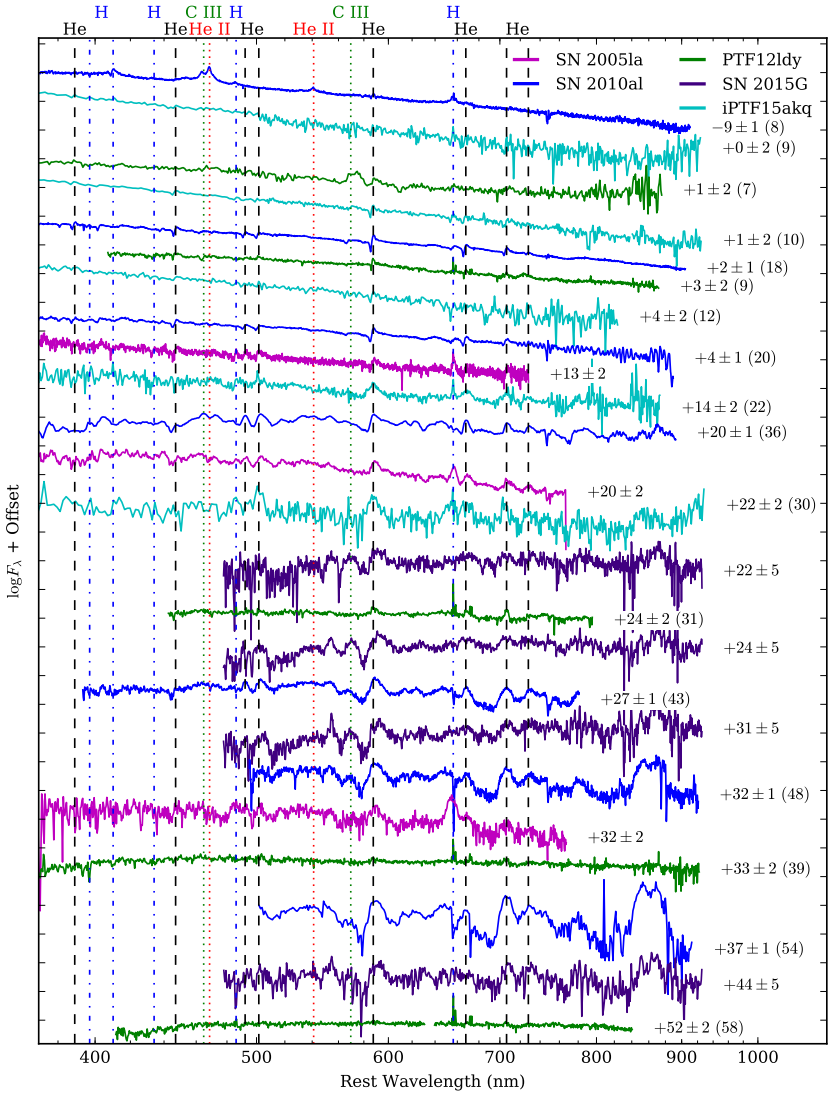

Figure 4.4: Combined spectral series of PTF12ldy, SN 2015G, and iPTF15akq, with representative spectra of SNe 2005la and 2010al for comparison. SN 2005la and iPTF15akq are transitional Ibn/IIn supernovae, meaning their spectra show relatively strong hydrogen features. Phase is indicated to the right of each spectrum, with rest-frame days from explosion in parentheses, where available. Vertical lines mark emission wavelengths of various elements, listed along the top axis. Tick marks on the vertical axes are 0.5 dex apart. Note the similarity between these objects and contrast with the early spectra in Figure 4.3. Also note the detection of C III in the first spectrum of PTF12ldy.

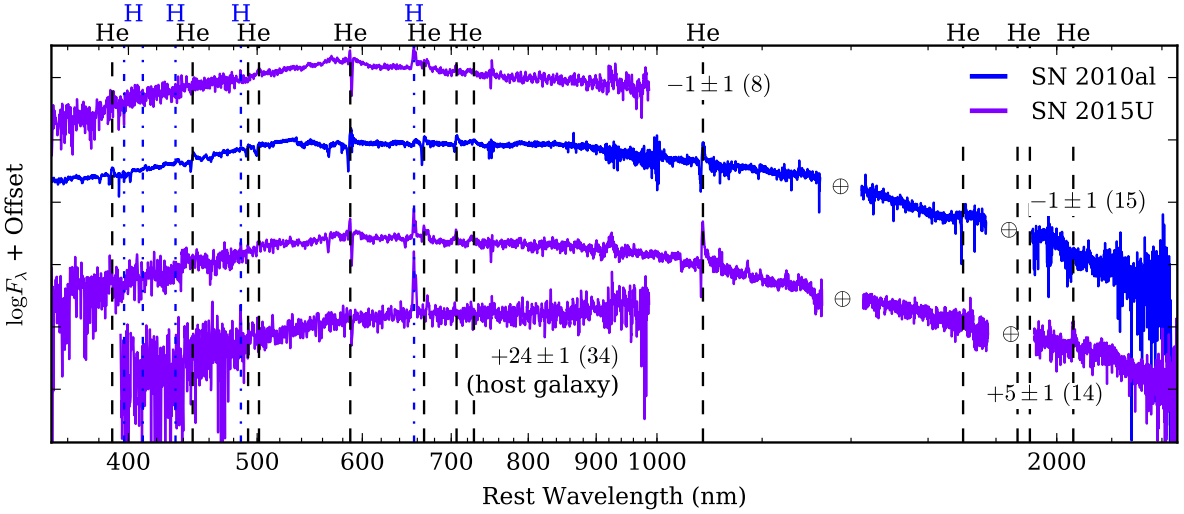

Figure 4.5: Spectra of the highly reddened SN 2015U with an optical through near-infrared spectrum of SN 2010al for comparison. The spectrum of SN 2010al has been reddened using the best-fit parameters for SN 2015U, $A_V = 2.06$ mag and $R_V = 2.4$ (as parametrized by CCM89). Phase is indicated near the right of each spectrum, with rest-frame days from explosion in parentheses. The spectrum from +5 days is a combination of an optical spectrum (range 320–900 nm; resolution 0.2 nm) from FLOYDS and a near-infrared spectrum (range 850–2500 nm; resolution 0.3 nm) from SpeX taken several hours apart. The host-dominated spectrum from +24 days is shown in order to identify host lines in the earlier spectra. Vertical lines mark emission wavelengths of various elements, listed along the top axis. The Earth symbol (⊕) marks regions trimmed to remove telluric contamination. Tick marks on the vertical axes are 0.5 dex apart. The P Cygni profile of the 1083 nm helium line links this to the subclass of objects in Figure 4.4.

of SN 2010al (from Pastorello et al. 2015a) at −1 day to match the observed continuum shape of SN 2015U.

We performed a similar analysis comparing iPTF15ul to SN 2000er. Lacking near-infrared data for iPTF15ul, we do not attempt to fit the total-to-selective extinction ratio, R_V. The resulting best-fit extinction parameters are $E(B-V) = 0.41 \pm 0.10$ mag with $R_V = 3.1$. This is illustrated in Figure 4.6, where we show a reddened spectrum of SN 2000er (from Pastorello et al. 2008a) together with the observed spectra of iPTF15ul.

This method assumes that SN 2015U and iPTF15ul follow a similar color evolution to SNe 2010al and 2000er, respectively. Under this assumption, our extinction estimate

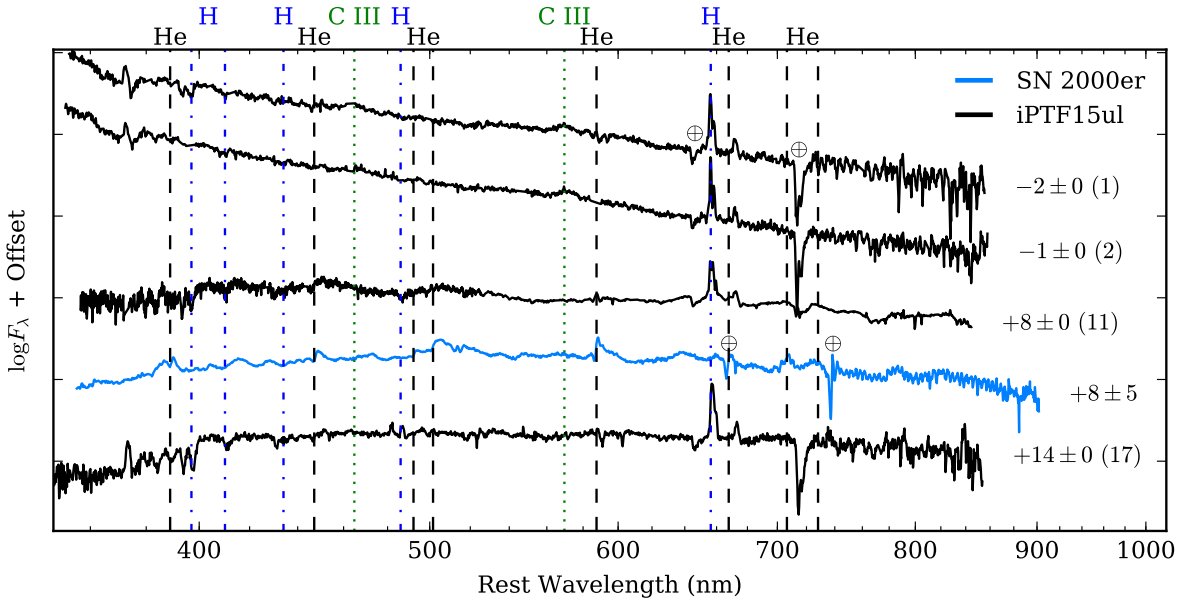

Figure 4.6: Spectra of iPTF15ul with a spectrum of SN 2000er for comparison. The spectrum of SN 2000er has been reddened using the best-fit parameters for iPTF15ul, $A_V = 1.27$ mag and $R_V = 3.1$ (as parametrized by CCM89). Phase is indicated near the right of each spectrum, with rest-frame days from explosion in parentheses, where available. Vertical lines mark emission wavelengths of various elements, listed along the top axis. The Earth symbol (⊕) marks features affected by telluric absorption. Tick marks on the vertical axes are 0.5 dex apart. Host contamination of iPTF15ul makes it difficult to identify features, but its spectral similarity with SN 2000er allows us to classify it as a SN Ibn. Also note the detection of C III in the premaximum spectra of iPTF15ul.

($A_R = 1.07 \pm 0.26$ mag) makes iPTF15ul the most luminous SN Ibn studied so far ($M_R = -20.64 \pm 0.29$ mag). However, given the small number of SNe Ibn with well-sampled multicolor light curves, our result should be treated with some caution.

We assume negligible host-galaxy extinction for the other five supernovae discussed here, as they are either well separated from their host galaxies or their hosts are relatively faint. The continuum shapes of their early spectra support this assumption.

4.3 Sample Analysis

4.3.1 Spectroscopy

In order to compare the spectral evolution of the objects in our sample, we collected all publicly available optical spectra of each object from WISeREP and added them to the spectra plotted in Figures 4.3–4.6.

Qualitative Classification

To begin, we examine the spectral series of all the objects in our sample. We find that, at early times ($\lesssim$ 20 days after peak), the spectra show some diversity in their helium line profiles. While all Type Ibn spectra have blue continua relative to most other supernova classes (after considering extinction and host contamination), some show only relatively narrow (1000 km s^{-1}) P Cygni lines of helium, while others exhibit narrow to intermediate-width (few thousand km s^{-1}) helium emission lines and broad features, sometimes with complex profiles. The latter are most similar to the earliest spectra of the traditional Type Ibn archetype, SN 2006jc, which unfortunately was not observed around maximum light.

At late times ($\gtrsim$ 20 days), the absorption components of the P Cygni lines become less pronounced and their velocities increase, making the two types of spectra less distinguishable. This means that early spectra of SNe Ibn may not look like those of the archetype SN 2006jc, similarity to which is often used as a basis for classification, although they will likely resemble it at later times. Early spectral time series will be essential to understanding this spectral diversity.[1]

[1]This represents a more general problem in supernova classification: classifications are usually announced after the first spectrum is obtained and not revised (at least not publicly) based on subsequent spectra. This can lead to misclassifications for several types of supernovae (e.g., Type II instead of Type IIb).

Until recently, all SNe Ibn in the literature observed prior to 12 days after peak showed P Cygni lines in their earliest spectra. However, spectra of PTF11rfh and iPTF14aki, although they resemble other SNe Ibn at late times, do not show P Cygni lines at early times. This confirms that Type Ibn spectra can have at least two morphologies during the first week after maximum light (see Figure 4.7).

With our current sparsely sampled, heterogeneous spectral data set, we cannot conclusively say whether these two morphologies arise from two distinct CSM configurations or from a continuum of CSM properties. A few supernovae do hint at a continuum of line profiles. For example, SNe 2014av and 2014bk both have dominant P Cygni lines at early times, but these lines are superimposed on broader emission features, not just blue continua. Weaker P Cygni lines are also superimposed on some emission-dominated spectra, such as those of SN 2006jc, PS1-12sk, and iPTF14aki. Nonetheless, for the purposes of this analysis, we will describe spectra as belonging to one of two different subclasses: the "P Cygni" subclass or the "emission" subclass.

Furthermore, we admit that a more physical analysis might group spectra by phase relative to explosion, rather than phase relative to maximum light, but weak constraints on the explosion times for many objects in our sample prevent this. It remains to be seen whether the spectral diversity would persist in such an analysis.

Since iPTF15akq and SNe 2005la and 2011hw exhibit relatively strong hydrogen features throughout their evolution, leading to their transitional classification as Type Ibn/IIn, it is not clear whether they belong in either of the two proposed classes. Nonetheless, with the exception of the hydrogen lines, their spectra are quite similar to those of other SNe Ibn, so we group them by line profile as well.

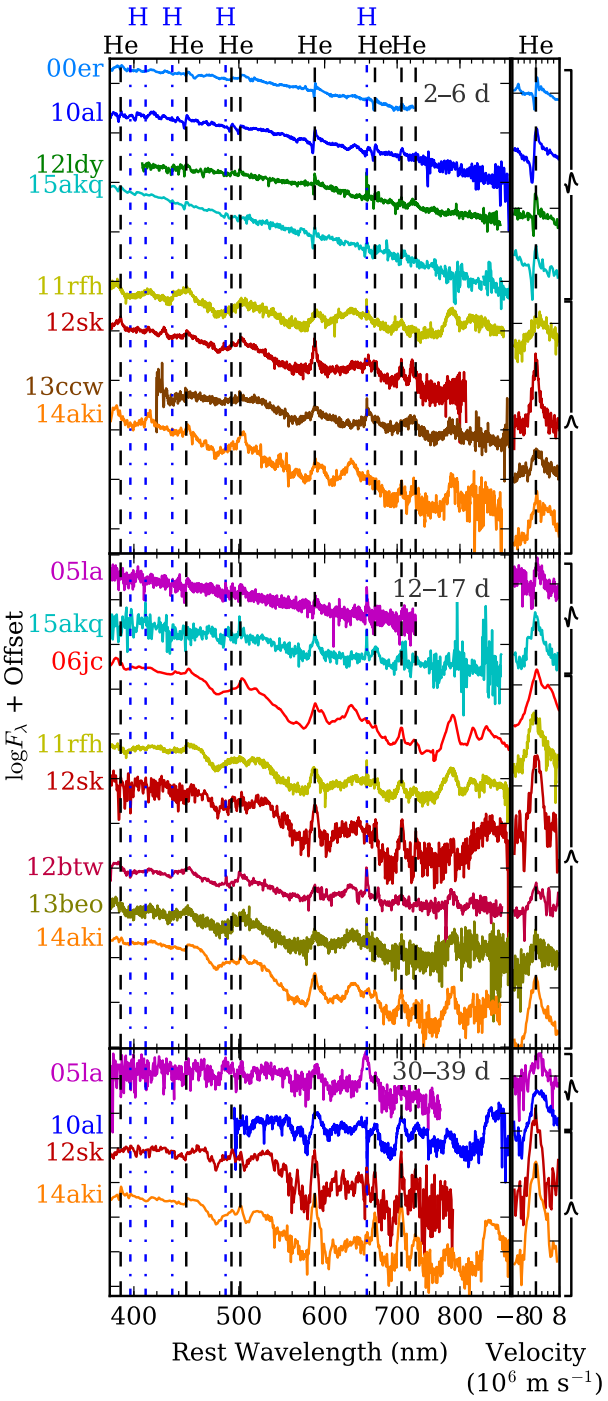

Figure 4.7: Spectra of SNe Ibn at three phase ranges. Individual supernovae are color-coded throughout this work (see legend in Figure 4.8 for full names): cool colors for the P Cygni subclass (top of each panel) and warm colors for the emission subclass (bottom of each panel). The column at right shows an expanded view of the helium emission line at 588 nm for each spectrum. Note the relative homogeneity within each subclass and the distinct difference between subclasses at early times ($\lesssim$ 20 days after peak). The distinction fades over the course of the first month.

Line Analysis

Of particular interest is the tentative detection of doubly ionized carbon (C III) at 465.0 and 569.6 nm in the earliest spectra of PTF12ldy (Figure 4.4) and iPTF15ul (Figure 4.6). C III has only appeared once before in a SN Ibn, in the earliest spectrum ever obtained of this class: that of SN 2010al nine days before maximum light (first spectrum in Figure 4.4). In that case, it appeared alongside other high-ionization species (N III and He II), which Pastorello et al. (2015a) interpreted as a sign of the flash-ionization of the CSM (as in Gal-Yam et al. 2014). To our knowledge, the spectrum of iPTF15ul is the third earliest (relative to peak) Type Ibn spectrum obtained, suggesting that these lines may still be C III recombining after shock breakout. We note, however, that the spectrum of SN 2010al showed only the 465.0 nm line, whereas the 569.6 nm lines in our spectra are stronger, possibly calling into question our tentative identification. Si II could be contributing at 567.0 nm, but we cannot identify any other Si II features. Although the features are relatively weak, they are notably broader than the narrow P Cygni lines that develop around maximum light. This may be caused by electron scattering (also as in Gal-Yam et al. 2014).

For each spectrum in our sample, we measure the expansion velocities and equivalent widths (EWs) of three neutral helium (He) lines (588, 668, and 707 nm) and hydrogen-α (Hα, 656 nm), where visible. The results are plotted in Figure 4.8.

Especially at late times, it is not trivial to distinguish broad P Cygni features on a blue continuum and broad emission on a flat continuum. We treat more symmetric lines as emission only (filled markers in Figure 4.8) and more asymmetric lines as P Cygni (open markers). For simplicity, we do not treat lines with multiple velocity components differently.

We fit emission lines with a Gaussian function on a constant or linear continuum

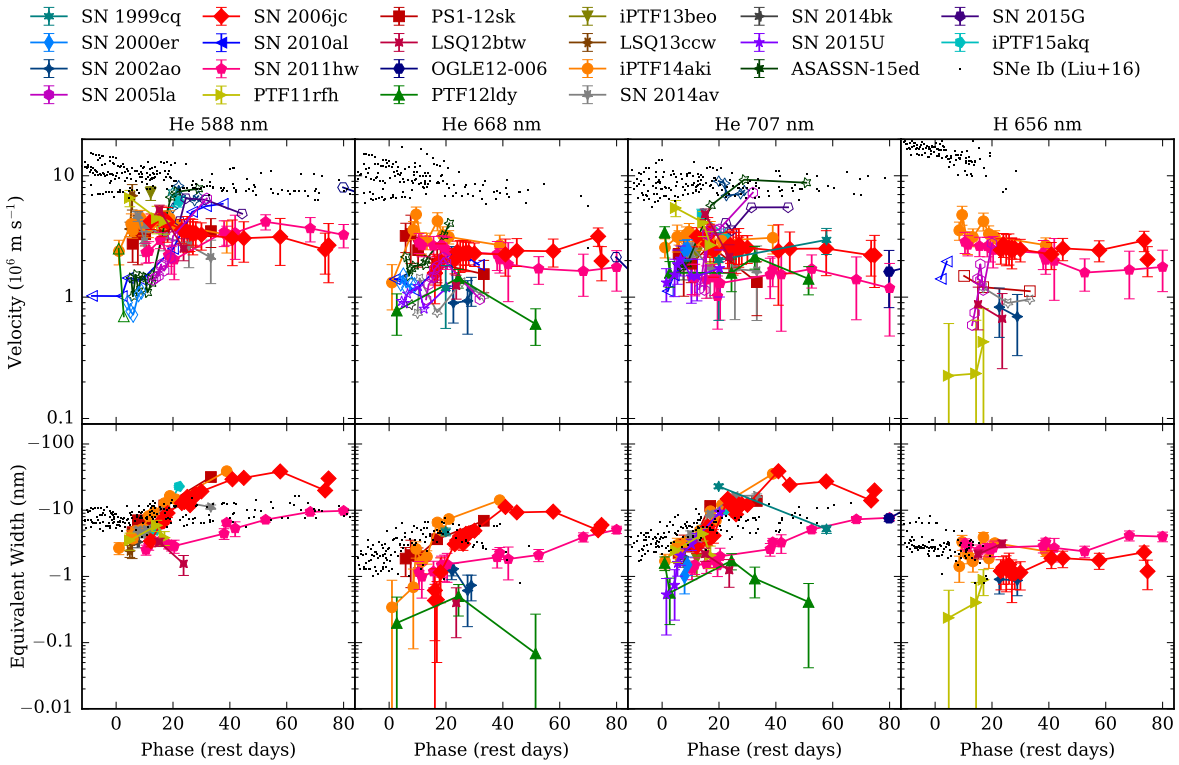

Figure 4.8: Top: velocity evolution of various spectral lines by object. Filled markers indicate pure emission lines, in which case the quoted velocity is the FWHM of the line. Open markers represent lines with P Cygni profiles, in which case the velocity comes from the absorption minimum. The increasing trend for P Cygni velocities likely does not mean the material is accelerating. Rather, at early times, we only see a slow-moving, optically thick CSM shell. As this shell becomes optically thin, we are increasingly able to see the faster-moving supernova ejecta. Otherwise, flat velocity curves simply suggest supernova ejecta in free expansion. Black dots represent absorption velocities of the Liu et al. (2016) sample of SNe Ib for comparison. Bottom: equivalent width (EW) evolution of various spectral lines by object. Only emission lines are shown. The upward trend in the helium lines suggests that circumstellar helium is being swept up by the ejecta. Black dots represent EWs of helium absorption in SNe Ib, also from Liu et al. (2016).

(depending on the object and the line) using a Markov chain Monte Carlo (MCMC) routine based on the `emcee` package (Foreman-Mackey et al. 2013). The velocity reported is derived from the FWHM intensity of the Gaussian. The EW is the integral of the flux normalized to the local continuum, which may or may not be constant over the width of the line. In cases where a nearby line might interfere with the measurement, we fit and subtract an additional Gaussian to the second line prior to integration.

We fit P Cygni lines with two Gaussians, one in absorption and one in emission, using the same MCMC routine. The velocity reported is derived from the wavelength difference between absorption and emission. We do not measure EW for P Cygni lines.

If the line is not clearly identifiable and visible above the noise, or if the width of the line is potentially unresolved by the spectrograph, we do not attempt a measurement. However, since the decision of whether or not to measure is based on a visual inspection, some misidentified lines may be included, and conversely some ambiguous lines may be omitted.

Error bars correspond to standard deviations of the fit-parameter distributions from the MCMC routine. They do not include systematic errors such as choosing the wrong line profile, ignoring multiple velocity components, etc.

Within each of the two spectral subclasses, especially within the emission subclass, there is very little variation in spectral evolution between objects. In most cases we see a general increasing trend in the helium EW, whereas the Hα EW, if present at all, stays roughly constant. Line velocities of the emission spectra show little evolution over time. On the other hand, P Cygni lines visible in early spectra tend to morph into broader emission-dominated lines over the course of the first month. We discuss the implications of these results in Section 4.5.

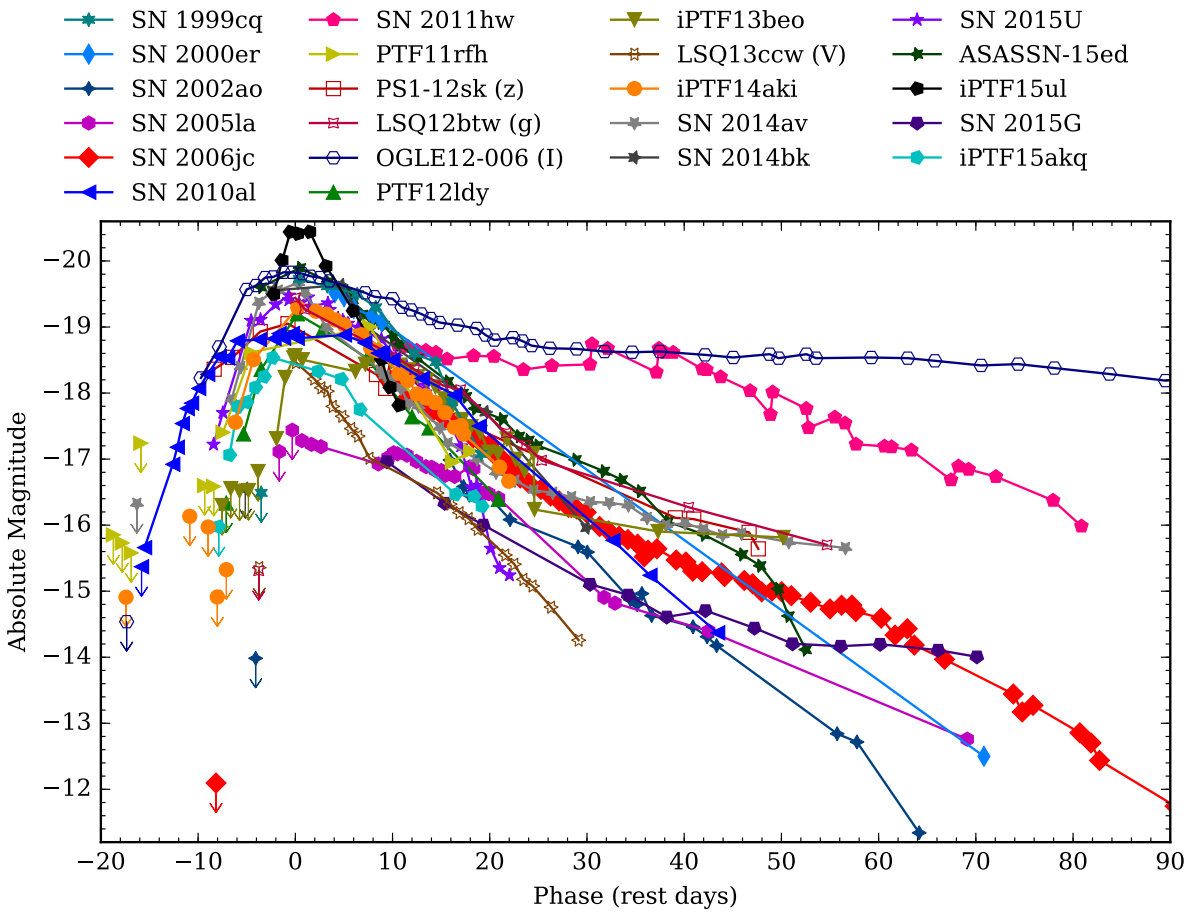

Figure 4.9: Rest-frame light curves used in the sample analysis. The R- or r- band was chosen unless a different filter had significantly better coverage, in which case an open marker is used and the filter is listed in parentheses. Note the homogeneity in light curve shape, even between subclasses, with a few significant exceptions.

4.3.2 Photometry

We obtained all published light curves of SNe Ibn from the literature. Most, but not all, objects have well-observed R- or r-band light curves, which we plot in Figure 4.9. Where this was not the case, we used light curves in a better-observed filter and noted this next to the supernova name in Figure 4.9. Although supernovae do not always have the same behavior in all filters, we assume that these differences are small compared to the uncertainties involved in our estimates below. We also do not apply K-corrections

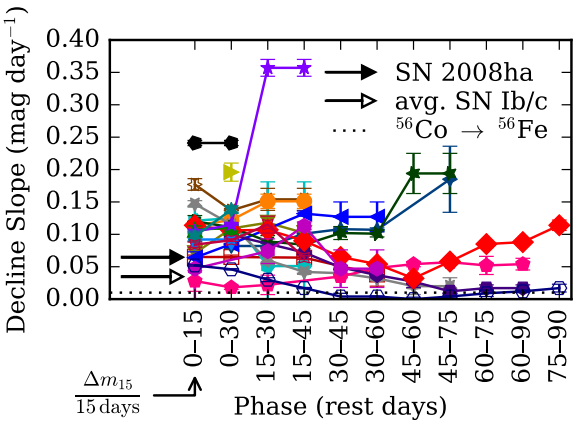

Figure 4.10: Slopes of the post-maximum light curves. Three comparisons are provided: $\Delta m_{15}(R) = 0.97$ for the 02cx-like SN 2008ha (Foley et al. 2009 black arrow), the weighted average $\Delta m_{15}(r') = 0.52$ mag of the stripped-envelope supernovae in Bianco et al. (2014 white arrow), and the ^{56}Co to ^{56}Fe decay rate (0.01 mag day^{-1}, dashed line). Note the clustering around 0.10 mag day^{-1} during the first month after peak, faster than all the comparisons. This may suggest that SNe Ibn are powered by a short period of circumstellar interaction and/or that their ^{56}Ni production and explosion energy are smaller than those of other hydrogen-poor supernovae (Moriya & Maeda 2016 but see Section 4.3.2).

to the light curves, for the same reason.

Several of the parameters we wish to explore depend on the determination of the time of maximum light of the supernovae, but unfortunately, over half of the objects have few or no points in their light curve around peak brightness. SN 2005la, SN 2011hw, and iPTF13beo have two peaks; in what follows, we consider only the first peak.

Decline Slope and Peak Magnitude

With an estimate of the epoch of maximum light of each supernova, we can determine the slope of the post-maximum decline. We divide the rest-frame light curve into six 15 day bins, starting with 0–15 days after peak, and five overlapping 30 day bins, starting with 0–30 days after peak. For each of these bins that includes three or more photometry points, we use weighted least-squares regression to determine a best-fit line (magnitude vs. phase) to that portion of the light curve. This effectively gives a coarse derivative of the data without fitting a function to the entire light curve. The slopes of these lines are plotted against the centers of their bins in Figure 4.10.

Most supernovae have several-day errors on the peak date, which in theory affects this calculation. However, since the light curve slopes generally change slowly after maximum light, we neglect this contribution to the error. Errors on the slope are the standard errors of the fit.

SN 2005la, SN 2011hw, and iPTF13beo have a second peak in the light curve during one or more of these bins. We omit any bins where the light curve is not consistent with a monotonically decreasing function. Note that lines in Figure 4.10 interpolate over these gaps in coverage, hiding the fact that some slopes become negative (rebrightening) for a short period.

The intercept of the earliest linear fit to the light curves is an estimate of the peak magnitude. In most cases this is the 0–15 day bin. For PTF11rfh and SNe 2002ao, 2014bk, and 2015G, which have fewer than three points in the 0–15 day bin, the intercept from the 0 to 30 day bin is used. The errors on the peak magnitudes include contributions from the estimated error on the peak date, the standard errors on the slope and intercept, and the slope-intercept covariance of the fit.

In cases where the peak is well sampled, we can use the measured peak brightness as a basis for comparison. We consider the peak magnitude to be measured if we have a photometry point within one day of the estimated peak date. Note that, in most cases where we have data, the extrapolated peak is brighter than the observed peak. This is expected since we are fitting a straight line to a concave-down portion of the light curve. Since the maximum difference between estimated and observed peak magnitude is 0.27 mag, we prefer to accept this bias rather than using a more sophisticated method to fit the well-sampled peaks.

Explosion Epoch and Rise Time

In order to determine the rise time, we must estimate the epoch of explosion. Where possible, we fit a parabola (flux vs. phase) to the premaximum light curve. We use the zero of this fit as our estimate of the explosion time. For objects not observed before maximum light, it is impossible to independently estimate the explosion epoch and the peak date. For those objects, we place an upper limit on the rise time that corresponds to the time between the last nondetection and the first detection. The last nondetections of SN 2005la and ASASSN-15ed are not deep enough to constrain the epoch of explosion, so we do not estimate their rise times. We then calculate the rise time as the time between our estimated explosion date and our estimated peak date in the rest frame of the supernova.

Results

The most striking result of the photometric analysis is the relative homogeneity in the shapes of Type Ibn light curves. Whereas Type IIn light curves can decline in a few weeks or last for many months (see, e.g., Kiewe et al. 2012 their Figures 17 and 18), almost all Type Ibn light curves decline at rates of 0.05–0.15 mag day^{-1} during the first month after maximum light (see Figure 4.10). These fast decline rates rule out radioactive decay as a significant power source for the late-time light curves of all but the most extreme outlier (OGLE12-006). We are therefore in agreement with the rest of the literature that circumstellar interaction most likely powers SNe Ibn.

However, since one might expect interaction-powered light curves to be as diverse as the set of possible CSM density profiles that generate them, our data suggest a relatively homogeneous set of progenitor systems and/or explosion parameters. Moriya & Maeda (2016) explain this homogeneity by proposing that the duration of circumstellar

interaction is shorter for SNe Ibn than for Type IIn supernovae, despite similar explosion properties and CSM configurations. Our photometry also supports this hypothesis. Our sample of spectra, on the other hand, continue to show evidence of interaction several weeks after maximum light. In particular, spectra of SNe Ibn show narrow emission lines and are bluer than those of other hydrogen-poor supernovae well over a month after maximum light (see bottom panel of Figure 4.1). Together, the light curves and spectra seem to indicate decreased interaction at later times: strong enough to produce narrow lines and blue spectra but weak enough not to significantly affect the light curves.

Peak magnitudes of Type IIn supernovae have a wider observed distribution than those of SNe Ibn (see Figure 4.11). However, with only 22 objects, we are unable to rule out the possibility that they arise from the same underlying distribution. We perform the Kolmogorov–Smirnov test, comparing the sample distributions of Type IIn and Ibn peak magnitudes, which yields a statistically insignificant result: the maximum distance between the cumulative distribution functions of the two samples is $D = 0.23$ with $p = 0.32$. Furthermore, the faster decline rates of SNe Ibn might cause an observational bias against discovering fainter objects, making the underlying distributions more similar.

Finally, we search for correlations between the three parameters we estimate: decline slope, peak magnitude, and rise time. For each pair of parameters, we calculate the weighted Pearson correlation coefficient (r_P, which down-weights points with large error bars but assumes the variables have Gaussian distributions), the Spearman rank correlation coefficient (r_S, which does not assume Gaussian distributions but weights all points equally), and their associated p-values (see Figure 4.12). We do not find any correlations that are statistically significant in both r_P and r_S.

In the figures throughout this paper, objects in the emission subclass are assigned cool colors (green/blue/purple) while objects in the P Cygni subclass are assigned warm colors (pink/red/orange/yellow). Objects not obviously belonging to either class are

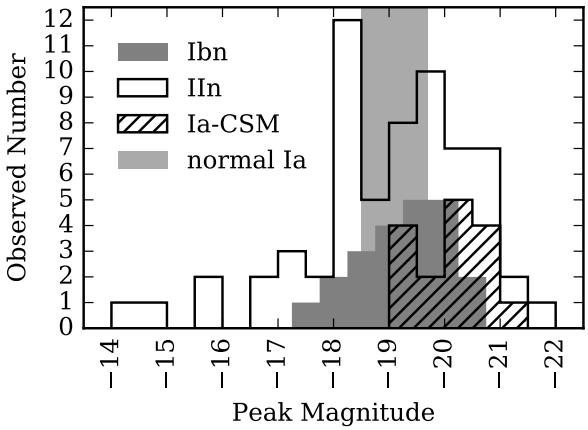

Figure 4.11: Observed distribution of the estimated peak absolute magnitudes (R- or r-band where possible); see Section 4.3.2) of SNe Ibn compared to those of Type IIn, Type Ia-CSM, and normal SNe Ia (all in the r-band), all of which are relatively luminous compared to normal CCSNe. Data for Type IIn and Ia-CSM supernovae are from Silverman et al. (2013). The Type Ibn distribution appears narrower than the Type IIn distribution, but the difference is not statistically significant.

colored gray and black. Since warm and cool colors appear to be well mixed in each plot, we conclude that light curve properties do not correlate strongly with the two spectral subclasses.

4.4 Light Curve Templates

Motivated by the observed homogeneity in Type Ibn light curves, we set out to define a region in magnitude–phase space that contains $\sim 95\%$ of the photometric points in our sample. We call this the Type Ibn light curve template. For the purposes of the template, we exclude the extreme outlier light curve of OGLE12-006 and the three double-peaked light curves (iPTF13beo and SNe 2005la and 2011hw), as their light curves may reflect different physical processes that we do not wish to capture.

First, we use a Gaussian process to fit a smooth curve through the combined light curves of the 18 remaining objects. We perform the fit in log–log space, specifically magnitude vs. log(phase + 20), in order to ensure consistent smoothness between the densely sampled early light curve and the sparsely sampled late light curve. This yields the average Type Ibn light curve. We then use two more independent Gaussian processes to fit the positive and negative residuals, respectively, from the average light curve. These

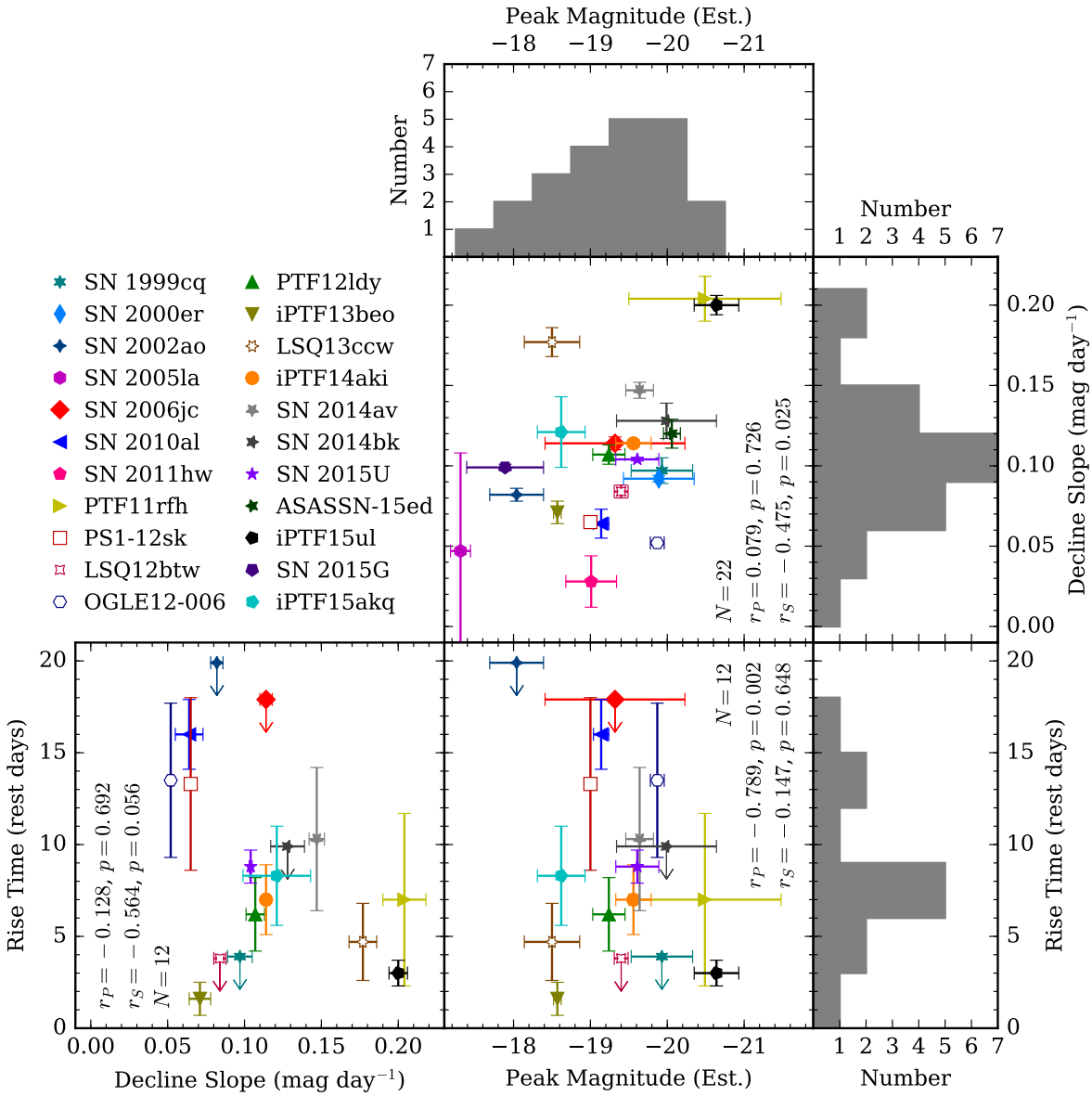

Figure 4.12: Histograms and scatter plots of light curve parameters. The weighted Pearson correlation coefficient (r_P), the Spearman rank correlation coefficient (r_S), and the associated p-values (probability of chance correlation) are given for each pair of parameters. Histograms and statistics exclude points with rise-time upper limits. For consistency, the estimated peak magnitude (see Section 4.3.2) is plotted for all objects, regardless of whether their peaks were well observed. We do not find any correlations that are statistically significant in both r_P and r_S.

result in upper and lower 1σ boundaries for the region. We plot the 95% probability region in the upper panel of Figure 4.13. Although all phases were included in the fit, we only report the template for phases during which more than one supernova was observed. We consider a supernova to be observed during a given phase if its published light curve contains points both before and after that phase.

Photometric nondetections are completely ignored in the fit, which severely biases the prepeak results. Many objects have extremely short rise times (a few days) that are not contained in the template region, while the few objects with longer rise times pull the fit to brighter magnitudes at early times. When comparing this template to future SNe Ibn, objects with arbitrarily short rise times should not be considered inconsistent. The purpose of the template is mainly to showcase the fast, homogeneous decline rate and bright peak magnitude.

We also produce a normalized Type Ibn light curve template by first normalizing all the light curves in our sample to their estimated peak magnitudes and then applying the method described above. Note that although all the normalized light curves pass through 0 mag at 0 days (neglecting the difference between estimated and observed peak magnitudes), the Gaussian process prevents the center and the edges of the template region from passing exactly through this point in order to preserve smoothness. The normalized template also appears in the lower panel of Figure 4.13.

4.5 Discussion: Implications for the Progenitor

Stepping back to Type Ib supernovae in general, two main progenitor scenarios have been suggested, each with a different way to remove the hydrogen envelope from a massive star. Gaskell et al. (1986), for example, propose a single massive WR star with a high mass-loss rate to remove the hydrogen envelope before explosion. Podsiadlowski

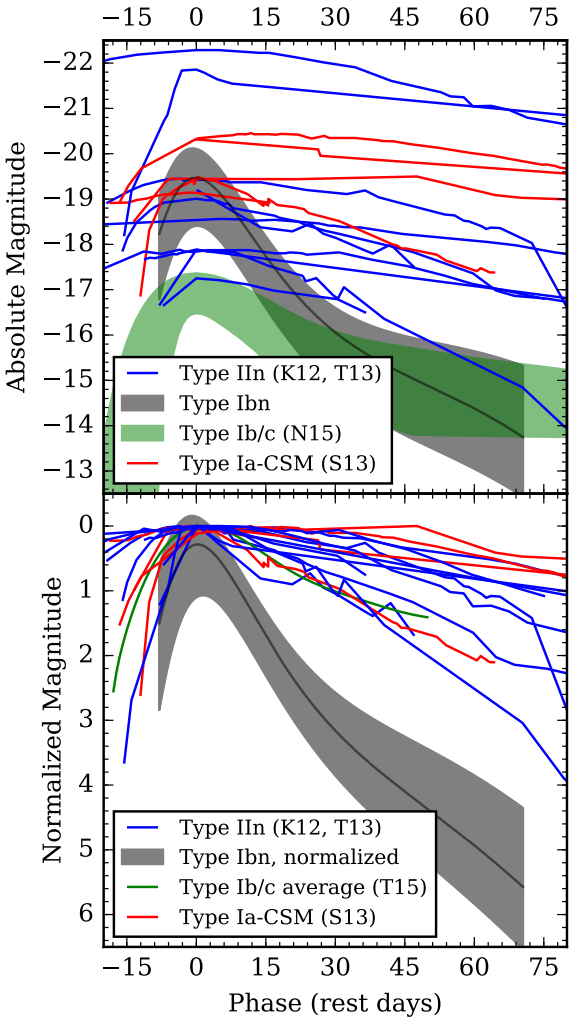

Figure 4.13: Type Ibn templates compared to analogous Type Ib/c templates (Nicholl et al. 2015; Taddia et al. 2015) and samples of Type IIn (Kiewe et al. 2012; Taddia et al. 2013 and references therein) and Type Ia-CSM (Silverman et al. 2013 and references therein) light curves. The upper panel shows the comparison of absolute magnitudes, and the lower panel illustrates the comparison when all light curves are normalized to peak. SNe Ibn are much more homogeneous and faster evolving than other interacting supernovae. They are also brighter and faster evolving than non-interacting SNe Ib/c.

et al. (1992), on the other hand, propose a close binary system, where binary interaction strips the hydrogen layer from the supernova progenitor. To date, only a single Type Ib supernova progenitor candidate has been detected: that of iPTF13bvn. In that case, Cao et al. (2013) found that the candidate was consistent with a WR star. However, hydrodynamical modeling by Fremling et al. (2014, 2016) and Bersten et al. (2014) show that the supernova properties are inconsistent with a single massive star and suggest a binary progenitor. A re-analysis of the photometry by Eldridge et al. (2015) also supports the binary hypothesis.

The literature on SNe Ibn contains many comprehensive discussions of possible progenitor scenarios (see, e.g., Foley et al. 2007; Pastorello et al. 2007, 2016; Sanders et al. 2013), but they fall roughly along the same lines as for normal SNe Ib: either binary interaction or stellar winds have stripped the outer layers from a massive star, leaving it surrounded by helium-rich CSM. If the CSM is dense enough, it can interact with supernova ejecta significantly, adding narrow emission lines to the spectra. Although observations of many SNe Ibn are consistent with single WR progenitors, without a direct progenitor detection, the binary scenario is difficult to rule out. Even the detection of an LBV-like eruption at the location of SN 2006jc two years before explosion could be explained either by an LBV companion or by residual LBV behavior in a recently transitioned WR star (Pastorello et al. 2007; Tominaga et al. 2008), although the lack of hydrogen in late-time spectra makes the former scenario less appealing. To complicate things further, Sanders et al. (2013) find that PS1-12sk exploded in a brightest cluster galaxy, and thus may have had a degenerate helium-rich progenitor rather than a massive star. (However, a low-surface-brightness star-forming region might have escaped detection.)

Exploring the dichotomy between spectra that exhibit early P Cygni lines and those that do not might aid in determining the range of properties of SN Ibn progenitors. To

be clear, we do not suggest that the two subclasses correspond to two entirely different populations of progenitor stars (this makes the late-time similarity hard to explain), but rather that different CSM initial conditions result in at least two varieties of early spectra. We also consider the possibility that *all* SNe Ibn exhibit helium P Cygni lines in their spectra immediately after explosion but that our observations thus far have not been sufficiently early to see them for all objects. If this proves to be the case, then the following discussion can be interpreted as explaining why some explosions result in only *short-lived* P Cygni lines while others show P Cygni lines for weeks.

One potential explanation for the spectral diversity is optical-depth effects in the CSM. If we attribute the presence of narrow P Cygni lines to slow-moving, dense circumstellar helium previously ejected by the progenitor, then the optical depth of that material at the time of explosion will determine how it manifests itself in the supernova spectra. If the material is optically thick, it will be backlit by supernova photons. This would result in slow-moving helium features superimposed on a hot thermal continuum. Then as the ejecta sweep up the material, the P Cygni lines transition into broad supernova features. On the other hand, if the material were optically thin by the time of explosion, broad features would dominate over the CSM emission. Spectra that exhibit very weak helium P Cygni lines on top of the emission features, such as those of SN 2014av, could represent an intermediate stage, where the circumstellar helium has an optical depth near 1.

A second option is that a viewing-angle effect controls whether P Cygni lines are visible in early Type Ibn spectra. If the CSM is not spherically symmetric about the progenitor—imagine, for example, a torus of circumstellar helium—then P Cygni lines may only be visible if the torus is viewed edge-on, whereas emission lines are produced when the torus is face-on. For this scenario to be successful, it must be able to account for the relative frequency of P Cygni to emission events. This ratio is difficult to estimate,

since there are only a small number of events in each class and the classification is not straightforward without early spectra. Nonetheless, with roughly equal numbers in each class, the proposed torus would seem to occupy a large portion of the progenitor star's solid angle.

The uniformity and rapid declines of Type Ibn light curves could indicate they are powered by interaction with a spatially confined shell of circumstellar helium surrounded by a less dense region of CSM. If the shell is thin enough, strong interaction between the ejecta and the CSM would last only a short time, rather than continuing to power the light curve for many months, as in SNe IIn. Quataert et al. (2016) suggest that super-Eddington winds tend to produce a CSM shell when driven by energy deposited near the stellar surface, either in the course of binary interaction or by unstable fusion or wave heating in a single star. The wind speed increases as the energy deposition radius decreases, so as the star loses material and shrinks, the ejected mass begins to pile up in a shell around the star. In fact, SN 2014C, which evolved from a hydrogen-poor SN Ib into a hydrogen-interacting SN IIn over the course of several months, could represent an extreme case where a massive star ejects its entire hydrogen envelope into a dense shell decades to centuries before explosion. Ejecta from SN 2014C then had to travel through a low-density bubble (during which time it was hydrogen-poor) before reaching and interacting with the circumstellar hydrogen (Milisavljevic et al. 2015; Margutti et al. 2017). WR stars and massive binaries are promising candidates for this type of behavior.

Unfortunately, none of these proposals can definitively differentiate between a binary progenitor and a single WR star. For nearby objects, X-ray and radio observations can help directly constrain the CSM properties and provide clues about progenitor mass loss (e.g., Chevalier et al. 2006). For the rest, early (pre-maximum or first-week-post-maximum) spectroscopy and detailed modeling of the interaction between supernova ejecta and various CSM configurations will be essential to resolving the remaining un-

knowns.

4.6 Summary

We have presented photometry and spectroscopy of six new SNe Ibn: PTF11rfh, PTF12ldy, iPTF14aki, iPTF15ul, SN 2015G, and iPTF15akq. We find PTF11rfh and iPTF14aki to be nearly identical to the archetype of the Ibn class, SN 2006jc. Helium P Cygni lines in early spectra of PTF12ldy link it to SNe 2000er and 2010al. Spectra of iPTF15ul are heavily contaminated by host-galaxy light, but nonetheless resemble those of SN 2000er. Late-time optical spectra of SN 2015G also show similarities to spectra of SN 2010al. iPTF15akq exhibits significant hydrogen in its spectra, making it resemble the transitional Type Ibn/IIn SN 2005la. When added to objects from the literature, these new events result in a sample of 22 SNe Ibn. We also presented new data on SN 2015U, previously discussed by Pastorello et al. (2015b), Tsvetkov et al. (2015), and Shivvers et al. (2016), including a near-infrared spectrum quite similar to that of SN 2010al.

We analyzed the full sample of Type Ibn light curves and spectra in order to determine the properties of this rare class of objects. Unlike the more commonly observed SNe IIn, whose interaction with hydrogen-rich CSM has been shown to generate a wide variety of light curve shapes, light curves of SNe Ibn are more homogeneous and faster evolving, with decline rates clustered closely around 0.1 mag day^{-1} during the first month after maximum light. We also find that, in the first week after maximum light, two types of Type Ibn spectra exist: those that consist of helium P Cygni lines superimposed on a blue continuum and those with broader features that resemble spectra of SN 2006jc.

We hypothesize that both the light curve uniformity and the transition in some objects from narrow P Cygni lines to broader features can be explained by the presence of a thin shell of circumstellar helium around the progenitor star surrounded by a less dense

region of CSM. An optically thick shell backlit by the explosion results in narrow P Cygni lines that eventually transition into broad emission lines as the shell is swept up by the supernova ejecta. Spectra without P Cygni lines imply that any previously ejected shell be optically thin at the time of explosion. Alternatively, the spectral diversity might be explained by a viewing-angle effect.

Last, we strongly emphasize that more theoretical modeling work is needed in order to make progress on the progenitor question for SNe Ibn. In addition, early ($\lesssim$ 1 week after peak brightness) observations of future SNe Ibn will be crucial to constraining these models.

Bibliography

Adelman-McCarthy, J. K., Allam, S. S., Allende Prieto, C., et al. 2007, ApJS, 175, 297

Aihara, H., Allende Prieto, C., An, D., et al. 2011, ApJS, 193, 29

Albareti, F. D., Prieto, C. A., Almeida, A., et al. 2017, ApJS, 233, 25

Arcavi, I. 2016, in Handbook of Supernovae, ed. A. W. Alsabti & P. Murdin (Cham: Springer)

Arcavi, I., Hosseinzadeh, G., Howell, D. A., & McCully, C. 2016a, TNSCR, 35, 1

Arcavi, I., Hosseinzadeh, G., Howell, D. A., McCully, C., & Valenti, S. 2017a, TNSCR, 1478, 1

Arcavi, I., Hosseinzadeh, G., Howell, D. A., et al. 2016b, TNSCR, 43, 1

Arcavi, I., McCully, C., Hosseinzadeh, G., et al. 2017b, TNSCR, 911, 1

Baade, W., & Zwicky, F. 1934, PNAS, 20, 254

Barbon, R., Buondi, V., Cappellaro, E., & Turatto, M. 2008, yCat, 1, 2024

Barbon, R., Ciatti, F., & Rosino, L. 1979, A&A, 72, 287

Becker, A. 2015, HOTPANTS: High Order Transform of PSF ANd Template Subtraction, Astrophysics Source Code Library, ascl:1504.004

Benetti, S., Patat, F., Turatto, M., et al. 1994, A&A, 285, L13

Bersten, M. C., Benvenuto, O. G., Folatelli, G., et al. 2014, AJ, 148, 68

Bianco, F. B., Howell, D. A., Sullivan, M., et al. 2011, ApJ, 741, 20

Bianco, F. B., Modjaz, M., Hicken, M., et al. 2014, ApJS, 213, 19

Bloom, J. S., Kasen, D., Shen, K. J., et al. 2012, ApJL, 744, L17

Breeveld, A. A., Curran, P. A., Hoversten, E. A., et al. 2010, MNRAS, 406, 1687

Brown, P. J., Breeveld, A. A., Holland, S., Kuin, P., & Pritchard, T. 2014, Ap&SS, 354, 89

Brown, P. J., Dawson, K. S., Harris, D. W., et al. 2012a, ApJ, 749, 18

Brown, P. J., Dawson, K. S., de Pasquale, M., et al. 2012b, ApJ, 753, 22

Brown, T. M., Baliber, N., Bianco, F. B., et al. 2013, PASP, 125, 1031

Burke, J., Hiramatsu, D., Arcavi, I., et al. 2018, TNSCR, 2018-761, 1

Cao, Y., Kulkarni, S. R., Gal-Yam, A., et al. 2016, ApJ, 832, 86

Cao, Y., Kasliwal, M. M., Arcavi, I., et al. 2013, ApJ, 775, L7

Cao, Y., Kulkarni, S. R., Howell, D. A., et al. 2015, Natur, 521, 328

Cardelli, J. A., Clayton, G. C., & Mathis, J. S. 1989, ApJ, 345, 245

Cenko, S. B., Fox, D. B., Moon, D.-S., et al. 2006, PASP, 118, 1396

Chevalier, R. A., Fransson, C., & Nymark, T. K. 2006, ApJ, 641, 1029

Childress, M. J., Scalzo, R. A., Sim, S. A., et al. 2013, ApJ, 770, 29

Chugai, N. N. 1991, MNRAS, 250, 513

Chugai, N. N., & Utrobin, V. P. 2000, A&A, 354, 557

Conley, A., Sullivan, M., Hsiao, E. Y., et al. 2008, ApJ, 681, 482

Crowther, P. A. 2007, ARA&A, 45, 177

Dilday, B., Howell, D. A., Cenko, S. B., et al. 2012, Sci, 337, 942

Drake, A. J., Djorgovski, S. G., Mahabal, A., et al. 2009, ApJ, 696, 870

Eggleton, P. P. 1983, ApJ, 268, 368

Eldridge, J. J., Fraser, M., Maund, J. R., & Smartt, S. J. 2015, MNRAS, 446, 2689

Faber, S. M., Phillips, A. C., Kibrick, R. I., et al. 2003, SPIE, 4841, 1657

Fan, Z., Wang, H., Jiang, X., et al. 2016, PASP, 128, 115005

Faran, T., Poznanski, D., Filippenko, A. V., et al. 2014, MNRAS, 442, 844

Ferrarese, L., Mould, J. R., Kennicutt, R. C., et al. 1999, ApJ, 529, 745

Ferretti, R., Amanullah, R., Bulla, M., et al. 2017, ApJL, 851, L43

Filippenko, A. V. 1997, ARA&A, 35, 309

Filippenko, A. V., Li, W. D., Treffers, R. R., & Modjaz, M. 2001, ASPC, 246, 181

Firth, R. E., Sullivan, M., Gal-Yam, A., et al. 2015, MNRAS, 446, 3895

Foley, R. J., Berger, E., Fox, O., et al. 2011, ApJ, 732, 32

Foley, R. J., Smith, N., Ganeshalingam, M., et al. 2007, ApJ, 657, L105

Foley, R. J., Zheng, W., Filippenko, A. V., & Dyk, S. D. V. 2015, ATel, 7298, 1

Foley, R. J., Chornock, R., Filippenko, A. V., et al. 2009, AJ, 138, 376

Foreman-Mackey, D., Hogg, D. W., Lang, D., & Goodman, J. 2013, PASP, 125, 306

Fox, O. D., Dyk, S. D. V., Dwek, E., et al. 2017, ApJ, 836, 222

Fremling, C., Sollerman, J., Taddia, F., et al. 2014, A&A, 565, A114

—. 2016, A&A, 593, A68

Gal-Yam, A. 2012, Sci, 337, 927

Gal-Yam, A. 2016, in Handbook of Supernovae, ed. A. W. Alsabti & P. Murdin (Cham: Springer)

Gal-Yam, A., & Leonard, D. C. 2009, Natur, 458, 865

Gal-Yam, A., Kasliwal, M. M., Arcavi, I., et al. 2011, ApJ, 736, 159

Gal-Yam, A., Arcavi, I., Ofek, E. O., et al. 2014, Natur, 509, 471

Ganeshalingam, M., Li, W., Filippenko, A. V., et al. 2012, ApJ, 751, 142

Garavini, G., Folatelli, G., Goobar, A., et al. 2004, AJ, 128, 387

Garnavich, P. M., & Ann, H. B. 1994, AJ, 108, 1002

Gaskell, C. M., Cappellaro, E., Dinerstein, H. L., et al. 1986, ApJ, 306, L77

Goobar, A., Kromer, M., Siverd, R., et al. 2015, ApJ, 799, 106

Groh, J. H. 2014, A&A, 572, L11

Guevel, D., & Hosseinzadeh, G. 2017, PyZOGY, v0.0.1, Zenodo, doi:10.5281/zenodo.1043973

Guy, J., Astier, P., Baumont, S., et al. 2007, A&A, 466, 11

Hakobyan, A. A., Adibekyan, V. Z., Aramyan, L. S., et al. 2012, A&A, 544, A81

Hamuy, M. 2003, ApJ, 582, 905

Hamuy, M., & Pinto, P. A. 2002, ApJL, 566, L63

Hayden, B. T., Garnavich, P. M., Kasen, D., et al. 2010, ApJ, 722, 1691

Heckman, T. M., & Thompson, T. A. 2017, in Handbook of Supernovae, ed. A. W. Alsabti & P. Murdin (Cham: Springer)

Hiramatsu, D., Arcavi, I., Burke, J., et al. 2018a, TNSCR, 672, 1

—. 2018b, TNSCR, 679, 1

—. 2018c, TNSCR, 693, 1

—. 2018d, TNSCR, 712, 1

—. 2018e, TNSCR, 715, 1

—. 2018f, TNSCR, 2018-760, 1

Hodge, P. W., & Kennicutt, Jr., R. C. 1983, AJ, 88, 296

Hook, I. M., Jørgensen, I., Allington-Smith, J. R., et al. 2004, PASP, 116, 425

Hosseinzadeh, G., Arcavi, I., Burke, J., et al. 2018a, TNSCR, 485, 1

Hosseinzadeh, G., Arcavi, I., Howell, D. A., McCully, C., & Valenti, S. 2016a, TNSCR, 131, 1

—. 2016b, TNSCR, 141, 1

—. 2016c, TNSCR, 145, 1

—. 2016d, TNSCR, 187, 1

—. 2016e, TNSCR, 219, 1

—. 2016f, TNSCR, 263, 1

—. 2016g, TNSCR, 294, 1

—. 2016h, TNSCR, 364, 1

—. 2016i, TNSCR, 386, 1

—. 2016j, TNSCR, 414, 1

—. 2016k, TNSCR, 595, 1

—. 2016l, TNSCR, 639, 1

—. 2016m, TNSCR, 721, 1

—. 2016n, TNSCR, 753, 1

—. 2016o, TNSCR, 865, 1

—. 2016p, TNSCR, 897, 1

—. 2016q, TNSCR, 926, 1

—. 2017a, TNSCR, 429, 1

—. 2017b, TNSCR, 434, 1

—. 2017c, TNSCR, 539, 1

—. 2017d, TNSCR, 835, 1

—. 2017e, TNSCR, 844, 1

—. 2017f, TNSCR, 1002, 1

—. 2017g, TNSCR, 1369, 1

—. 2017h, TNSCR, 58, 1

—. 2017i, TNSCR, 132, 1

—. 2017j, TNSCR, 172, 1

—. 2017k, TNSCR, 241, 1

—. 2017l, TNSCR, 253, 1

Hosseinzadeh, G., Arcavi, I., McCully, C., Howell, D. A., & Valenti, S. 2016r, TNSCR, 447, 1

—. 2017m, TNSCR, 579, 1

Hosseinzadeh, G., Arcavi, I., Valenti, S., Howell, D. A., & McCully, C. 2016s, TNSCR, 213, 1

—. 2016t, TNSCR, 226, 1

—. 2016u, TNSCR, 236, 1

—. 2017n, TNSCR, 751, 1

Hosseinzadeh, G., Ellman, N., McCully, C., et al. 2016v, TNSCR, 272, 1

—. 2016w, TNSCR, 303, 1

Hosseinzadeh, G., Hiramatsu, D., Arcavi, I., et al. 2018b, TNSCR, 162, 1

—. 2018c, TNSCR, 313, 1

—. 2018d, TNSCR, 373, 1

Hosseinzadeh, G., Howell, D. A., Arcavi, I., McCully, C., & Valenti, S. 2016x, TNSCR, 239, 1

—. 2016y, TNSCR, 401, 1

—. 2016z, TNSCR, 411, 1

—. 2016aa, TNSCR, 785, 1

—. 2017o, TNSCR, 536, 1

—. 2017p, TNSCR, 729, 1

—. 2017q, TNSCR, 1022, 1

—. 2017r, TNSCR, 228, 1

Hosseinzadeh, G., McCully, C., Arcavi, I., Howell, D. A., & Valenti, S. 2017s, TNSCR, 43, 1

Hosseinzadeh, G., McCully, C., Valenti, S., Arcavi, I., & Howell, D. A. 2017t, TNSCR, 775, 1

Hosseinzadeh, G., Smartt, S., Arcavi, I., et al. 2016ab, TNSCR, 227, 1

Hosseinzadeh, G., Tucker, B., Arcavi, I., et al. 2017u, TNSCR, 864, 1

Hosseinzadeh, G., Valenti, S., Arcavi, I., Howell, D. A., & McCully, C. 2016ac, TNSCR, 634, 1

—. 2017v, TNSCR, 858, 1

—. 2017w, TNSCR, 1259, 1

Hosseinzadeh, G., Valenti, S., Arcavi, I., et al. 2017x, TNSCR, 169, 1

Hosseinzadeh, G., Valenti, S., Howell, D. A., Arcavi, I., & McCully, C. 2017y, TNSCR, 865, 1

Hosseinzadeh, G., Valenti, S., Sand, D., et al. 2018e, TNSCR, 433, 1

Hosseinzadeh, G., Yang, Y., Arcavi, I., et al. 2016ad, TNSCR, 73, 1

Hosseinzadeh, G., Yang, Y., Howell, D. A., et al. 2016ae, TNSCR, 367, 1

—. 2016af, TNSCR, 214, 1

Hosseinzadeh, G., Yang, Y., McCully, C., et al. 2016ag, TNSCR, 162, 1

Hosseinzadeh, G., Yang, Y., Valenti, S., et al. 2016ah, TNSCR, 105, 1

Hosseinzadeh, G., Sand, D. J., Valenti, S., et al. 2017z, ApJL, 845, L11

Hosseinzadeh, G., Howell, D. A., Sand, D., et al. 2017aa, TNSCR, 300, 1

Hosseinzadeh, G., Valenti, S., Bostroem, K. A., et al. 2017ab, TNSCR, 368, 1

Hosseinzadeh, G., Valenti, S., McCully, C., et al. 2018f, ApJ, in press

Howell, D. A. 2011, NatCo, 2, 350

Howell, D. A., Sullivan, M., Nugent, P. E., et al. 2006, Natur, 443, 308

Huang, F., Li, J.-Z., Wang, X.-F., et al. 2012, RAA, 12, 1585

Iben, I., & Tutukov, A. V. 1984, ApJS, 54, 335

Im, M., Choi, C., Yoon, S.-C., et al. 2015, ApJS, 221, 22

Immler, S., Modjaz, M., Landsman, W., et al. 2008, ApJ, 674, L85

Itagaki, K. 2016, TNSTR, 234, 1

Jerkstrand, A. 2017, in Handbook of Supernovae, ed. A. W. Alsabti & P. Murdin (Cham: Springer)

Jerkstrand, A., Ertl, T., Janka, H.-T., et al. 2018, MNRAS, 475, 277

Jha, S., Riess, A. G., & Kirshner, R. P. 2007, ApJ, 659, 122

Jones, M. I., Hamuy, M., Lira, P., et al. 2009, ApJ, 696, 1176

Jordi, K., Grebel, E. K., & Ammon, K. 2006, A&A, 460, 339

Kasen, D. 2010, ApJ, 708, 1025

Khazov, D., Yaron, O., Gal-Yam, A., et al. 2016, ApJ, 818, 3

Kiewe, M., Gal-Yam, A., Arcavi, I., et al. 2012, ApJ, 744, 10

Kromer, M., Fremling, C., Pakmor, R., et al. 2016, MNRAS, 459, 4428

Kulkarni, S. R. 2013, ATel, 4807, 1

Kumar, S., Yuk, H., Zheng, W., et al. 2015, CBET, 4164, 1

Kushnir, D., Katz, B., Dong, S., Livne, E., & Fernández, R. 2013, ApJL, 778, L37

Landolt, A. U. 1992, AJ, 104, 340

Law, N. M., Kulkarni, S. R., Dekany, R. G., et al. 2009, PASP, 121, 1395

Leonard, D. C. 2007, ApJ, 670, 1275

Leonard, D. C., Filippenko, A. V., Barth, A. J., & Matheson, T. 2000, ApJ, 536, 239

Levanon, N., & Soker, N. 2017, MNRAS, 470, 2510

Li, W., Van Dyk, S. D., Filippenko, A. V., et al. 2006, ApJ, 641, 1060

Lisakov, S. M., Dessart, L., Hillier, D. J., Waldman, R., & Livne, E. 2017, MNRAS, 466, 34

—. 2018, MNRAS, 473, 3863

Liu, Y.-Q., Modjaz, M., Bianco, F. B., & Graur, O. 2016, ApJ, 827, 90

Liu, Z.-W., Moriya, T. J., & Stancliffe, R. J. 2015, MNRAS, 454, 1192

Maeda, K., Kutsuna, M., & Shigeyama, T. 2014, ApJ, 794, 37

Maoz, D., Mannucci, F., & Nelemans, G. 2014, ARA&A, 52, 107

Margutti, R., Kamble, A., Milisavljevic, D., et al. 2017, ApJ, 835, 140

Marion, G. H., Brown, P. J., Vinkó, J., et al. 2016, ApJ, 820, 92

Matheson, T., Filippenko, A. V., Chornock, R., Leonard, D. C., & Li, W. 2000, AJ, 119, 2303

Mattila, S., Lundqvist, P., Sollerman, J., et al. 2005, A&A, 443, 649

Mauerhan, J. C., Smith, N., Filippenko, A. V., et al. 2013, MNRAS, 430, 1801

Maund, J. R., Smartt, S. J., & Danziger, I. J. 2005, MNRAS, 364, L33

McMullin, J. P., Waters, B., Schiebel, D., Young, W., & Golap, K. 2007, ASPC, 376, 127

Milisavljevic, D., Chilingarian, I., Berlind, P., et al. 2016, ATel, 8861, 1

Milisavljevic, D., Margutti, R., Kamble, A., et al. 2015, ApJ, 815, 120

Miller, J. S., & Stone, R. P. S. 1994, The Kast Double Spectograph, Lick Observatory Tech. Rep. No. 66 (Santa Cruz: Lick Observatory)

Minkowski, R. 1941, PASP, 53, 224

Mo, H., van den Bosch, F. C., & White, S. 2010, Galaxy Formation and Evolution (Cambridge Univ. Press)

Modjaz, M., Blondin, S., Kirshner, R. P., et al. 2014, AJ, 147, 99

Moriya, T. J., & Maeda, K. 2016, ApJ, 824, 100

Moriya, T. J., Tominaga, N., Langer, N., et al. 2014, A&A, 569, A57

Morozova, V., Piro, A. L., & Valenti, S. 2017, ApJ, 838, 28

—. 2018, ApJ, 858, 15

Nakano, S., Itagaki, K., Puckett, T., & Gorelli, R. 2006, CBET, 666, 1

Nicholl, M., Smartt, S. J., Jerkstrand, A., et al. 2015, MNRAS, 452, 3869

Niemela, V. S., Ruiz, M. T., & Phillips, M. M. 1985, ApJ, 289, 52

Noebauer, U. M., Kromer, M., Taubenberger, S., et al. 2017, MNRAS, 472, 2787

Nugent, P. E., Sullivan, M., Cenko, S. B., et al. 2011, Natur, 480, 344

Ochner, P., Benetti, S., Pastorello, A., et al. 2015, ATel, 7105, 1

Ofek, E. O., Sullivan, M., Cenko, S. B., et al. 2013, Natur, 494, 65

Ofek, E. O., Sullivan, M., Shaviv, N. J., et al. 2014, ApJ, 789, 104

Oke, J. B., & Gunn, J. E. 1982, PASP, 94, 586

Oke, J. B., Cohen, J. G., Carr, M., et al. 1995, PASP, 107, 375

Pakmor, R., Kromer, M., Taubenberger, S., et al. 2012, ApJL, 747, L10

Pan, Y.-C., Foley, R. J., Kromer, M., et al. 2015, MNRAS, 452, 4307

Parrent, J., Friesen, B., & Parthasarathy, M. 2014, Ap&SS, 351, 1

Parrent, J. T., Thomas, R. C., Fesen, R. A., et al. 2011, ApJ, 732, 30

Pastorello, A., Zampieri, L., Turatto, M., et al. 2004, MNRAS, 347, 74

Pastorello, A., Sauer, D., Taubenberger, S., et al. 2006, MNRAS, 370, 1752

Pastorello, A., Smartt, S. J., Mattila, S., et al. 2007, Natur, 447, 829

Pastorello, A., Mattila, S., Zampieri, L., et al. 2008a, MNRAS, 389, 113

Pastorello, A., Quimby, R. M., Smartt, S. J., et al. 2008b, MNRAS, 389, 131

Pastorello, A., Benetti, S., Brown, P. J., et al. 2015a, MNRAS, 449, 1921

Pastorello, A., Tartaglia, L., Elias-Rosa, N., et al. 2015b, MNRAS, 454, 4293

Pastorello, A., Wang, X.-F., Ciabattari, F., et al. 2016, MNRAS, 456, 853

Patat, F., Barbon, R., Cappellaro, E., & Turatto, M. 1994, A&A, 282, 731

Pejcha, O., & Prieto, J. L. 2015, ApJ, 806, 225

Perley, R., Napier, P., Jackson, J., et al. 2009, IEEEP, 97, 1448

Perlmutter, S., Gabi, S., Goldhaber, G., et al. 1997, ApJ, 483, 565

Perlmutter, S., Aldering, G., Goldhaber, G., et al. 1999, ApJ, 517, 565

Phillips, M. M. 1993, ApJ, 413, L105

Pierce, M. J. 1994, ApJ, 430, 53

Piro, A. L., Chang, P., & Weinberg, N. N. 2010, ApJ, 708, 598

Piro, A. L., & Morozova, V. S. 2016, ApJ, 826, 96

Piro, A. L., & Nakar, E. 2013, ApJ, 769, 67

—. 2014, ApJ, 784, 85

Planck Collaboration, Ade, P. A. R., Aghanim, N., et al. 2016, A&A, 594, 13

Podsiadlowski, P., Joss, P. C., & Hsu, J. J. L. 1992, ApJ, 391, 246

Polshaw, J., Benitez, S., Taubenberger, S., et al. 2014, ATel, 6091, 1

Poole, T. S., Breeveld, A. A., Page, M. J., et al. 2007, MNRAS, 383, 627

Pumo, M. L., Zampieri, L., Spiro, S., et al. 2017, MNRAS, 464, 3013

Quataert, E., Fernández, R., Kasen, D., Klion, H., & Paxton, B. 2016, MNRAS, 458, 1214

Quimby, R. M., Wheeler, J. C., Höflich, P., et al. 2007, ApJ, 666, 1093

Rabinak, I., Livne, E., & Waxman, E. 2012, ApJ, 757, 35

Rau, A., Kulkarni, S. R., Law, N. M., et al. 2009, PASP, 121, 1334

Rayner, J. T., Toomey, D. W., Onaka, P. M., et al. 2003, PASP, 115, 362

Reichart, D., Nysewander, M., Moran, J., et al. 2005, NCimC, 28, 767

Riess, A. G., Filippenko, A. V., Challis, P., et al. 1998, AJ, 116, 1009

Rockosi, C., Stover, R., Kibrick, R., et al. 2010, SPIE, 7735E, 0R

Roming, P. W. A., Kennedy, T. E., Mason, K. O., et al. 2005, SSRv, 120, 95

Ross, T. W., Channa, S., Molloy, J. D., Zheng, W., & Filippenko, A. V. 2016, ATel, 8875, 1

Sand, D. J., Hsiao, E. Y., Banerjee, D. P. K., et al. 2016, ApJL, 822, L16

Sand, D. J., Graham, M. L., Botyánszki, J., et al. 2018, ApJ, in press

Sanders, N. E., Soderberg, A. M., Foley, R. J., et al. 2013, ApJ, 769, 39

Sapir, N., & Waxman, E. 2017, ApJ, 838, 130

Schlafly, E. F., & Finkbeiner, D. P. 2011, ApJ, 737, 103

Schlegel, E. M. 1990, MNRAS, 244, 269

—. 2001, ApJL, 556, L25

Science Software Branch at STScI. 2012, PyRAF: Python alternative for IRAF, Astrophysics Source Code Library, ascl:1207.011

SDSS Collaboration, Albareti, F. D., Allende Prieto, C., et al. 2017, ApJS, 233, 25

Shapley, H. 1939, PNAS, 25, 569

Shappee, B. J., Piro, A. L., Stanek, K. Z., et al. 2018, ApJ, 855, 6

Shappee, B. J., Piro, A. L., Holoien, T. W.-S., et al. 2016, ApJ, 826, 144

Shen, K. J., & Bildsten, L. 2014, ApJ, 785, 61

Shivvers, I., Groh, J. H., Mauerhan, J. C., et al. 2015, ApJ, 806, 213

Shivvers, I., Zheng, W., Mauerhan, J., et al. 2016, MNRAS, 461, 3057

Silverman, J. M., & Filippenko, A. V. 2012, MNRAS, 425, 1917

Silverman, J. M., Foley, R. J., Filippenko, A. V., et al. 2012, MNRAS, 425, 1789

Silverman, J. M., Nugent, P. E., Gal-Yam, A., et al. 2013, ApJS, 207, 3

Skrutskie, M. F., Cutri, R. M., Stiening, R., et al. 2006, AJ, 131, 1163

Smartt, S. J. 2009, ARA&A, 47, 63

Smartt, S. J., Gilmore, G. F., Trentham, N., Tout, C. A., & Frayn, C. M. 2001, ApJL, 556, L29

Smartt, S. J., Valenti, S., Fraser, M., et al. 2015, A&A, 579, A40

Smith, N. 2016, in Handbook of Supernovae, ed. A. W. Alsabti & P. Murdin (Cham: Springer)

Smith, N., Foley, R. J., & Filippenko, A. V. 2008, ApJ, 680, 568

Smith, N., Li, W., Silverman, J. M., Ganeshalingam, M., & Filippenko, A. V. 2011, MNRAS, 415, 773

Smith, N., Miller, A., Li, W., et al. 2010a, AJ, 139, 1451

Smith, N., Li, W., Miller, A. A., et al. 2010b, ApJ, 732, 63

Spiro, S., Pastorello, A., Pumo, M. L., et al. 2014, MNRAS, 439, 2873

Stetson, P. B. 2000, PASP, 112, 925

Strauss, M. A., Huchra, J. P., Davis, M., et al. 1992, ApJS, 83, 29

Taddia, F., Stritzinger, M. D., Sollerman, J., et al. 2013, A&A, 555, A10

Taddia, F., Sollerman, J., Leloudas, G., et al. 2015, A&A, 574, A60

Tartaglia, L., Sand, D. J., Valenti, S., et al. 2018, ApJ, 853, 62

Thomas, R. C., Nugent, P. E., & Meza, J. C. 2011, PASP, 123, 237

Tominaga, N., Limongi, M., Suzuki, T., et al. 2008, ApJ, 687, 1208

Tsvetkov, D. Y., Volkov, I. M., & Pavlyuk, N. N. 2015, IBVS, 6140, 1

Tully, R. B. 1988, Nearby Galaxies Catalog (Cambridge: Cambridge Univ. Press)

Turatto, M., Mazzali, P. A., Young, T. R., et al. 1998, ApJL, 498, L129

Valenti, S., Sand, D., Tartaglia, L., et al. 2017a, TNSCR, 613, 1

—. 2017b, TNSCR, 757, 1

Valenti, S., Sand, D. J., & Tartaglia, L. 2017c, TNSTR, 294, 1

Valenti, S., Howell, D. A., Stritzinger, M. D., et al. 2016, MNRAS, 459, 3939

Valenti, S., Bostroem, K. A., Sand, D., et al. 2017d, TNSCR, 516, 1

Van Dyk, S. D. 2016, in Handbook of Supernovae, ed. A. W. Alsabti & P. Murdin (Cham: Springer)

Waxman, E., & Katz, B. 2017, in Handbook of Supernovae, ed. A. W. Alsabti & P. Murdin (Cham: Springer)

Webbink, R. F. 1984, ApJ, 277, 355

Whelan, J., & Iben, I. 1973, ApJ, 186, 1007

Yaron, O., & Gal-Yam, A. 2012, PASP, 124, 668

Yaron, O., Perley, D. A., Gal-Yam, A., et al. 2017, NatPh, 13, 510

Yusa, T., Buczynski, D., Noguchi, T., et al. 2015, CBET, 4087, 1

Zackay, B., Ofek, E. O., & Gal-Yam, A. 2016, ApJ, 830, 27

Zampieri, L., Shapiro, S. L., & Colpi, M. 1998, ApJL, 502, L149

Zhang, K., Wang, X., Zhang, J., et al. 2016, ApJ, 820, 67

Zheng, W., Silverman, J. M., Filippenko, A. V., et al. 2013, ApJL, 778, L15

Zheng, W., Shivvers, I., Filippenko, A. V., et al. 2014, ApJL, 783, L24

Zheng, W., Filippenko, A. V., Mauerhan, J., et al. 2017, ApJ, 841, 64